Bactericidal surfaces with nanoparticles and light activated agents to inhibit healthcare associated infections

This thesis is presented to UCL in partial fulfilment of the requirements

for degree of Doctor of Philosophy

Gi-Byoung Hwang

2017

Supervised by

Professor Ivan P. Parkin

Material Chemistry Centre, UCL Department of Chemistry

Doctor Elaine Allan

Department of Microbial Diseases, UCL Eastman Dental Institute

1

Declaration

I, Gi-Byoung Hwang, confirmed that the work presented in this thesis is my own. Where information has been derived from other sources, I confirm that this has been indicated in the thesis

Acknowledgements

Abstract

This thesis details the anti-biofouling property of superhydrophobic surface and white light-activated bactericidal polymers, and self-cleaning and bactericidal paints for preventing hospital associated infection.

To investigate the anti-biofouling property of superhydrophobic surface over a long period of time, superhydrophobic surfaces were made using 1H, 1H, 2H, 2H-perfluorooctyltriethoxysilane, P25 TiO_2 nanoparticles, ethanol, and double sided tape. The bacteria adhesion of the superhydrophobic surface was tested through full immersion of four different bacteria suspensions for 1, 4, 8, 16, and 24 h and then the result was compared with other surfaces containing glass, polystyrene, and polyurethane. Changes of the tested surfaces were investigated by water contact angle meter, SEM, AFM, and confocal microscope.

Through a simple swell-encapsulation shrink process, white light-activated bactericidal polyurethane was produced. Toluidine blue O and silver nanoparticles were encapsulated into a polyurethane and characterised by water contact angle meter, UV/Vis spectrometer, fluorescence microscope, and material testing and inspection device.

Crystal violet and acrylic latex, which is a widely used paint material for home decoration, were mixed together to produce photobactericidal paints for the first time. At various mixing ratio, crystal violet and acrylic latex were combined together. The paint coated slide was characterised using water contact angle meter, and UV/Vis spectrometer, and its stability was investigated through liquid leaching test

Crystal violet, toluidine blue O, P25 TiO_2 nanoparticles, and 1H, 1H, 2H, 2H-perfluorooctyltriethoxysilane were used to produce dual functional paints with superhydrophobic and bactericidal behaviour. TiO_2, TBO, and CV paints were fabricated *via* physical and chemical reaction. The dual functional paint coated slides were investigated in terms of water repellence, self-cleaning, and anti-biofouling properties, and was also characterised by SEM, AFM, and UV/Vis spectrometer.

Bactericidal properties of the treated polyurethane and paint, dual functional paints were assessed with *Escherichia coli* and *Staphylococcus aureus*. The tested samples demonstrated not only potent photobactericidal activity in white light (typical

hospital lamp) but also bactericidal activity in dark. It is expected that bactericidal materials detailed in this thesis will be useful for use in healthcare facilities in order to reduce hospital associated infections.

CONTENTS

List of Figures

nanoparticles.

List of Tables

List of Abbreviations

Healthcare-associated infections (HAIs)

National Health Service (NHS)

Staphylococcus aureus (*S. aureus*)

Methicillin sensitive *Staphylococcus aureus* (MSSA)

Methicillin resistant *Staphylococcus aureus* (MRSA)

Escherichia coli (*E. coli*)

Clostridium difficile (*C. difficile*)

Pseudomonas aeruginosa (*P. aeruginosa*)

vancomycin-resistant *Enterococcus* (VRE)

Klebsiella species (*Klebsiella spp.*)

Enterococcus species (*Enterococcus spp.*)

Acinetobacter species (*Acinetobacter spp.*)

Aerosol-assisted chemical vapor deposition (AACVD)

1H, 1H, 2H, 2H-perfluorooctyltriethoxysilane (PFOTES)

Titanium dioxide (TiO$_2$)

Polystyrene A (PSA)

Polystyrene B (PSB)

Polyurethane (PU)

Polydimethylsiloxane (PDMS)

Brain-heart-infusion (BHI)

Carbapenem-nonsusceptible and extended-spectrum cephalosporin-resistant *Escherichia coli* (CRE)

Deionized water (DI water)

Phosphate buffered saline (PBS)

Scanning electron microscopy (SEM)

Atomic force microscopy (AFM)

Contact angle hysteresis (CAH)

Colony forming unit (CFU)

Toluidine blue O (TBO)

Methylene blue (MB)

Crystal violet (CV)

Light activated bactericidal agents (LABAs)

Reactive oxygen species (ROS)

Silver (Ag)

Gold (Au)

Graphene oxide (GO)

Zinc oxide (ZnO)

Titanium dioxide (TiO_2)

Transmission electron microscopy (TEM)

Dispersive X-ray spectroscopy (EDS)

Ultraviolet and Visible (UV/Vis)

Mixtures of Au and Ag nanoparticles (Mix Ag/Au NPs)

Nanoparticles (NPs)

Occupational Safety and Health Administration (OSHA)

Singlet oxygen ($^1O_2$)

Triplet oxygen ($^3O_2$)

Superoxide anion ($O_2^{-\bullet}$)

Hydrogen peroxide (H_2O_2),

Food and Drug Administration in US (FDA)

Polytetrafluoroethylene (PTFE)

Water contact angle (WCA)

Hydroxly radicals ($\bullet OH$)

Perfluorinated chemicals (PFOs)

Perfluorooctanoic acid (PFOA)

Perfluorooctane sulfonate (PFOS)

Perfluorobutane sulfonate (PFBS)

Perfluorodecanoic acid (PFDA)

International Agency for Research on Cancer (IARC)

US Food & Drug Administration (FDA)

Thesis Purpose and Structure

Purpose

The aim of this thesis was to developing white light-activated bactericidal surfaces incorporated with nanoparticles, toluidine blue O, crystal violet, and polymers, and to investigate their potential as bactericidal and anti-biofouling surface treatments. The ultimate purpose is to make antimicrobial surfaces which show bactericidal and anti-biofouling properties for inhibiting the spread of healthcare-associated infections in hospitals.

Structure

Chapter 1 details current issues caused by healthcare-associated infections (HAIs), the pathogens role in HAIs spread, current scheme in hospitals to prevent HAIs, and development and function of antimicrobial surfaces including bactericidal and/or anti-biofouling surfaces. In Chapter 2, anti-biofouling property of superhydrophobic surfaces was investigated over a long period of time. In Chapter 3, the effect of silver nanoparticles on photobactericidal activity of toluidine blue O incorporated polyurethane was investigated. In Chapter 4, photobactericidal paint made from combination of crystal violet and acrylic latex was used to kill bacteria under the real world conditions. Chapter 5, dual functional surfaces with superhydrophobic and photobactericidal properties produced by chemical and physical combination of 1H, 1H, 2H, 2H-perfluorooctyltriethoxysilane, TiO_2 nanoparticles, crystal violet, and toluidine blue O was investigated. The final chapter details conclusions from the studies conducted in this thesis and suggestion for future research.

Chapter 1: Introduction

1.1 Healthcare-associated infections

Healthcare-associated infections (HAIs), which are also known as nosocomial infections, are the infections obtained as a consequence of a patient's treatment by doctors, nurses and other healthcare workers[1-3]. Hospitalized elderly, babies, and people with weakened immune system are at a high risk of HAIs[4]. HAIs produce a variety of symptoms in patients from minor pain to long term or permanent disability, and even patient death in some cases[4,5].
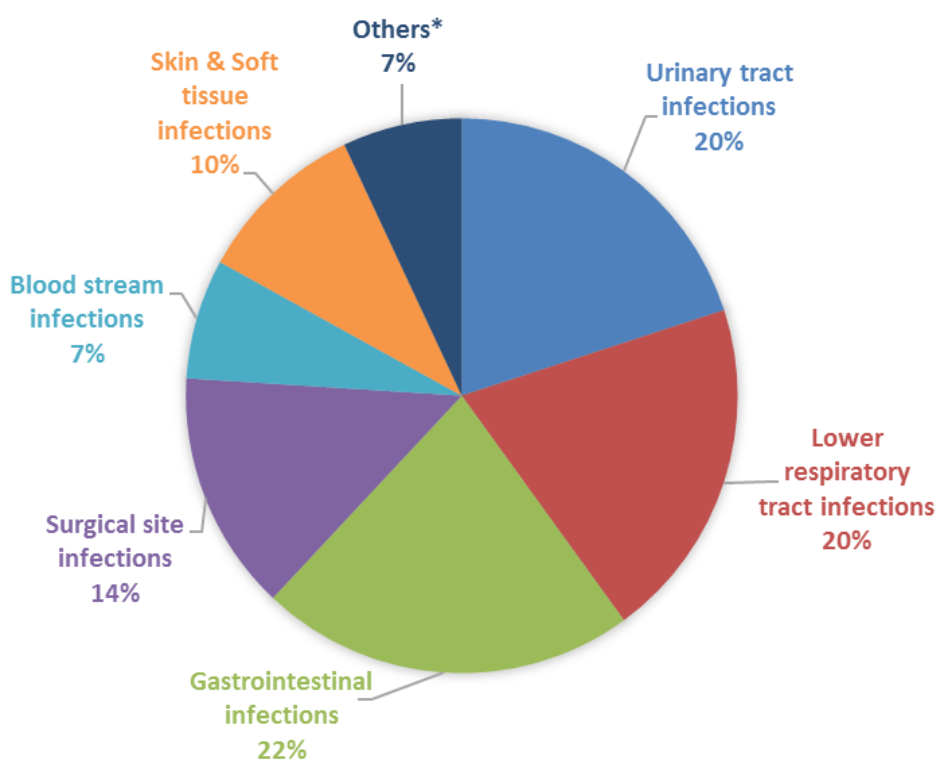
Fig.1.1 Type of HAIs in hospitals in England
*Others: infections of bone, nervous system, and joints

According to prevalence surveys of HAIs in acute hospitals in England[4,5], 8% of patients in hospitals had HAIs and among them, 9,000 people were killed from the infection. The main HAIs are urinary tract infections, lower respiratory tract infections, gastrointestinal, surgical site infections, blood stream infections, skin and

soft tissue infections (Figure 1.1)[4,5]. The majority of HAIs are caused by bacteria

and there are various bacteria producing different types of HAIs[4].

1.1.1 Hospital pathogen

Since the discovery of antibiotics in 1930, common sicknesses produced by bacterial

infection have become curable with antibiotics and they have made an important

contribution to public health[6]. However, after several decades, as bacteria have

evolved to protect themselves from antibiotics, antibiotic treatment to control

infections became futile[7]. As a result, the infections by antibiotic resistant bacteria

have become one of the key issues in hospitals[4]. Since 2004, The National Health

Service (NHS) has been conducting various schemes relating to legislation,

mandatory surveillance, inspection, and disinfection[4,8,9]. In particular, significant

endeavour was devoted to prevention of HAIs caused by methicillin sensitive

Staphylococcus aureus (MSSA), Methicillin resistant *Staphylococcus aureus*

(MRSA), *Escherichia coli* (*E. coli*), and *Clostridium difficile* (*C. difficile*)[8].

1.1.1.1 Methicillin resistance *Staphylococcus aureus*

MRSA is a Gram-positive bacterium and it genetically differs from other

Staphylococcus aureus strains[10]. It is difficult to treat patients infected by MRSA

because it is multi-drug resistant: MRSA has resistance to methicillin, oxacillin,

penicillin, and cephalosporins[10]. In 1961, the methicillin resistant bacteria were

identified and since 1990s, it has been endemic in hospitals[11-13]. MRSA is well

known HAI pathogen. It is responsible for 4 % of blood stream infection[4]. Although

its infection rate was relatively low, 1,517 patients were killed by MRSA infection

in England in 2007[2,14]. Due to its fatality and resistance to antibiotics, it has been

classified into mandatory surveillance category of pathogens in the NHS since 2005[4,8,15].

1.1.1.2 Methicillin sensitive *Staphylococcus aureus*

MSSA is also a Gram positive coccus[16]. It is found in the nose, skin, and respiratory tract of around one third of people[17]. Although MSSA is normally harmless to human health, it can produce an infection when the bacteria enter the human body with compromised immune system such as abscess, respiratory infections, boils, and it can cause an infection on skin breaks from surgical treatment and grazes[4,18,19]. It can produce septicaemia which is a life threatening blood poisoning when it gets into bloodstream[4]. In hospitals, MSSA is associated with lower respiratory infections, tissue infections, bloodstream and surgical site infections[4]. Since 2011, it has been classified into mandatory surveillance pathogen in NHS because of high infection rate of it[8,20].

1.1.1.3 *Escherichia coli*

E. coli is a Gram-negative bacterium and has a rod like shape[21]. *E. coli* is found in food, and the intestine of human, cattle, sheep, and other animals[22]. It has various groups and most of them is not harmful to human health. However, some of them can be pathogenic producing urinary tract infections, blood stream infections, respiratory illness, diarrhea, and fever[22,23]. It can cause the death to senior patients and young children (< 5 year), patients with weakened immune system[24,25]. *E. coli* was added to Public Health England mandatory surveillance scheme in 2011[8].

1.1.1.4 *Clostridium difficile*

C. difficile is a Gram-positive bacterium with rod like shaped[26]. It is difficult to treat *C. difficile* infection because of its antibiotic resistance and spore forming property[27]. *C. difficile* is resistant to fluoroquinolone antibiotic such as levofloxacin and ciprofloxacin[28]. *C. difficile* initiates sporulation process producing dormant spores when it is exposed to environmental stimuli including starvation, quorum sensing and other stresses[29]. The spores are responsible for the spread of *C. difficile* infections in hospitals[29] and they are resistant to widely used chemicals (ethanol, butanol, chloroform and sodium hypochlorite) to disinfection and sanitization for hospital surfaces[30]. *C. difficile* produces a variety of symptoms including diarrhoea, fever, weight loss, and dehydration[31]. According to the NHS surveys of HAIs[4], 70 % of gastrointestinal infections in hospitals was caused by *C. difficile*, and 7,916 patients were killed by *C. difficile* infection in 2007[4]. For these reasons, *C. difficile* was included in Public Health England mandatory surveillance scheme in 2004[8].

1.1.1.5 *Pseudomonas aeruginosa*

P. aeruginosa is Gram-negative and rod-shaped bacterium[32]. *P. aeruginosa* is multi-antibiotic resistant including fosfomycin, levofloxacin, ceftazidime piperacillin, imipenem, piperacillin, and tobramycin[33]. The bacterium is a dangerous pathogen and it is one of major causes of severe HAIs in England[5]. *P. aeruginosa* infections mainly occur in surgical sites within hospitals[5]. Surgical site infection, pneumonia and blood infections by the bacteria can cause a severe illnesses or patient's death in some cases[5]. The bacteria were included in extended NHS surveillance of pathogens in 2017[34].

1.1.2 Current scheme to reduce the number of HAIs

In 2000, The National Audit Office published a report about concerns of the management and control of HAIs[35], and a report from the House of Common committee of Public Account in 2004/05 brought attention to the fact that the progress of HAIs reduction was patchy and there was a lack of urgency for incidents of HAIs infection[36]. Since then, the Department of Health has instigated/initiated vigorous schemes including mandatory surveillance, legislation, inspection and advice on infection management and prevention in order to decrease the number of infection[4,8,9].

Mandatory surveillance: The output of mandatory surveillance is to investigate progress to control key HAIs and offers epidemiological evidence[8]. The surveillance contains patients details such as associated care details, sex, admission data, NHS number, date birth, hospital number and others[8]. All information of the cases is collected and analysed by the Trusts through real-time surveillance system which was named after the "Healthcare Associated Infection Data Capture System"[8]. Since April 2004, it has been mandatory that NHS acute Trusts report all of MRSA and *C. difficile* cases, and *E. coli* and MSSA have was included a mandatory surveillance pathogen since 2011[8,20].

Legislation: To strengthen HAI control, the health and Social Care Act 2008 was legislated[9]. It is applied to the healthcare provider and it shows not only how to comply with the infection inhibition requirement which is in regulations but also how to keep high levels of infection inhibition[9]. Healthcare providers do not need to comply with the regulation guide to prevent HAIs, but they must meet the

regulations in other way[9].

Inspection: All NHS trusts have an annually health check by the Healthcare commission[9]. The trusts are assessed on the basis of Core Standard which is related to HAI prevention and control[4,9]. They were assessed in terms of national target of HAI[4,9]. With Health and Social Care Act 2008, the inspection of HAIs was strengthen and trusts which failed to stick to the Code of Practice was fined[4,9].

Advice on infection management and prevention: Health Protection Agency and its regional Protection Units have a responsible for advising and supporting the NHS and other healthcare facilities to reduce HAIs[4,37]. They help healthcare facilities to identify, manage, and minimize the HAI related risk[4,37].

Other schemes: Since 2004, healthcare worker training has been revised on infection and control practice[4]. Currently, it is a mandatory training along with fire, health, and safety training[4]. The relationship between hand hygiene and infection rate has been acknowledged since 2000[4]. National Patient Safety Agency and Trusts have taken on campaigns of hand hygiene to reduce the number of HAIs[4].

Since 2004, the effort to reduce the number of HAIs has had some achievement. In hospital, MRSA bloodstream infection dropped by 40%, the number of MRSA case fell by 65% in 2008, and the number of *C. difficile* was reduced by 50%[4]. According to annual epidemiological commentary[15,20,38,39], although the numbers of MRSA and C. *difficile* in hospitals has decreased since 2008, the reduction rate is low, and in contrast with that of MRSA and C. *difficile,* the number of MSSA and *E. coli* have increased[4,15].

1.1.3 The role of hospital surfaces in the prevalence of hospital-associated infection

In the past, hospital surfaces had been considered to have negligible contribution to the spread of hospital pathogens[40]. However, recent research has showed that surfaces contaminated by bacteria have a significant contribution to the prevalence of pathogen which can cause HAIs[40-43]. Hospital surfaces in the vicinity of infected patients have more chance to be contaminated than other surfaces in hospitals, and small number of pathogens (such as *C. difficile* spores) may be able to initiate HAIs[44-46]. Previous study reported that some pathogens are able to survive on hospital surfaces including intensive care units, and surgical wards over a long period of time[46]. As shown in Table 1.1, *Klebsiella species (Klebsiella spp.)*, *S. aureus*, *Enterococcus species* (*Enterococcus spp.*)*,* and *P. aeruginosa* had an ability to survive on dry inanimate surfaces for more than 1 year[40,47], and in particular, vancomycin-resistant *Enterococcus* (VRE) showed a remarkable survivability in that it kept its viability on surfaces for more than 4 years[48]. Although it was clearly unknown how the bacteria can survive on the hospital surfaces over a long period of time, it was reported that some bacteria are able to survive on surfaces without any nutrient source[49,50].

Table 1.1 Survival period of pathogens related to HAIs on dry inanimate surfaces.

Bacteria	Survival period
Klebsiella spp.	more than 30 months
Acinetobacter spp.	11 months
Staphylococcus aureus (containing MRSA)	More than 12 months
Clostridium difficile	More than 5 months
Enterococcus spp. (*containing* VRE)	More than 46 months
Pseudomonas aeruginsosa	16 months

When hospital surfaces including catheters, keyboards, ward beds, and other medical devices are contaminated by bacteria, they can accelerate the spread of pathogens between patients and healthcare workers. As shown in Figure 1.2, the bacteria contaminated surfaces in hospitals can act as pathogen reservoirs contributing to pathogen transmission *via* touch by workers and patients. Once hospital surfaces are contaminated, a cyclic issue is produced because the pathogens can be transmitted to other surface or patients or healthcare worker in the vicinity of it[51]. Washing hands of healthcare workers may control pathogen spread to some extent, but it is not possible to prevent the surface contamination nor pathogen transfer by patients resulting in the transmission cycle remaining. For these reasons, surface cleaning and /or disinfection have been commonly conducted to be sure that a hospital surface is appropriately disinfected and safe for patients[52]. Many researches have been conducted to determine the efficiency of cleaning and disinfection. Previous research has reported that after cleaning/disinfection, the surface was often contaminated by the pathogen, and even multiple repetition of disinfection was not enough to remove pathogen on surfaces[53-55]: for instance, 27%

of surfaces in rooms were still contaminated by MRSA or *Acinetobacter baumannii* after cleaning 4 times using disinfectant[54].
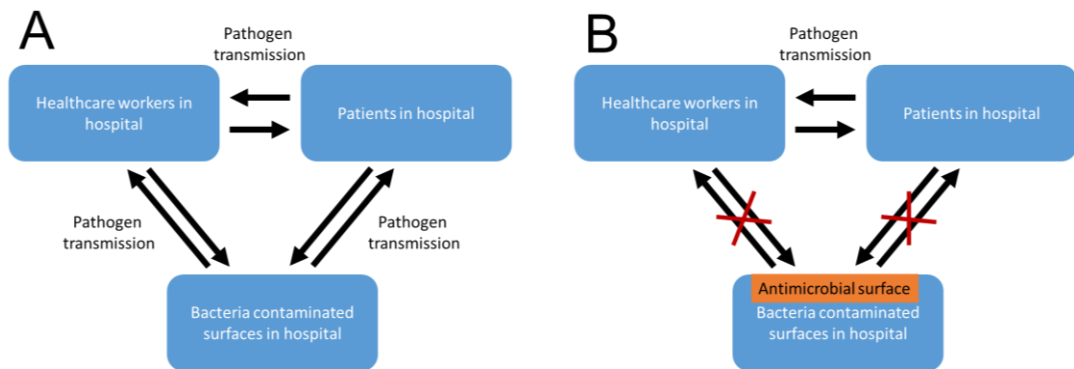
Fig. 1.2 Role of (a) hospital surface or (b) antimicrobial surface on the transmission of HAIs[51]

To address the problem of HAIs, techniques that can prevent bacterial contamination of surfaces are necessary. The development of antimicrobial surfaces can make a significant contribution to inhibit the contamination resulting in the address of the cyclic issue. The antimicrobial surface could significantly decrease the contamination on hospital surfaces without any external interventions, and it could enhance hospital hygiene[51]. Through prevention of the surface contamination in hospitals, it is possible to destroy the cycle of pathogen transmission[51]. As a result, the issue would be left into person to person transmission in hospitals which can be solved by proper washings and disinfection on hands of healthcare workers and patients[51].

1.2 Antibacterial surface

Since the first recognition on bacterial attachment and reproduction on surfaces in 1930s, many studies have been extensively performed to reduce bacteria attachment

or biofilm formation on surfaces[56,57]. As a promising strategy, antibacterial surfaces have been studied for several decades. Antibacterial surfaces imply that it is resistant to bacteria attachment by causing bacterial death in contact with surfaces indicating bactericidal effect or representing anti-biofouling activities[58-60]. In this section, a variety of techniques is detailed in terms of anti-biofouling and bactericidal surfaces.

1.2.1 Anti-biofouling surface

Anti-biofouling surface is a surface that resists bacterial attachment because of its unfavourable surface structure or chemical substance to bacteria[57].

1.2.1.1 Superhydrophobic surface

Water droplet contact angle is the measured angle where the liquid-vapor interface meets a solid surface. If the angle is higher than 90 °, the surface is considered hydrophobic, and if the angle is smaller than 90°, it is considered hydrophilic (Figure 1.3)[61].
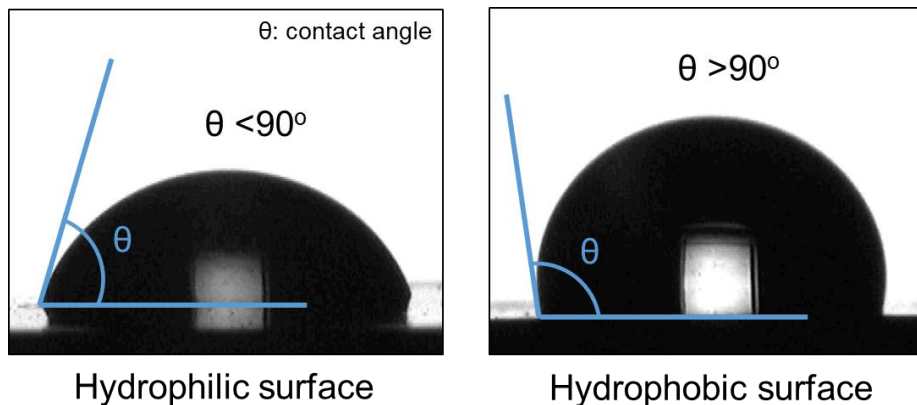
Fig. 1.3 Water droplet contact angle of hydrophilic and hydrophobic surfaces

Rolling off angle is the inclination angle of the surface where a water droplet rolls

off. Contact angle hysteresis is defined as the difference of advancing angle (water injection) and receding angle (water withdrawal) (Figure 1.4)[61].
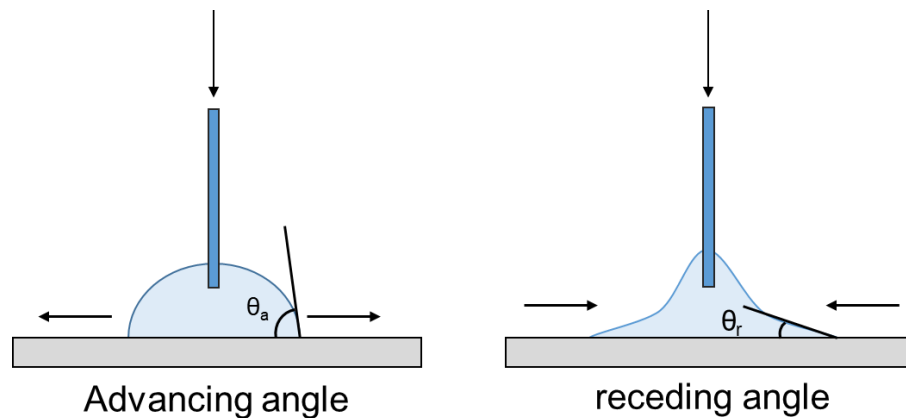
Fig. 1.4 Contact angle hysteresis: difference of advancing angle and receding angles

Superhydrophobic surface is a surface which is extremely difficult to wet and it has high water contact angle (>150°), low rolling off angle (<5 °) and contact angle hysteresis (<5 °)[62,63]. The superhydrophobic surface resulting from a rough surface structure with low surface energy[64]. In nature, butterfly and Cicada wings, Taro and Lotus leaves exhibited superhydrophobic and self-cleaning properties[65-67]. When the natural surfaces were immersed in water, it is resistant to bacteria biofouling[68]. Due to anti-biofouling property of superhydrophobic surface, man-made superhydrophobic surfaces were produced in an effort of decreasing biofouling, and they were tested at various settings[65,68-70]. In previous studies, it was observed that polydimethylsiloxane (PDMS) based or elastomeric superhydrophobic surface had a reduced bacteria adhesion of 50–80%, compared to intact glass, and bacteria adhesion on silica colloid coated surface which is a superhydrophobic surface was >98% lower than the surface without the colloid[65,68,71]. Additionally, superhydrophobic polystyrene, polycarbonate, and polyethylene exhibited low bacteria adhesion and a good removal efficiency[69]. Although the exact mechanism

of the property was not clearly explained, several ideas were suggested. Ivanova *et al* proposed that the reduction was mainly due to the morphological difference while other studies proposed that the air-bubbles entrapped on a superhydrophobic surface, which is in Cassie-Baxter state, prevent bacterial adhesion because it is difficult for bacteria to penetrate the water/air interface[60,68].

1.2.1.2 Lubricant surface

Lubricant surface, which is also called a slippery surface, was introduced by the Aizenberg group in Harvard university[72,73]. Lubricant surface was inspired from pitcher plants which use their leaves to make insects slide off and entrap them in a cavity and is resistant to water, blood, and oil[72,74]. The surface is produce through coating of lubricant fluid (silicone oil) on the superhydrophobic or porous surfaces: when the rough surface was exposed to silicone oil, it penetrated into the surface and formed a lubricant layer on the surface[75,76]. The lubricant layer is stable, immobilized and extremely slippery[74,75,77]. The surface has a sliding of a water droplet at 60 º tilted angle, and resists external force[75,78]. Recently, anti-biofouling property of the lubricant surface was reported[73,79-81]. Aizenberg group showed that after 7 days of bacteria exposure, the lubricant surface had 96-99.6 % less attachment of *P. aeruginosa, E. coli* and *S. aureus,* compared to a polytetrafluoroethylene (PTFE) surface[73], and the surface is much less adhesive on green microalgae containing *Chlamydomonas reinhardtii*, *Dunaliella salina, Botryococcus braunii*, and *Nannochloropsis oculata* than glass and PDMS treated surfaces[81].

1.2.1.3 Graphene treated surface

Graphene is a form of carbon molecules, and it is a single layer of carbon atom with a hexagonal lattice[82]. In 2004, the material was discovered, and characterized by Adre Geim[83,84] and it has been actively studied because of mechanical, optical, and electronical novelties[85-87]. In recent years, a few researches reported anti-biofouling properties of graphene coated surfaces[88,89]. Previous study has showed that graphene coated surface has less biofilm formation compared to *Halomonas spp*[89]. Although the anti-biofouling mechanism of graphene treated surface was not clearly explained, it is speculated that surface energy modification from hydrophilic to hydrophobic and electrostatic interaction (repulsive force by the negatively charged surface) with bacterial cells cause a reduction on biofilm formation[89].

1.2.2 Bactericidal surface

Bactericidal surface is the surface that kills bacteria in contact through largely a chemical reaction[57].

1.2.2.1 Silver treated surface

For several centuries, silver has been known and used for antibacterial materials[90-92]. Silver was used for treatment of burn and silver vessels were used for making water potable[91,92]. More recently, silver nitrate was used for medical purpose to deal with various diseases including venereal infection, bone and perianal diseases, fistulae, and eye disease[93,94]. The accurate mechanism of bactericidal behaviour of silver against bacteria is still unknown but silver ions play an important role to disinfect bacteria[6]. When silver ions penetrate inside of a bacterial cell, the ions

make bacteria lose their ability for DNA replication, and ultimately leads to bacterial death[95,96]. Because silver represented good bactericidal activity against various bacteria strains, the metallic substance was applied to medical devices, medical dressing, and textile fabrics[97-101]. In previous studies, it was shown that the treatment of silver nanoparticles into polymeric medical device and surgical masks enhanced their bactericidal efficiency, and dressing cream containing silver and sulfonamide exhibited a broad spectrum of antibiotic behaviour and was utilized for treatment of burns[97,98]. Moreover, it was shown that silver nanoparticles coated fabrics or air/water filters represented strong bactericidal activities against bacteria[102,103]. Although many studies suggested that silver is non-toxic, it has been considered that large quantity use of silver nanoparticles can be hazardous to the environment and human health[104].

1.2.2.2 Copper treated surface

Copper has been used as a bactericidal substance for centuries. Ancient Greeks used copper to treat pulmonary diseases and to purify water[105]. Copper and its alloys not only exhibited antibacterial activities but also showed antiviral, antifungal and molluscicidal activities[105]. Copper has been considered as a promising and novel bactericidal materials because it has strong antimicrobial activity against a range of microorganisms including anti-biotic resistant organisms, and the copper is cheaper and more readily available than silver[105,106]. In previous studies, copper treated surface showed antimicrobial activity against *E. coli* O157, MRSA, *C. difficile* and influenza virus which are key hospital pathogens, and tests of stainless steel and copper coupons showed that *C. difficile* were completely killed on a

31

copper coupon within 48 h whereas viability of the bacteria did not change on a stainless steel coupon[107-110]. Moreover, Sehmi *et al.* (2015) showed that after copper nanoparticles are encapsulaed into polyurethane and silicone, the polymers showed very potent bactericidal activity[111]. It was speculated that the bactericidal mechanism of copper is similar to that of silver. Firstly, copper ions disturb biochemical process after penetration inside bacterial cells resulting in cell death [106]. Secondly, copper interacts with the cell wall and it produces bacterial membrane damage with an increase of permeability resulting in bacterial viability reduction [106].

1.2.2.3 Graphene oxide treated surface

Graphene oxide (GO) is a single monolayer of graphite with oxygens[112-114]. GO is synthesized by chemical oxidation of graphite and then followed by exfoliation through ultrasonication[114]. Because of its stability and low cost in production, it is considered as a promising material in various fields such as a precursor and a building material[114,115]. In recent years, many studies reported that GO exhibited strong bactericidal activities against a range of microorganisms including *S. aureus, Pseudomonas* syringae*, Xanthomonas campestris, E. coli,* and *Cupriavidus metallidurans*[116-120]. It is considered that when a GO sheet is in direct contact with a bacterial cell, it produces chemical/physical interactions resulting in membrane damage and then cell death. The membrane damage could be produced by atomically sharp edges of GO that could pierce the membrane, and the damage may occur through lipid peroxidation induced by the oxidative character of GO[116,121,122]. Due to its bactericidal actions, various bactericidal surfaces based on graphene oxide such as stainless steel,

polymer film, cotton fabric and water treatment membrane were produced and studied[119,123-125].

1.2.2.4 Light activated bactericidal surface

Recently, light-activated bactericidal agents have become a new emerging strategy to disinfect bacteria. Even though the bactericidal activity of the agents were reported in early 1900s, because of the wide spread development of antibiotics, and their potential for use in hospitals, the potential of light activated agents were not extensively studied[126-130]. However, with the spread of drug-resistant bacteria, light activated bactericidal agents have gained significant attention as a promising alternative because they have different bacterial kill mechanisms to antibiotics.

1.2.2.4.1 Titanium dioxide treated surface

Titanium dioxide (TiO_2), which is also called titania or titanium oxide, is a photocatalytic material[131]. The photobactericidal activity of TiO_2 was reported for the first time in 1985, and since then, many studies have been performed to investigate antimicrobial activities against bacteria, viruses, and fungi[132-137]. As shown in Figure 1.5, the antimicrobial mechanism of TiO_2 is widely known[138,139]. TiO_2 is considered as a n-type semiconductor indicating that electrons are the major carrier and that it has larger electron concentration than hole concentration[83,140]. When TiO_2 is exposed to ultraviolet (UV) irradiation, it establishes a redox environment[141]. TiO_2 acts as sterilizer due to light induced redox process. TiO_2 has a unique electronic structure that is characterized by an electron empty conduction band and an electron filled valance band. TiO_2 has a band gap energy of 3.0 to 3.2

eV indicating energy difference between conduction band and valance band[141]. During UV irradiation, TiO_2 absorbs UV photons and an electron is excited the conduction band from the valance band, resulting in production of an electron hole pair[141]. At the TiO_2 surface, the free electron (e⁻) and hole (h+) created reactions between photoexcited TiO_2 and H_2O, oxygen, and hydroxide groups on the surface, resulting in hydroxyl radicals, singlet oxygens and superoxide anions (equation 1-1 to 1-5)[138,139].

$$TiO_2 + hv \rightarrow e^- + h^+ \qquad (1-1)$$

$$h^+ + H_2O \rightarrow HO^\bullet + H^+ \qquad (1-2)$$

$$h^+ + OH^- \rightarrow OH^\bullet \qquad (1-3)$$

$$e^- + O_2 \rightarrow O_2^{\bullet-} \qquad (1-4)$$

$$2O_2^{\bullet-} + 2H_2O \rightarrow 2HO^\bullet + 2OH^- + O_2 \qquad (1-5)$$
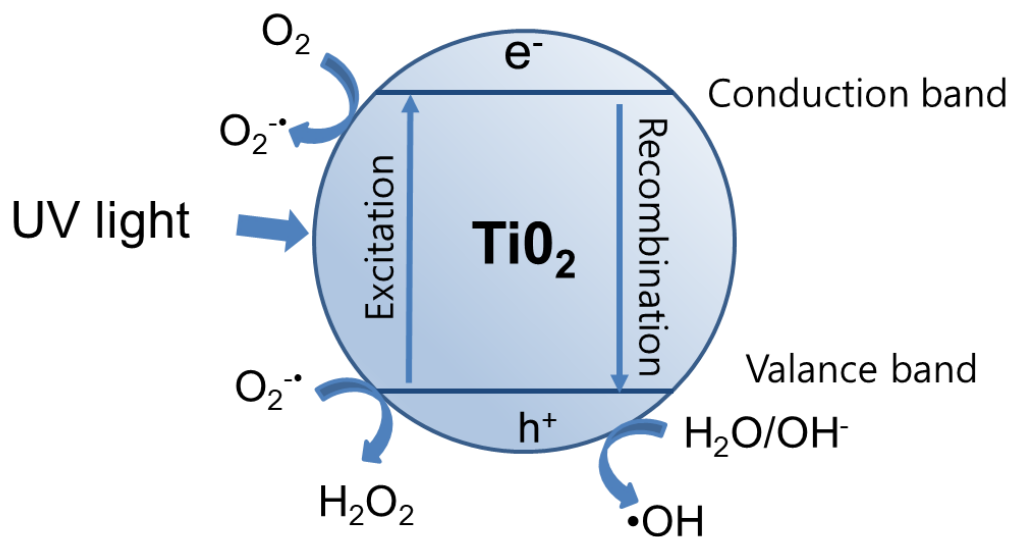
Fig. 1.5 Photoreaction process of TiO_2

These are a very potent radical with ability to kill various microorganisms. One

drawback of this material is that it is activated by UV light only because excitation of TiO$_2$ requires radiation with a wavelength of <400 nm [141]. Thus, its bactericidal activity is weakened under indoor lighting which mainly use visible light sources.

1.2.2.4.2 Zinc oxide treated surface

Zinc oxide (ZnO) materials have had broad attention because of their electronic and optical properties[142]. Since the 1960s, synthesis and application of ZnO particles were extensively studied in terms of sensors, catalysts, and transducers, and bactericides[143]. ZnO has been known as a bactericidal substance and it is classified as "generally recognized as safe" by the U.S. Food and Drug Administration (FDA), and it has been widely used as a food additive such as food cans, and packages of meat, corn, and pea in order to prevent contaminations[144]. Although several ideas on bactericidal mechanism of ZnO was suggested, exact toxic mechanism was not completely explained, and is still controversial[145]. It was reported that bactericidal activity of ZnO is dependent on size and concentration because small size (<100 nm) has high surface to volume ratio of ZnO resulting in higher interaction with bacteria[144]. The material has been known to have a wide range of bactericidal behaviour against Gram-negative and -positive bacteria such as *E. coli*, *Salmonella*, *Listeria monocytogenes*, and *S.* aureus[146]. It was mainly believed that the bactericidal mechanism of zinc oxide occurs in two ways: I) through photoreaction induced by UV or visible light, generation of reactive oxygen species (ROS) containing hydroxyl radical (•OH), superoxide anion ($O_2^{-\bullet}$), hydrogen peroxide (H$_2$O$_2$), and singlet oxygen (^{1}O$_2$); II) interaction between zinc oxide particles and bacteria cell resulting in disturbance of cellular activity and

bacterial death[147].

ZnO is considered as n-type semiconductor[148]. ZnO has an electron empty conduction band and an electron filled valance band, and it has a band gap energy of 3.2 eV which is similar to TiO_2[141,148]. The photocatalytic mechanism of ZnO to produce ROS is similar to that of TiO_2. Upon light irradiation, ZnO absorbs the photon, and it is excited resulting in free electrons (e^-) in the conduction band and holes ($h+$) in the valance band are created and, the pair in interaction with water or bacteria produces hydroxyl radical ($\bullet OH$) superoxide anion ($O_2^{-\bullet}$), hydrogen peroxide (H_2O_2), and singlet oxygen ($^1O_2$) [145].

1.2.2.4.3 Light-activated bactericidal dye treated surface

Crystal violet, rose bengal, toluidine blue O, and methylene blue which have been historically for biological and surgical stains, and disinfections of wounds, were known to have light-activated bactericidal properties which are photoexcited by a visible light source (Figure 1.6) [149-151]. As shown Figure 1.7, when the dyes are exposed to a light source, they absorb photons from the light. The photon absorbed dye molecules transform from a ground state to an excited single state (paired electron spin)[152-154]. Depending on the environmental or molecular condition, they lose energy resulting in return to the ground state or they transform to a triplet state (unpaired electron spin) from an excited single state[152-154].

The molecules in a triplet state undergo two chemical reactions indicating photochemical reaction I and II[152,153]. In photochemical reaction I, they undergo redox reaction through interaction with the environment, resulting in generation of reactive oxygen species, and in photochemical reaction II, the molecular energy at a

triplet state is transferred triplet oxygen ($^3O_2$), resulting in production of singlet oxygen ($^1O_2$).
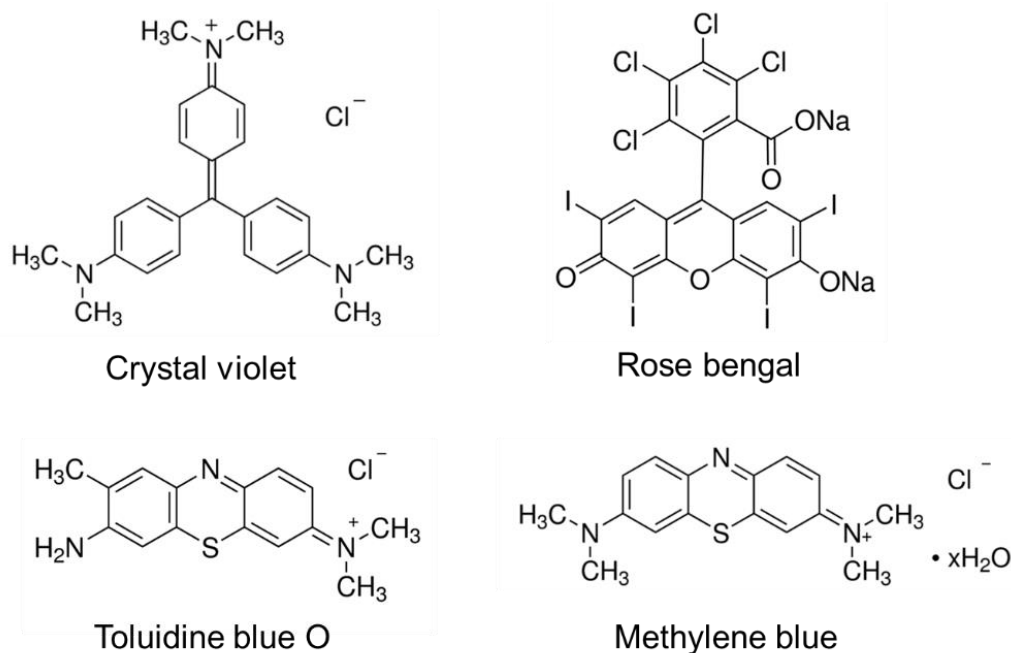
Fig1.6 Chemical structure of crystal violet, rose bengal toluidine blue O, and methylene blue

The generated reactive oxygen species (ROS) cause bacterial death through two different mechanism[152-154]. First, the oxygen species cause damage to the cytoplasmic membrane of the cell, resulting in a leakage of internal contents or inactivation of enzymes and membrane transport systems. Second, they break single or double stranded DNA of bacteria[152-155].

Because of their potent photobactericidal activity and ease in use, the light activated bactericidal dyes were used to treat infection of blood products, oral infections, and viral infection, and it was reported that they were effective to disinfect drug resistant bacteria, viruses, parasites, and yeasts[152].
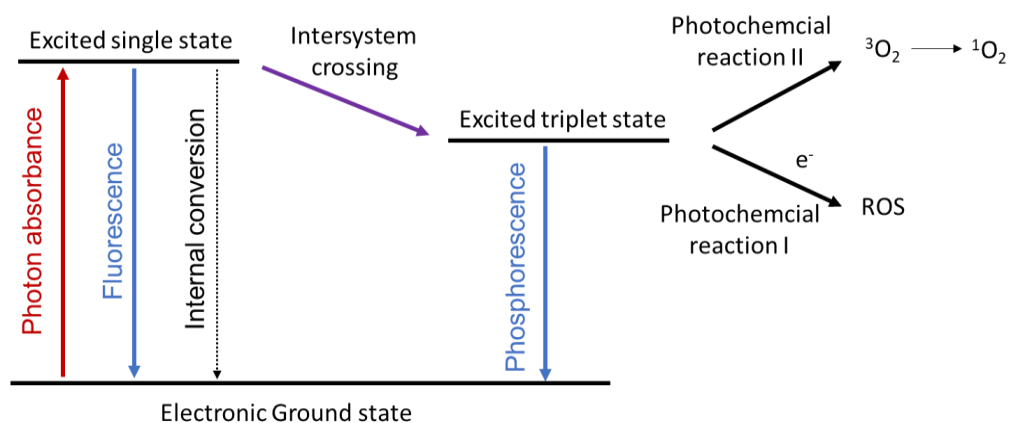
Fig.1.7 Jablonksi diagram showing photochemical reaction process of the light-activated bactericidal agent after light exposure

In recent years, various studies on surface application of the light activated bactericidal agents containing crystal violet, toluidine blue O, and methylene blue were actively performed in the Parkin group[156-160]. They showed that through a simple swell-encapsulated shrink process, silicone and polyurethane which are widely used in catheter, keyboard cover, and other hospital devices, can be easily transformed into photobactericidal materials, and additional encapsulation of nanoparticles such as gold, and zinc oxide nanoparticles into the polymer containing the dye significantly enhance photobactericidal activities against *E. coli*, *S. aureus*, and MRSA which are representative hospital pathogens[156-161].

In the next chapter, superhydrophobic surfaces, which are widely known anti-biofouling materials, were tested over a long period of time and compared to other surfaces in order to determine their applicability in the real world.

Chapter 2: Short-lived anti-biofouling properties of superhydrophobic surfaces and their transformation into a bacterial reservoir

2.1. Introduction

Healthcare-associated infections (HAIs) produced by a range of bacteria have been a serious problem in hospitals because it causes discomfort or long-term and permanent disability to patients and even it produces patients' death in some cases, and annually, it costs National Health Service £14 million to treat the infected patients and to prevent HAIs[4]. Bacterial biofilms on hospital surfaces act as a reservoir which can make a contribution to the spread of HAI pathogens through touch transmission between patients, doctors, nurses, and other hospital workers[51,162,163].

To prevent biofilm formation on hospital surfaces, various techniques have been proposed in terms of anti-biofouling surfaces and bactericidal surface[57]; anti-

biofouling surface implies preventing bacteria from attaching on the surfaces including carbon treated surface, superhydrophobic surface, lubricant surface[57,71,80,89], and bactericidal surface implies killing bacteria in contact with the surface through chemical mechanism, containing silver or copper doped surfaces, titanium dioxide, and zinc oxide coated surfaces[57,111,164-166].

Superhydrophobic coatings have been considered a promising way to prevent biofilm formation on surfaces because they can dramatically decrease bacteria attachment on surfaces[167-169]. Many researches have tested superhydrophobic surface to investigate its feasibility in a variety of settings; bacteria suspension flown over the surface or surface immersion in bacteria suspension[65,68-71]. Privett *et al.* (2011) demonstrated >98% adhesion reduction of *S. aureus* or *P. Aeruginosa* on silica-colloid-dope substrates, compared to substrates without silica-colloid[68], and Freshauf *et al.* (2012) showed that bacteria adhesion on polystyrene, polyethylene, and polycarbonate based surfaces was lower (bacteria adhesion reduction: about 98%) than other surfaces, and it also showed a good removal efficiency of bacteria from the surface through rinsing (bacteria remains after rinsing: approximately 0.1%)[69]. Crick *et al.* (2011), and Ozkan *et al.* (2016) showed decreased bacterial attachment on superhydrophobic surfaces made by aerosol-assisted chemical vapor deposition (AACVD)[68,71]. However, all of studies above tested the anti-biofouling property of superhydrophobic surface over a short period of time (<4h of bacteria exposure).

In this chapter, anti-biofouling property on superhydrophobic surfaces, which we produced, was tested over a long period of time. Experimental results clearly showed that the air-bubbles entrapped between bumps of superhydrophobic surface in water

significantly decreased the contact area between the surface and bacteria, resulting in a huge reduction in the number of attached bacteria after 1h of bacterial exposure. But, the bubble disappeared with increasing time in water, and after 24h exposure time, bacteria attachment on the surface significantly increased and the number of bacteria attached to superhydrophobic surface was >1.6 times higher than them on glass, polyurethane, and polystyrenes.

2.2. Experimental

2.2.1 Sample surface

Superhydrophobic surface: 1.0 g of 1H, 1H, 2H, 2H-perfluorooctyltriethoxysilane (PFOTES, $C_8F_{13}H_4Si(OCH_2CH_3)_3$, Sigma-Aldrich, St. Louis, MO, USA) and 99.0 g of pure ethanol (EDM Millipore Co., Billerica, MA, USA) were mixed together. TiO_2 nanoparticles (P25, Thermo fisher scientific, Waltham, MA, USA) was dispersed in 40 mL of the mixture, and then it was sonicated for 10 min. Sellotape double sided tape was attached on slide glass, it was dipped in the mixture of PFOTES, ethanol, TiO_2 nanoparticles, and then the treated slide was kept in dark for 24h.

Other sample surfaces: Glass (VWR, PA, USA), polystyrene A and B (PSA, Station Road Baseboards, Norwich, UK) and polyurethane (American Polyfilm Inc, Branford, CT, USA) were purchased. all of samples were prepared in the same size (2.5 cm × 5.5 cm). Additionally, polystyrene A and B have identical chemical composition but their surface roughness is different.

PDMS based superhydrophobic surface: 2 g of Polydimethylsiloxane (PDMS, Midland, MI, Dow Corning, USA) and 2.75 g of silica dioxide (SiO_2) nanoparticles (Sigma-Aldrich, St. Louis, MO, USA) were dispersed in 20 mL hexane (Sigma-Aldrich, St. Louis, MO, USA) under constant agitation. The glass slide was vertically dipped into the mixture for 5 s, the glass was gently withdrawn from the solution, then kept at 100 °C for 2 h, and then allowed to cool to room temperature.

2.2.2 Preparation of bacteria suspension

For this study, carbapenem-nonsusceptible and extended-spectrum cephalosporin-resistant *Escherichia coli* (CRE 1030), *Escherichia coli* (*E. coli* ATCC 25922), methicillin-resistant *Staphylococcus aureus* (MRSA 4742), and *Staphylococcus aureus* (*S. aureus* 8325-4), were used. CRE, *E. coli*, MRSA, and *S. aureus* which were stored in brain-heart-infusion broth (BHI broth, Oxoid Ltd., Hampshire, England, UK) with 20% (v/v) glycerol at –70°C, were propagated on nutrient agars (MacConkey agar for CRE and *E. coli*, and Mannitol salt agar for MRSA and *S. aureus*) (Oxoid Ltd., Hampshire, England, UK). One bacteria colony was inoculated in to10 mL of BHI broth and incubated at 37°C with shaking at 200 rpm.

2.2.3 Experiment of bacterial adhesion

BHI bacteria suspension: bacteria were cultured in BHI broth for 18 h, and then the bacteria suspension was diluted 10-fold by BHI broth to get ~10^8 colony forming units per milliliter (CFU/ mL).

PBS Bacteria suspension: Bacteria were culture in BHI for 18 h, and then they

were collected by centrifugation at 5000 rpm for 10 min. 10 mL of PBS was added into the bacteria, then vortexed for 10 min, and centrifugated again to get bacteria re-suspended in 10 mL of PBS. The bacteria suspension was diluted 10-fold resulting in ~10^8 CFU/mL

Glass, polystyrenes, polyurethane, and superhydrophobic surface were horizontally placed in the bacteria suspension, and kept at 37°C for 1, 4, 8, 16, and 24 h. After that, they were collected from bacteria suspension, washed by deionized (DI) water to get rid of bacteria which are weakly attached to the sample. The washed sample was placed into 0.1 % crystal violet solution for 15 min to stain the bacteria attached to the sample. The stained sample was vigorously washed by DI water twice, placed in 10 mL of pure ethanol, and then vortexed for 5 min to leach out crystal violet molecules from bacteria on the samples to ethanol. After that, the unnecessary residues in the solution was removed through centrifugation at 14,500 rpm for 2 min[73]. The absorption value of the solution at 590 nm was measured by a UV/Vis spectrometer to quantitatively determined the number of attached bacteria.

2.2.4 Measurement of bacteria surface coverage

Bacteria attached sample was stained by 0.1 % crystal violet solution, then it was washed by DI water twice, and dried in a dark room for 24 h. The stained sample was photographed, and the coverage of bacteria on samples were determined by the ImageJ software (http://imagej.nih.gov/ij/): colour threshold was selected, then hue, saturation, and brightness in threshold were manipulated to select bacteria covered area, and followed by selection of measurement in analysis.

2.2.5 Confocal microscopy

Live/Dead BacLight[TM] Bacterial Viability kit (L707; Invitrogen, Carlsbad, CA, USA) was used to determine bacteria attached to the sample. The kit contained SYTO 9, green fluorescent nucleic acid, and propidium iodide, red-fluorescent nucleic acid stain. SYTO 9 generally labels all bacteria including intact and damaged bacteria and propidium iodide stains bacteria with membrane damaged. The excitation/emission wavelengths of two stains are 485/530 nm for SYTO 9 and 490/635 nm for propidium iodide. In order to detect bacteria attached to sample, 3 μL of SYTO 9 was mixed with 1 mL of PBS solution. 1 mL of the fluorescent dye solution was inoculated on bacteria attached samples, and kept in a dark room for 15 min. The attached bacteria were visualized by confocal layer scanning microscopy (Bio-Rad Laboratories, Inc., Hercules, CA, USA).

2.2.6 SEM analysis

In order to determine surface morphology of sample, Scanning Electron Microscopy (SEM, JEOL Inc., Peabody, MA, USA) was employed. To prevent surface charging, the sample was coated by gold crystals for 60 s through sputter coating process, and then the surface morphology was observed by SEM at an accelerating voltage of 5 kV. Images of the sample was taken by SEMAfore software.

2.2.7 AFM analysis

To determined topography and roughness of the sample surface, Atomic force microscopy (AFM, EeasyScan 2 AFM, Nanosurf, Liestal, Switzerland) was employed. For tapping mode, NCLR mode and dynamic force mode was applied,

and the resonant frequent of the cantilever ranged from 150 to 200 kHz. Scanning area of AFM on the surface was about 50 µm × 50 µm.

2.2.8 Water contact angle

Figure 2.1 shows the method used for water contact angle measurement. The equilibrium water contact angle was determined on a test sample using a contact angle meter (First Ten Angstroms, Inc., Portsmouth, Virginia, USA). A water droplet (volume: 5 µL) was inoculated on the sample, its image was captured side on and analysed by Surftens 4.5 software. Manual mode of the software was employed to measure water contact angle.

Additionally, the contact angle hysteresis (CAH) on superhydrophobic surface was determined by an "add and remove volume" method[170]. Advanced and receding angles were measured and then the difference of them was calculated to get CAH.
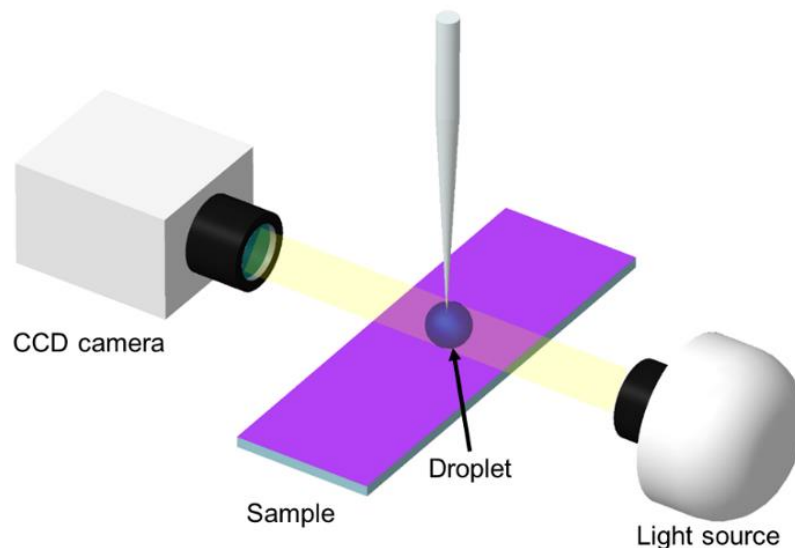
Fig. 2.1 Water contact angle measurement of sample

2.2.9 Measurement of water contact angle across superhydrophobic surface

The measurement of water contact angle across the surface was performed to test if superhydrophobic surface maintains its property after bacteria exposure. As shown in Figure 2.2, the angles were measured after 1, 4, 8, 16, and 24 h bacteria exposure.
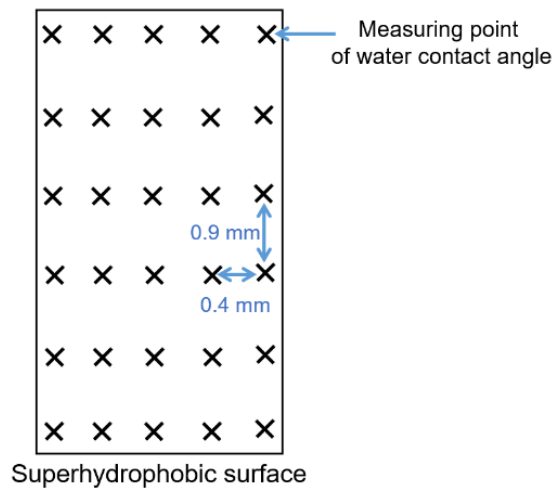
Fig. 2.2 Measurement of water contact angle across superhydrophobic surface

2.2.10 Plastron effect of air bubbles entrapped on superhydrophobic surface

When a superhydrophobic surface, which is in the Cassie-Baxter state, was vertically immersed in DI water and rotated about 49 degree, the surface changed from white into a mirror-like surface. This is called the plastron effect. The plastron effect is produced by light reflection, which is mainly due to air-bubbles entrapped on the surface[171]. The effect on the surface was monitored by Canon camera (Canon Inc. Tokyo, Japan) at intervals of 30 min.

2.2.11 Test of *S. aureus* and *S. aureus* Δ pbp4

S. aureus (strain JE2) and *S. aureus* Δ *pbp4* (transposon mutant NE679) which were stored in BHI broth with 20% (v/v) glycerol at –70ºC were propagated on Mannitol salt agar[172,173]. One bacteria colony was inoculated in to 10 mL of BHI broth and incubated for 18 h. As stated in section 2.2.3 Experiment of bacteria adhesion, BHI and PBS bacteria suspensions were prepared. The number of the bacteria is ~10^8 CFU/mL. Superhydrophobic surface was horizontally immersed in to bacteria suspension for 1 and 24 h at 37 ºC. After that, the sample was removed from bacteria suspension, washed by DI water twice, and then placed into 0.1 % crystal violet solution for 15 min. The stained sample was vigorously washed by DI water twice, placed in 10 ml of pure ethanol, and then vortexed for 5 min to recover crystal violet molecules from the sample. After that, residues of the solution were removed through centrifugation at 14,500 rpm for 2 min. The absorption of the solution at 590 nm was measured by a UV/Vis spectrometer.

2.2.12 Air-bubble layer on superhydrophobic surface

Uniformly structured surface was prepared and it was dipped into superhydrophobic paint (preparation of superhydrophobic paint was stated in Section 2.2.1) for 5 s and then withdrawn gently from the paint. It was dried in a dark room for 24 h. In order to determine air-bubble layer and its durability on a superhydrophobic surface, the coated surface was horizontally immersed in DI water and the air bubble layer entrapped on the surface was photographed side on at intervals of 20 min.

2.2.13 Measurement of remaining bacteria after cleaning process

Sample was horizontally immersed in bacteria suspension and it was incubated for 24 h at 37 °C. It was collected the sample from the suspension, and sample was washed using DI water twice and then dried in a dark room for 3 h. To confirmed remained bacteria on the sample after the cleaning process, gloved finger wiping was conducted across the sample surface. As shown in Figure 2.3, a finger was placed on to the sample and moved forth and back for 5.5 cm and then washed by DI water. It was repeated three time on each sample. After the cleaning process, the sample was immersed in 0.1 % crystal violet solution for 15 min, and then it was washed by DI water twice. The sample was then placed in 10 ml of ethanol solution, vortexed for 5 min, and centrifuged at 14,500 rpm for 2 min. The absorption value of the solution was measured at 590 nm
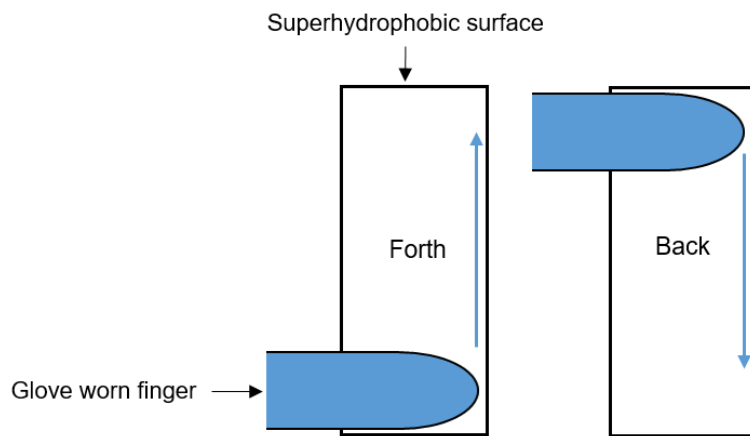
Fig. 2.3 Cleaning process

2.2.14 Statistical analysis

Experimental data were analysed by SPSS (IBM Corporation, Armonk, New York, USA) in terms of Mann–Whitney U test, T-test, and Pearson correlation coefficient.

2.3 Result and discussion

2.3.1 Surface roughness and water contact angle

Commercial glass slide, polyurethane, polystyrene A and polystyrene B were used, and a superhydrophobic surface was made using double sided tape, 1H, 1H, 2H, 2H-perfluorooctyltriethoxysilane, ethanol, and TiO_2 nanoparticles. Prior to the bacteria attachment process, the surface roughness and water contact angle of the test samples was investigated using an AFM and a water angle meter, respectively. Table 2.1 shows the water contact angle and surface roughness of glass slide, polyurethane, polystyrene A and B, superhyhydrophobic surface. The superhydrophobic surface had a water contact angle of 163.3 $^\circ$ with rolling off angle of <1 $^\circ$ and contact angle hysteresis of <1 $^\circ$. Of the samples, the superhydrophobic surface gave the highest water contact angle and surface roughness while the glass slide had the lowest surface roughness and water contact angle; surface roughness: glass slide < polystyrene A < polyurethane < polystyrene B < superhydrophobic surface, water contact angle: glass slide < polystyrene B < polystyrene A < polyurethane < superhydrophobic surface).

2.3.2 Bacteria attachment after 1h exposure in BHI and PBS

In the bacteria adhesion process, five different samples were placed in ~10^8 CFU/mL of bacteria suspension with (in BHI) or without (in PBS) nutrients and incubated for 1 h at 37 $^\circ$C. In order to compare the number of bacteria on the samples, the bacteria attached samples were stained by crystal violet solution, and the stained samples were placed in to ethanol to solubilized the crystal violet in ethanol.

Table 2.1 Surface roughness and water contact angle of glass slide, polyurethane, polystyrene A, polystyrene B, and superhydrophobic surface

Sample	Surface roughness (R_a)	Water contact angle (º)
Glass slide	4.9 ± 0.9 nm	5.7 ± 0.7 º
Polyurethane	182.9 ± 72.6 nm	102 ± 1.1 º
polystyrene A	160.5 ± 26.4 nm	88.9 ± 1.9 º
polystyrene B	436.2 ± 245.1 nm	84.8 ± 2.9 º
superhydrophobic surface	1212.9 ± 323.0 nm	163.3 ± 2.8º
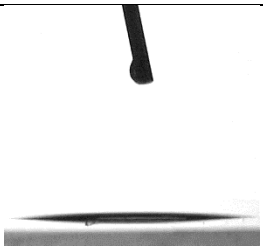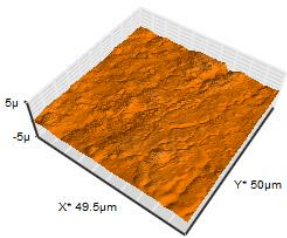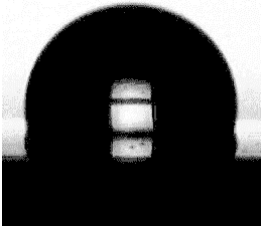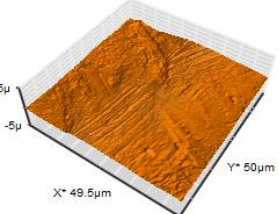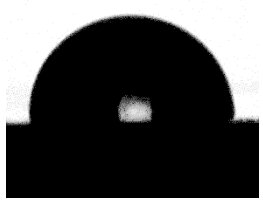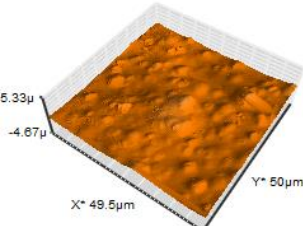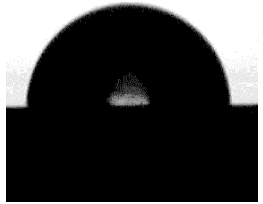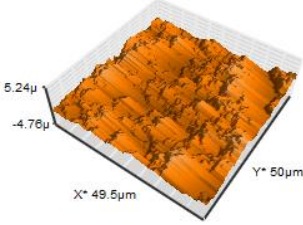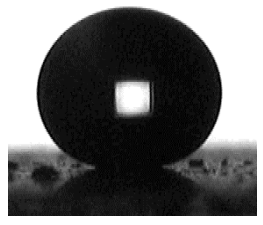
The absorption of crystal violet was measured at a wavelength of 590 nm, and the absorption is proportional to the number of attached bacteria[73,174]. In this chapter, *E. coli*, *S. aureus*, CRE, and MRSA were used. Prior to the bacteria attachment, it was confirmed that intact superhydrophobic surface was not stained by crystal violet solution[175] and that the crystal violet stain against glass slide, polyurethane, and polystyrenes was minor (absorption at 590 nm: <0.01).

Figure 2.4 shows the number of bacteria attached on glass slide, polyurethane, polystyrene A and B, and superhydrophobic surface after 1 h of bacteria exposure. After 1h of bacteria exposure in BHI or PBS, it was observed that the superhydrophobic surface had less bacteria attachment than the glass slide, polyurethane, polystyrene A and B samples (all of bacteria at BHI and PBS: *P*-value <0.5). In the experiment of *S. aureus*, MRSA, *E. coli*, and CRE in BHI, it was confirmed that bacteria adhesion on the superhydrophobic surface was >26% lower than the other surfaces, and the reduction in CRE attachment was about 91% compared with other surfaces. The experiment in PBS showed that bacteria adhesion on the superhydrophobic surface was >35% lower, compared to other samples, and the adhesion difference of the superhydrophobic surfaces and other surfaces containing glass slide, polyurethane, polystyrene A and B was the highest on *S. aureus* (69–82% less than the other samples).
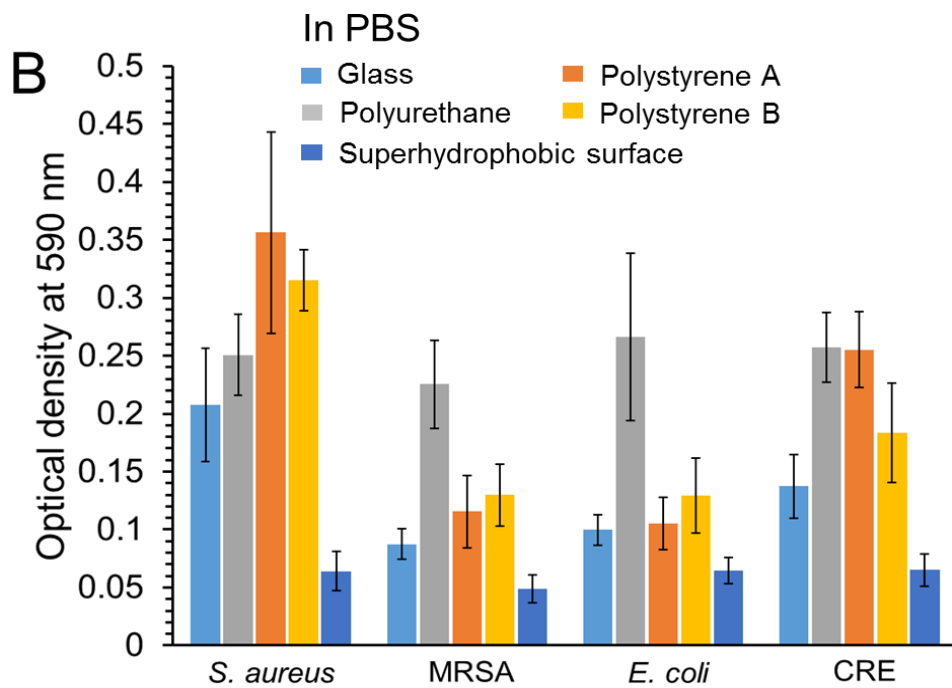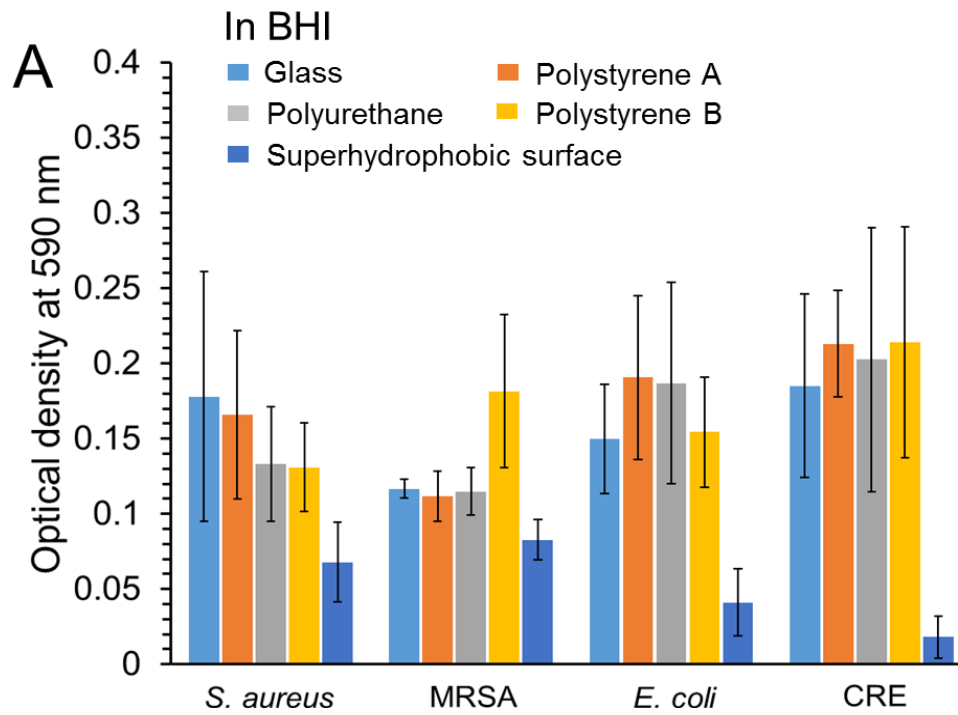
Fig. 2.4 Quantitative comparison of bacteria attached on glass, polyurethane, polystyrene A, polystyrene B, and superhydrophobic surface after 1 h of bacteria exposure. Error bars indicate standard deviation.

2.3.3 Bacteria attachment and surface colonization on superhydrophobic surface with exposure time

Figure 2.5 shows bacteria attachment on superhydrophobic surfaces with exposure time in BHI and PBS medium. The number of bacteria attached on superhydrophobic surface was minimal at 1 h of bacteria exposure. However, the number significantly increased with increasing exposure time. After 24 h of the exposure, the number of attached bacteria was >12 times higher, compared to that at 1 h exposure. The highest increase in bacteria adhesion was shown on CRE (BHI) and *S. aureus* (PBS), and the number of CRE and *S. aureus* attached to superhydrophobic surface after 24 h of bacteria exposure was 43 and 21 times higher than them after 1 h of bacteria exposure, respectively.

Figure 2.6 shows bacterial surface coverage of the superhydrophobic surfaces with exposure time. Violet colour on the insets represented the area where bacteria colonized. It was shown that at the beginning (4 h of bacteria exposure in BHI and PBS) bacterial colonization happened at an edge of the superhydrophobic surface, and the colonized area diffused across the surface with exposure time. After 24 h exposure, the bacteria colonized >95% and >92% of the superhydrophobic surfaces in BHI and PBS, respectively. The surface coverage by MRSA was the highest (the coverage: 99.7%) and fastest at both BHI and PBS.
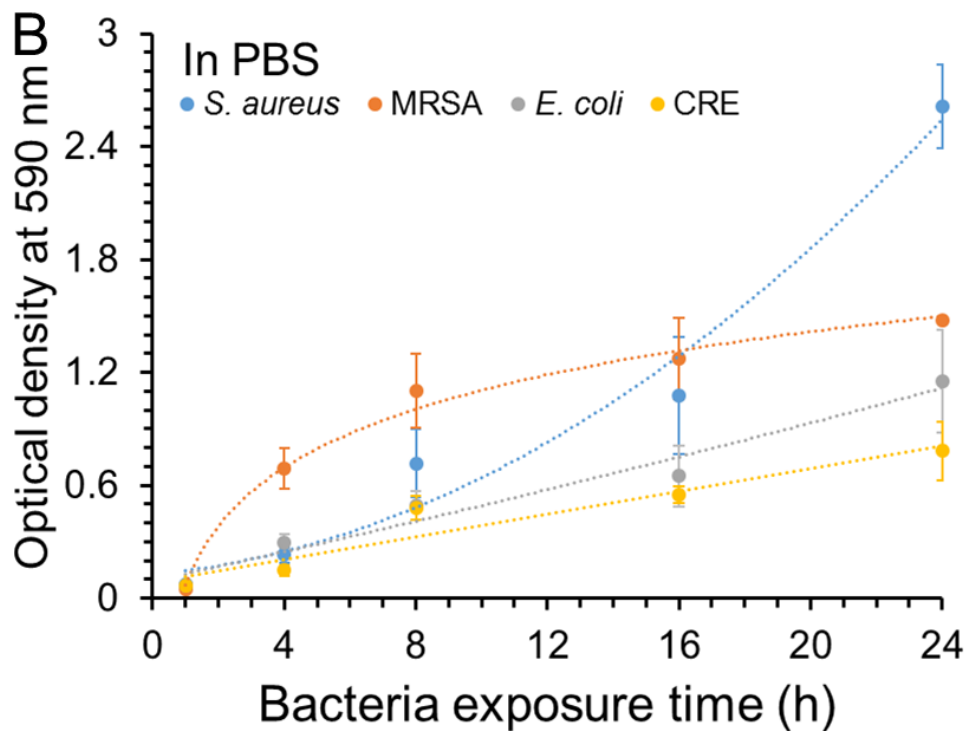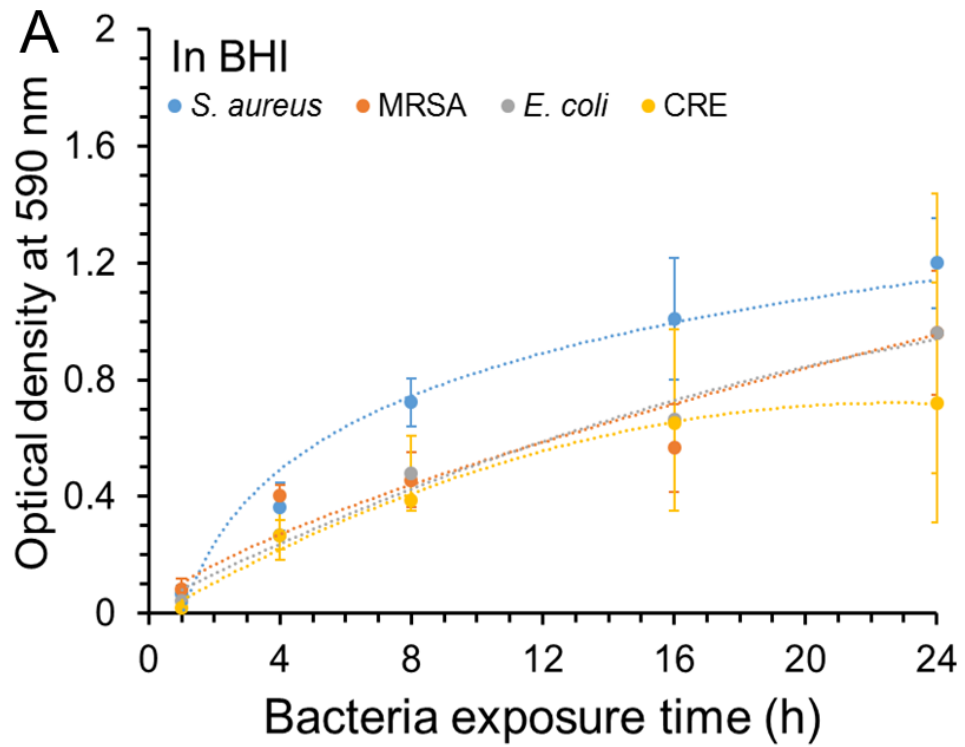
Fig. 2.5 Bacteria adhesion on superhydrophobic surface after 1, 4, 8, 16, and 24 h of bacteria exposure (a) in BHI and (b) in PBS
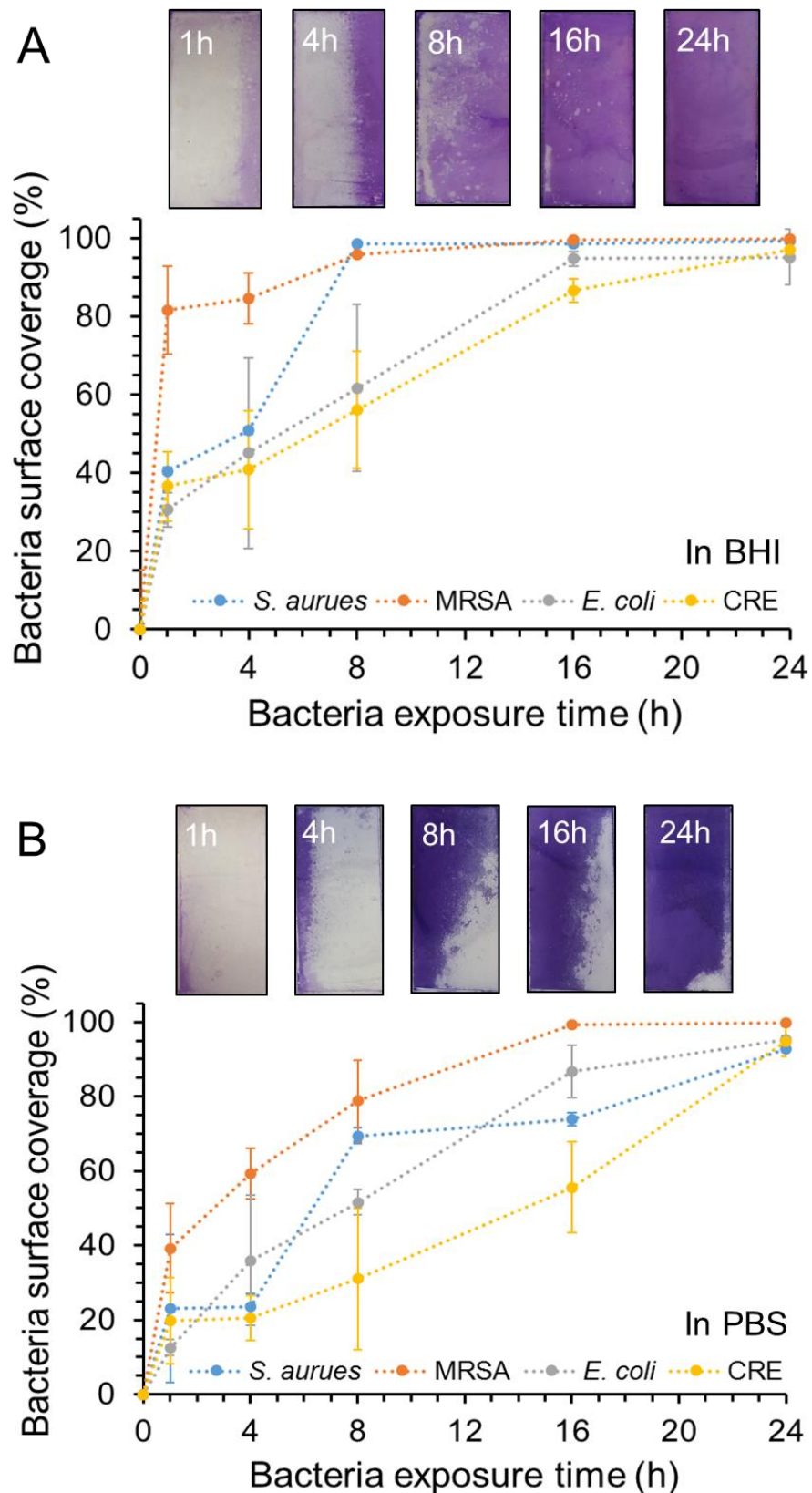
Fig. 2.6 Bacterial surface coverage on superhydrophobic surface after 1, 4, 8, 16, and 24 h of bacteria exposure (a) in BHI and (b) in PBS. Insets in the Figure shows bacterial surface coverage (violet colour) with the time.

2.3.4 Change of the water contact angle with increasing bacterial exposure time

Prior to the experiment, it was confirmed that PBS and BHI solutions did not give adverse effects on the water repellency to superhydrophobic surface. Figure 2.7 shows average water contact angle of superhydrophobic surface bacteria with exposure time in BHI and PBS. At 1 h of bacteria exposure in BHI and PBS, the superhydrophobic surface maintained its water repellency with an average water contact angle of >150.4 $^{\circ}$. However, the average angle reduced with exposure time, and after 24 h, the contact angle of the superhydrophobic surface was below 112 $^{\circ}$, indicating that the surface changed from superhydrophobic to hydrophobic.

Figure 2.8 shows the change of water contact angle across the superhydrophobic surface after 1, 4, 8, 16, and 24 h of bacteria exposure. Blue and red on the colour scale bar indicate low and high contact angles, respectively. It was observed that at the beginning of bacteria exposure, all areas of superhydrophobic surface maintained the water repellency (water contact angle of >150 $^{\circ}$), even although an edge of the surface had a small reduction of the contact angle. But, after 4 h exposure, a water contact angle on the edge of the surface was reduced by >50 $^{\circ}$ and the reduction diffused across the surface with time and, after 24h, the reduction was observed on all areas of the superhydrophobic surface. This is explained by that fact that the attachment of bacteria, which have a hydrophilic cell wall (Figure 2.9) produced a reduction in water repellency to the superhydrophobic surface. As shown Figure 2.10 and 2.11, SEM and confocal microscopic analyses showed that bacteria colonized across the superhydrophobic surface after 24 h. AFM analysis showed that due to bacterial colonization, the roughness of superhydrophobic surface

reduced to 501.8 nm from 1212.9 nm.
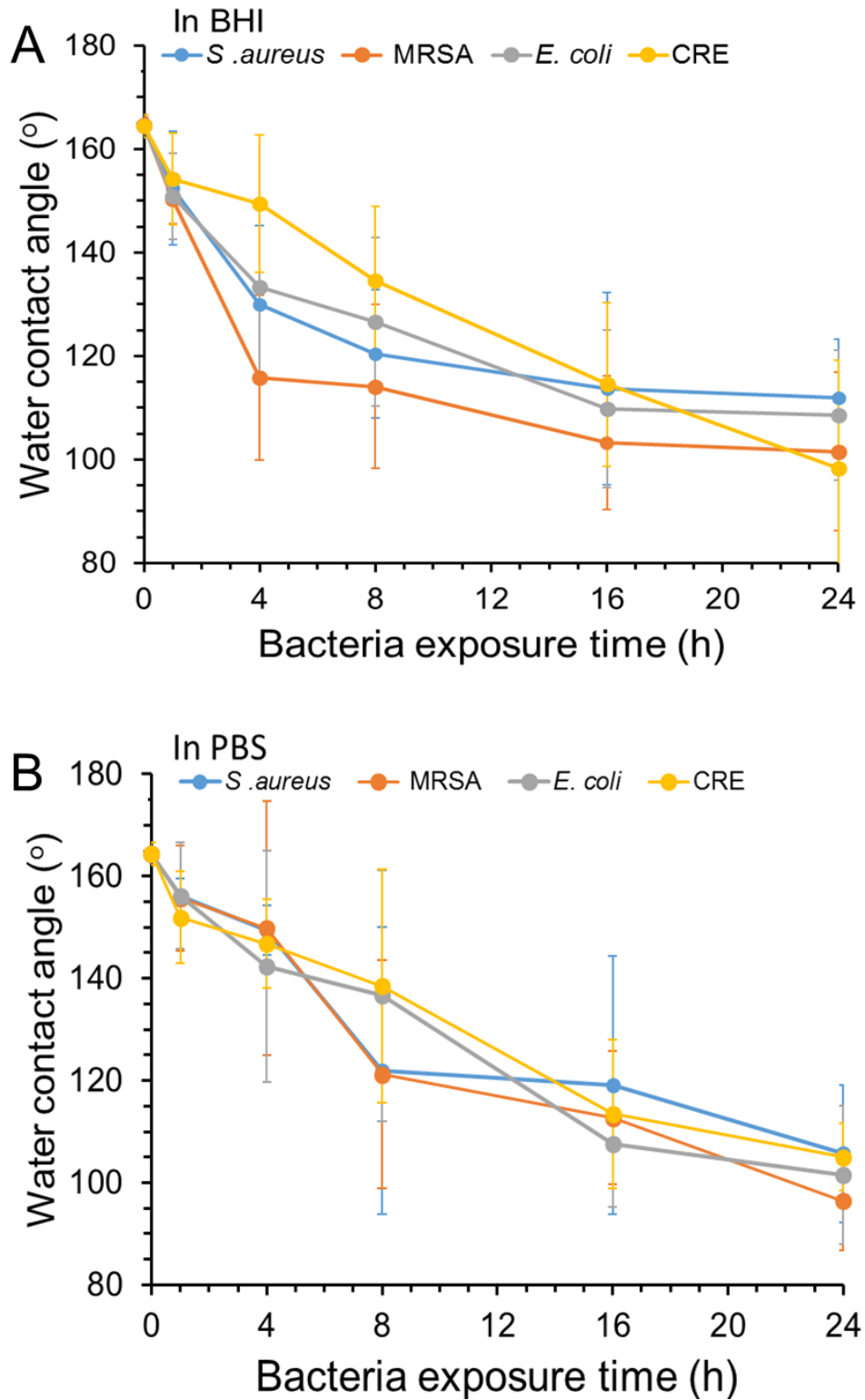
Fig. 2.7 Average water contract angle on superhydrophobic surface after 1, 4, 8, 16, and 24 h bacteria exposure: (a) in BHI and (b) in PBS
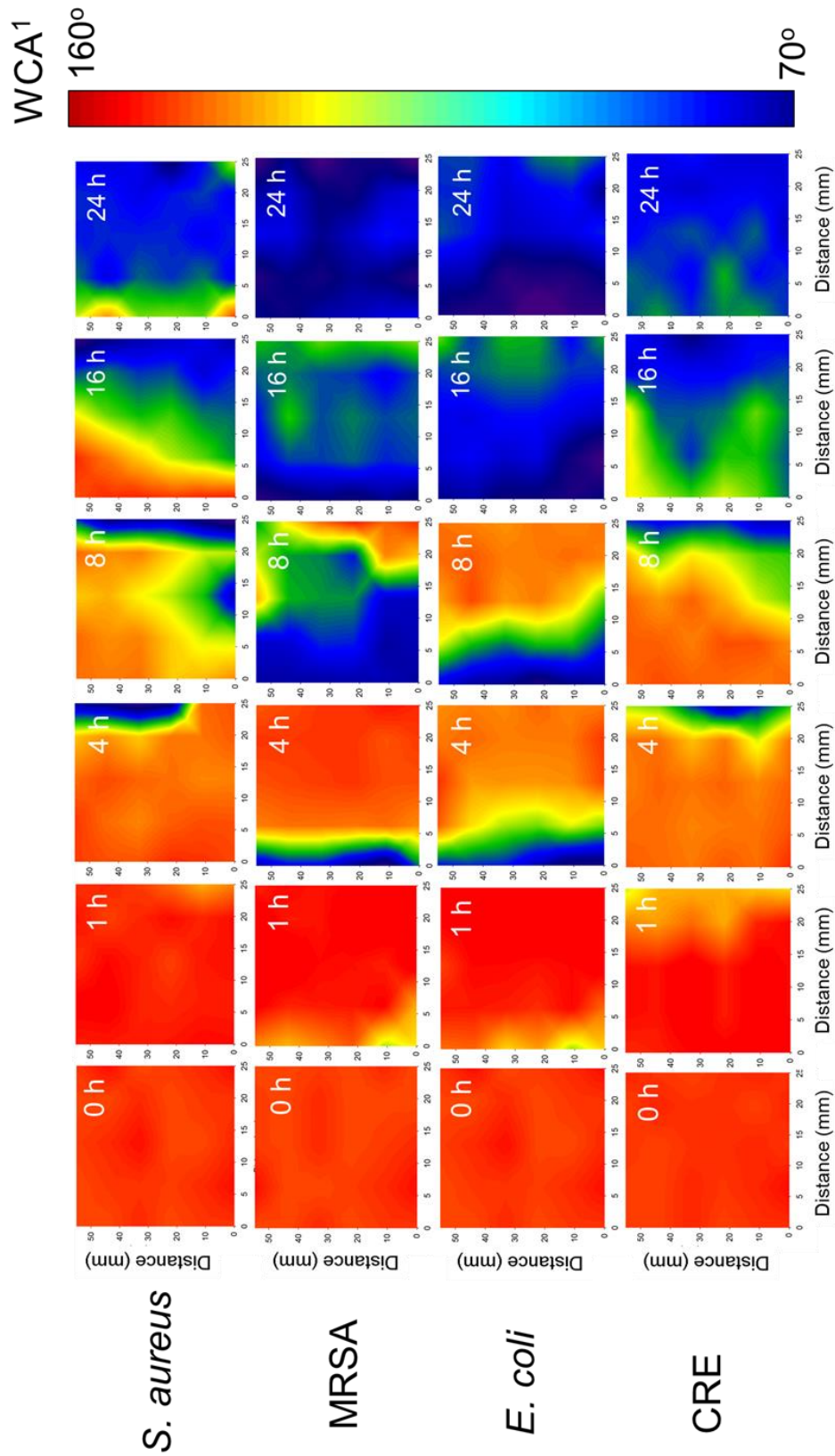
Fig. 2.8 Water contact angles across superhydrophobic surface after 1, 4, 8, 16, and 24 h of bacteria exposure

[1] WAC: water contact angle
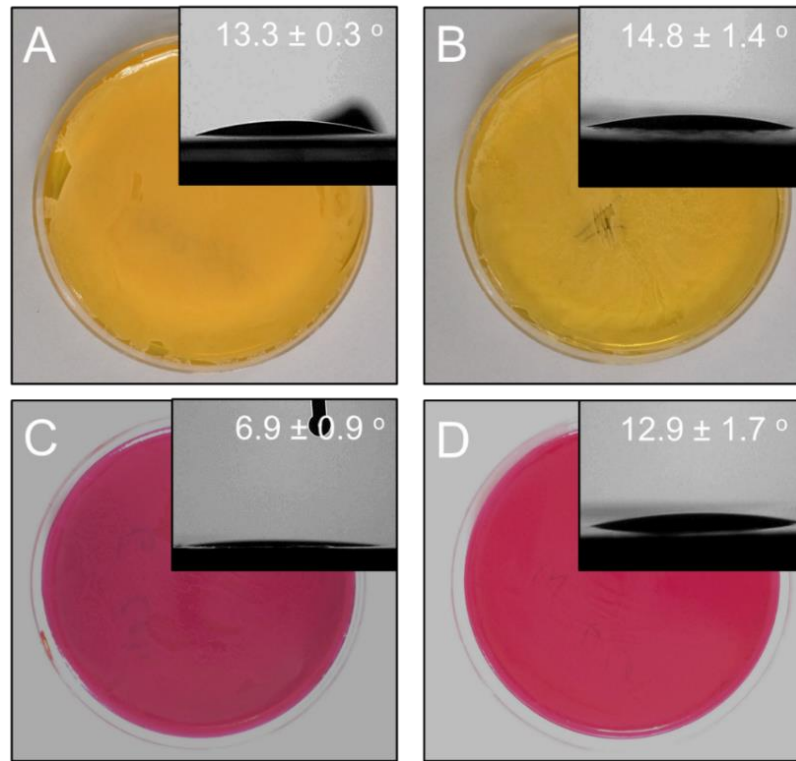
Fig. 2.9 Water contact angle of *S. aureus*, MRSA, *E. coli*, and CRE bacteria colonies.
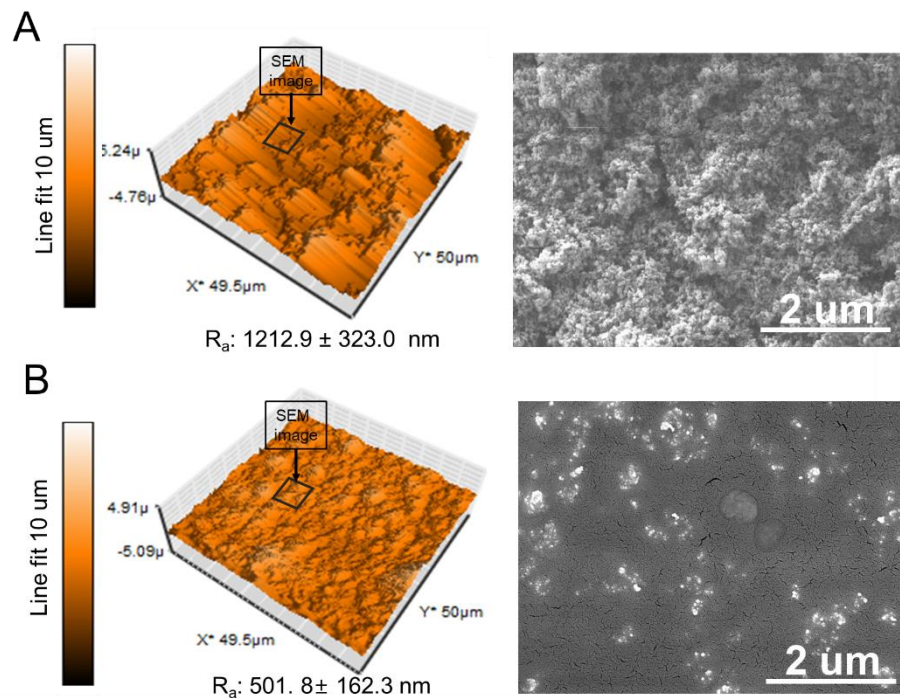
Fig. 2.10 AFM and SEM images of superhydrophobic surface (a) before and (b) after 24 h bacteria colonization in BHI and PBS.
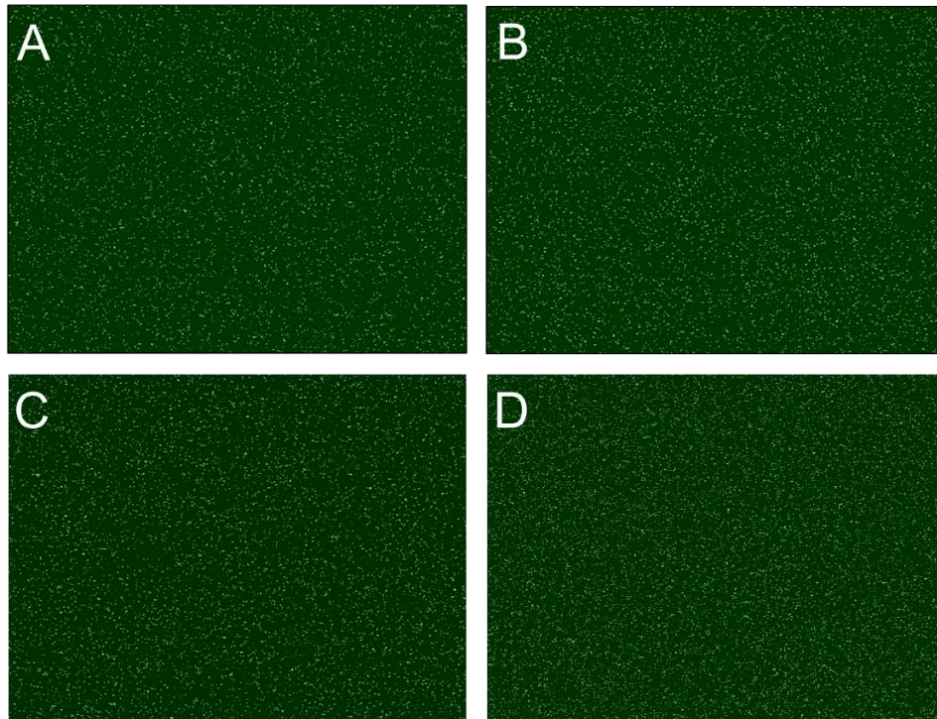
Fig. 2.11 Images of (a) *S. aureus*, (b) MRSA, (c) *E. coli*, and (d) CRE bacteria attached on superhydrophobic surface. The images of bacteria were taken using confocal microscopic system and SYTO 9 in live/dead staining kit.

2.3.5 Bacteria adhesion of glass, polystyrene A, polystyrene B, polyurethane, and superhydrophobic surface after 24 h

Figure 2.12 shows the quantitative comparison of bacteria adhesion on a glass slide, polyurethane, polystyrene A, polystyrene B, and superhydrophobic surfaces after 24 h bacteria exposure in BHI and PBS. It was observed that compared to samples at 1 h of bacteria exposure, the number of attached bacteria for all of tested samples significantly increased, and in contrast with that of 1 h exposure, the bacteria number on the superhydrophobic surface was much greater than that on a glass, polyurethane, polystyrene A, and polystyrene B: it was observed that the number of bacteria on superhydrophobic surface was >1.6 times higher than them on other samples (*P-value* <0.01 for all bacteria in BHI and PBS). In comparison of superhydrophobic

60

surface and glass, the difference in the attached bacteria number between them was significant. In particular, the CRE (in BHI) and MRSA (in PBS) numbers on superhydrophobic surface were 9.3 and 11.4 times higher than the glass, respectively.

To determine what factor affects the significant increase of bacteria adhesion on superhydrophobic surface, correlation of the number of bacteria on the samples and surface roughness or water contact angle was analysed because it was known that surface roughness and water contact angle influence bacteria adhesion on surfaces[176-179]. As shown in Figure 2.13, a significant correlation of the bacteria numbers and surface roughness of glass, polyurethane, polystyrene A, polystyrene B, and superhydrophobic surface was observed; the correlation coefficient of them ranged from 0.92 to 1 in BHI and PBS. Figure 2.14 shows correlation of the number of bacteria and water contact angle on samples after 24 h of bacteria exposure. the correlation coefficients of water contact angle on the samples and the attached bacteria numbers in BHI and PBS was lower than that of surface roughness of the samples: the coefficient ranged from $0.17 < r < 0.9$, and any trend of relation between them was not confirmed.

To validate our experimental results, bacteria adhesion on another superhydrophobic surface was tested. As shown in Table 2.2, the PDMS based superhydrophobic surface had a water contact of 153° with low rolling off angle and contact angle hysteresis, and a surface roughness of 808 nm. In the bacteria adhesion assay, MRSA was used.
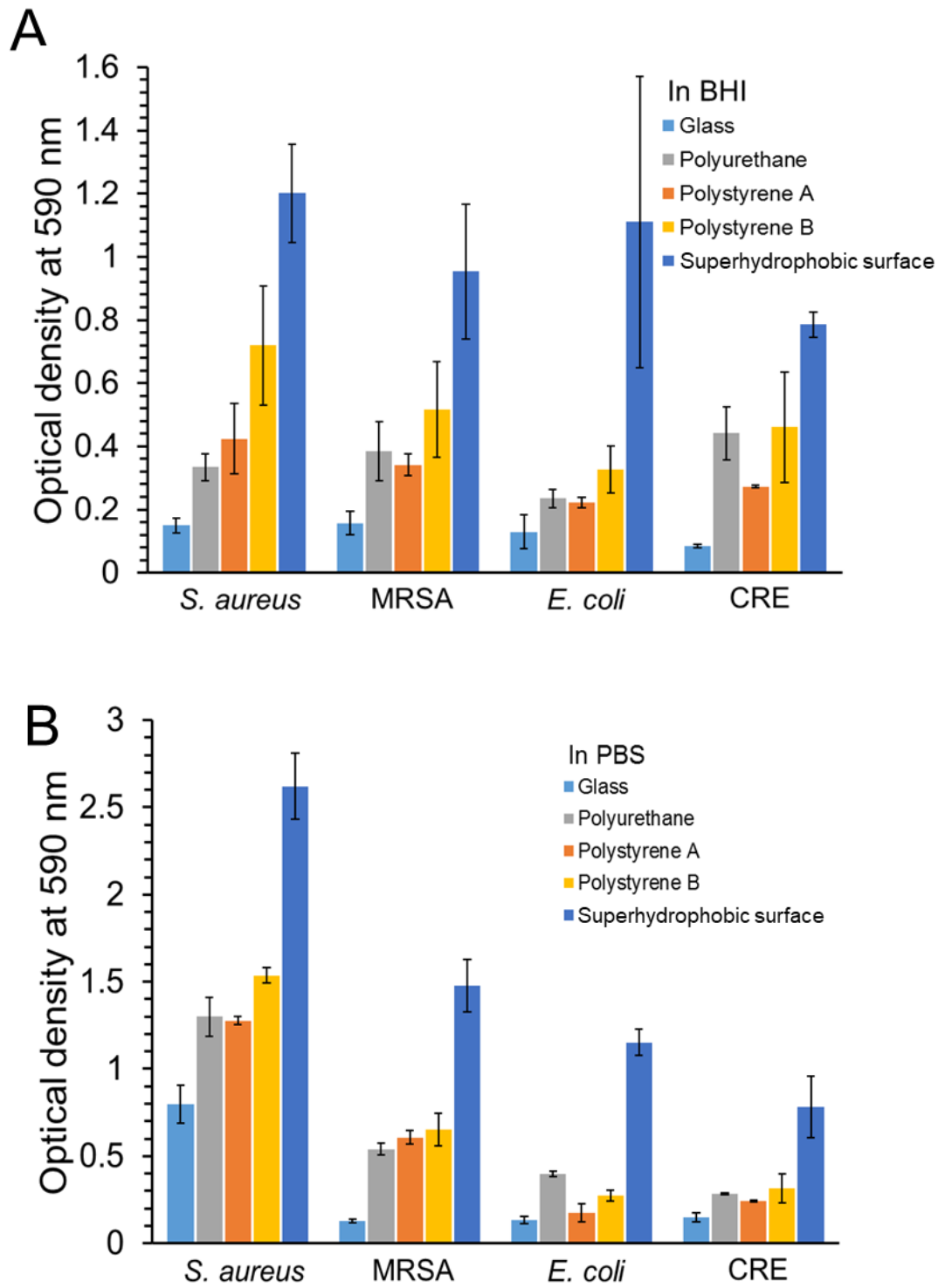
Fig. 2.12 Quantitative comparison of bacteria attached on glass, polyurethane, polystyrene A, polystyrene B, and superhydrophobic surface after 24 h exposure
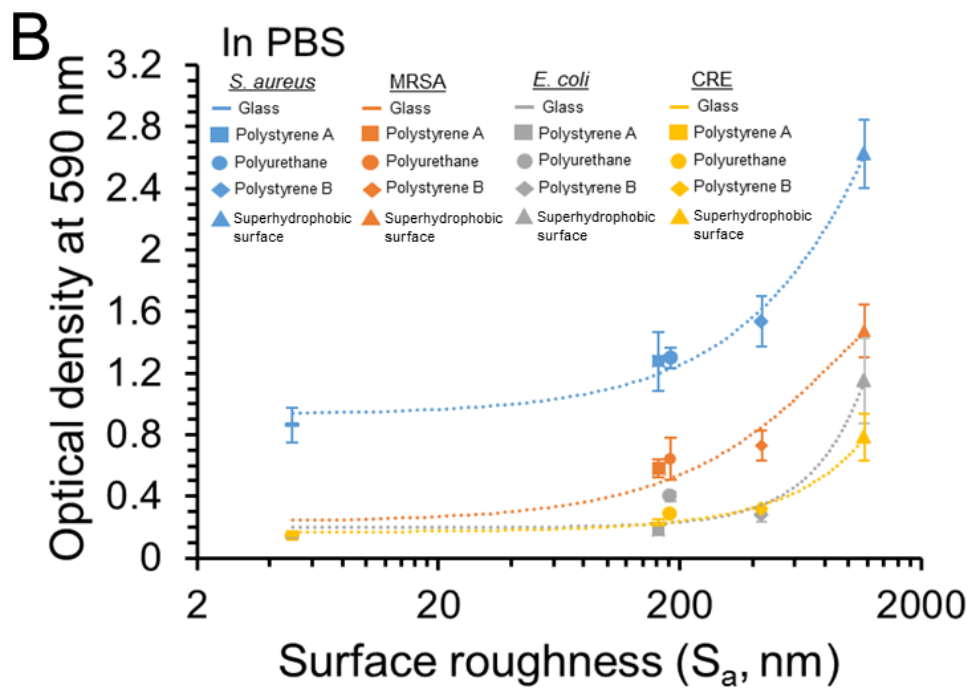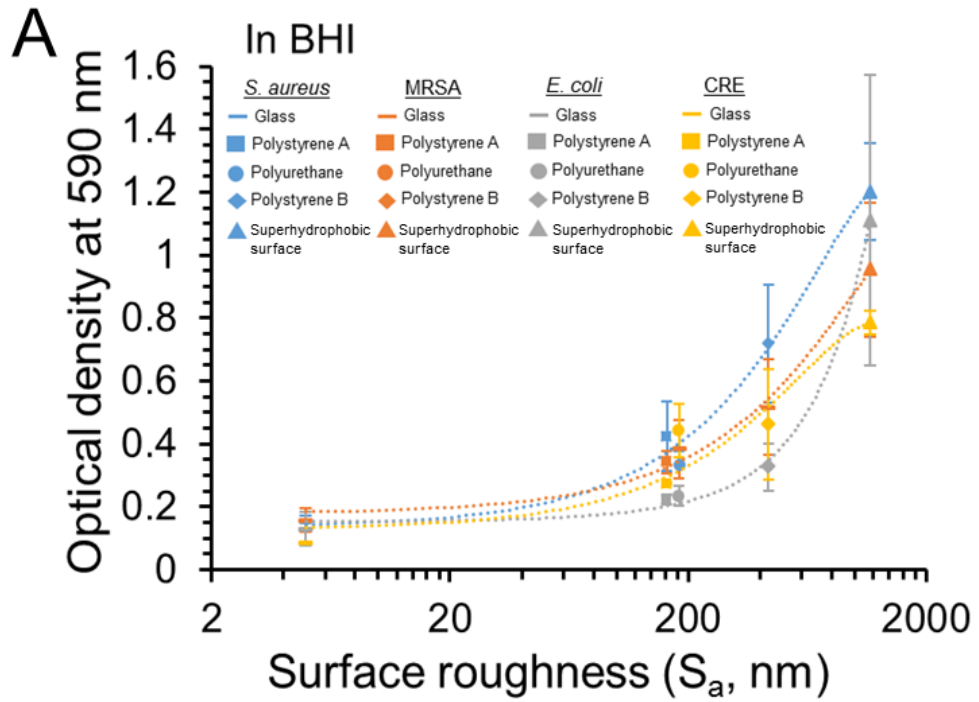
Fig. 2.13 Correlation of the number of bacteria and surface roughness on glass, polyurethane, polystyrene A, polystyrene B, and superhydrophobic surface after 24 h of bacteria exposure
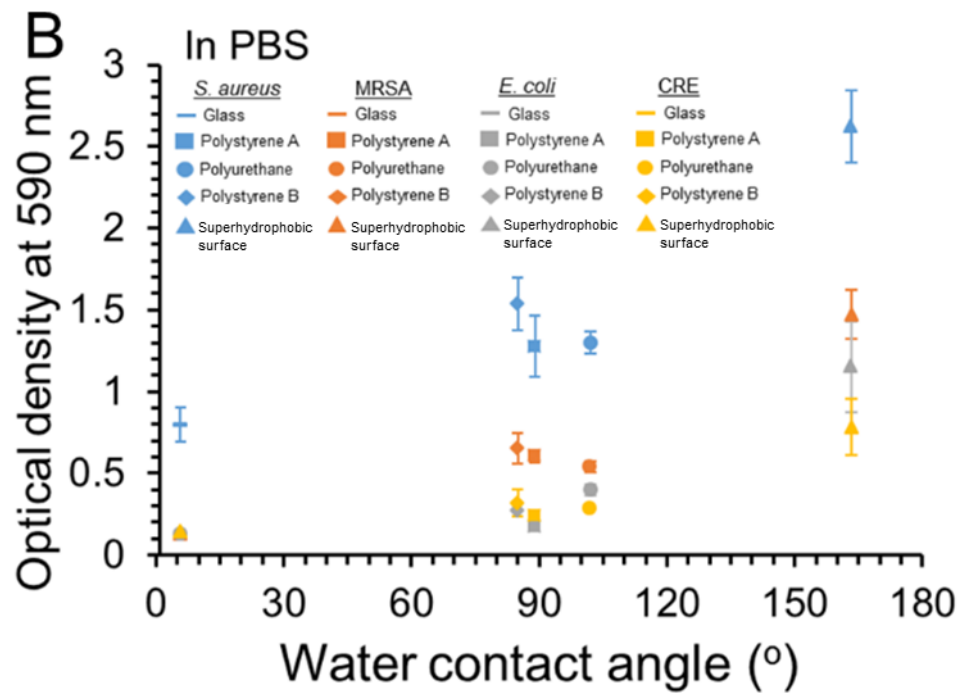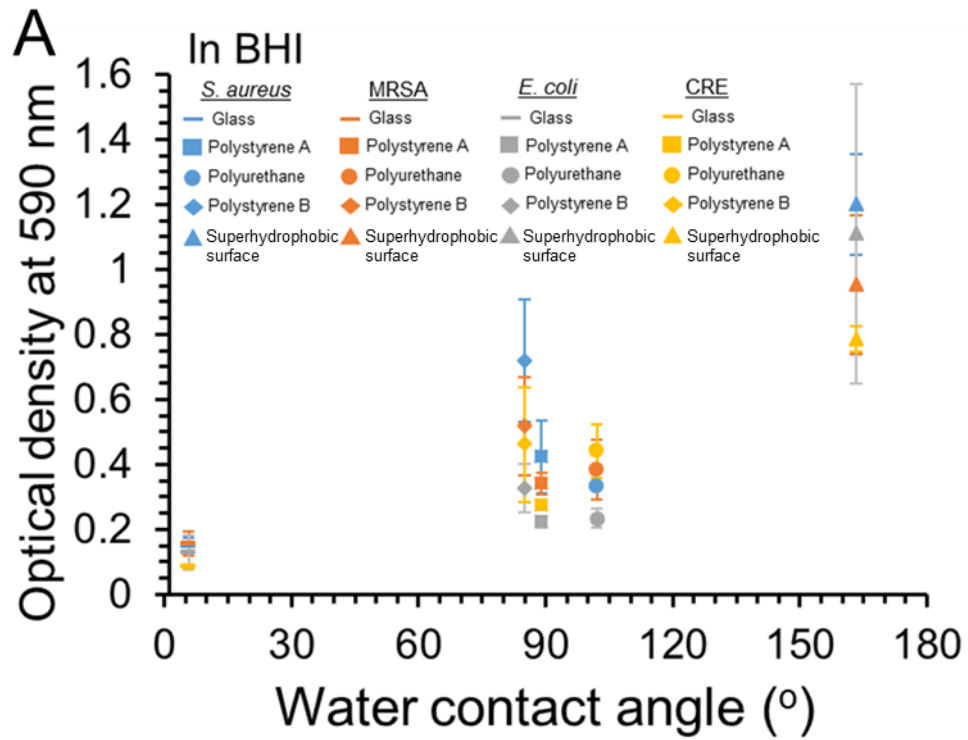
Fig. 2.14 Correlation of the number of bacteria and water contact angle on glass, polyurethane, polystyrene A, polystyrene B, and superhydrophobic surface after 24 h of bacteria exposure

As shown in Figure 2. 15, bacteria adhesion result against the PDMS surface was quite similar with the results shown in Section 2.3.5. It was observed that the number of bacteria attached to the surface was much more than on glass, polyurethane, polystyrene A, and polystyrene B (*P-value* <0.01), and statistically significant correlation between the number of attached bacteria and surface roughness on samples was confirmed (0.96 < *r* <0.98) and the correlation coefficient was higher than that of water contact angle (0.82< *r* <0.92).

Table 2.2 water contact angle, rolling off angle, contact angle hysteresis, and surface roughness of PDMS based superhydrophobic surface

	Water contact angle	Rolling off angle	Contact angle hysteresis	Surface roughness (S_a)
PDMS based superhydrophobic surface	$153.4 \pm 2.0\,^\circ$	$2.8 \pm 1.3\,^\circ$	$1.5 \pm 1.1\,^\circ$	808 ± 19.6 nm
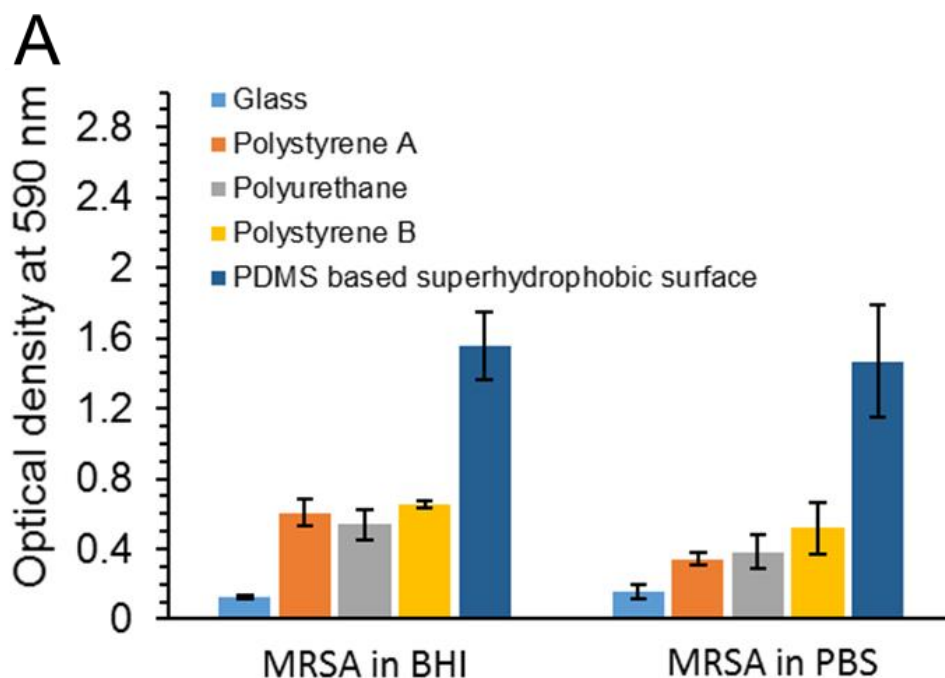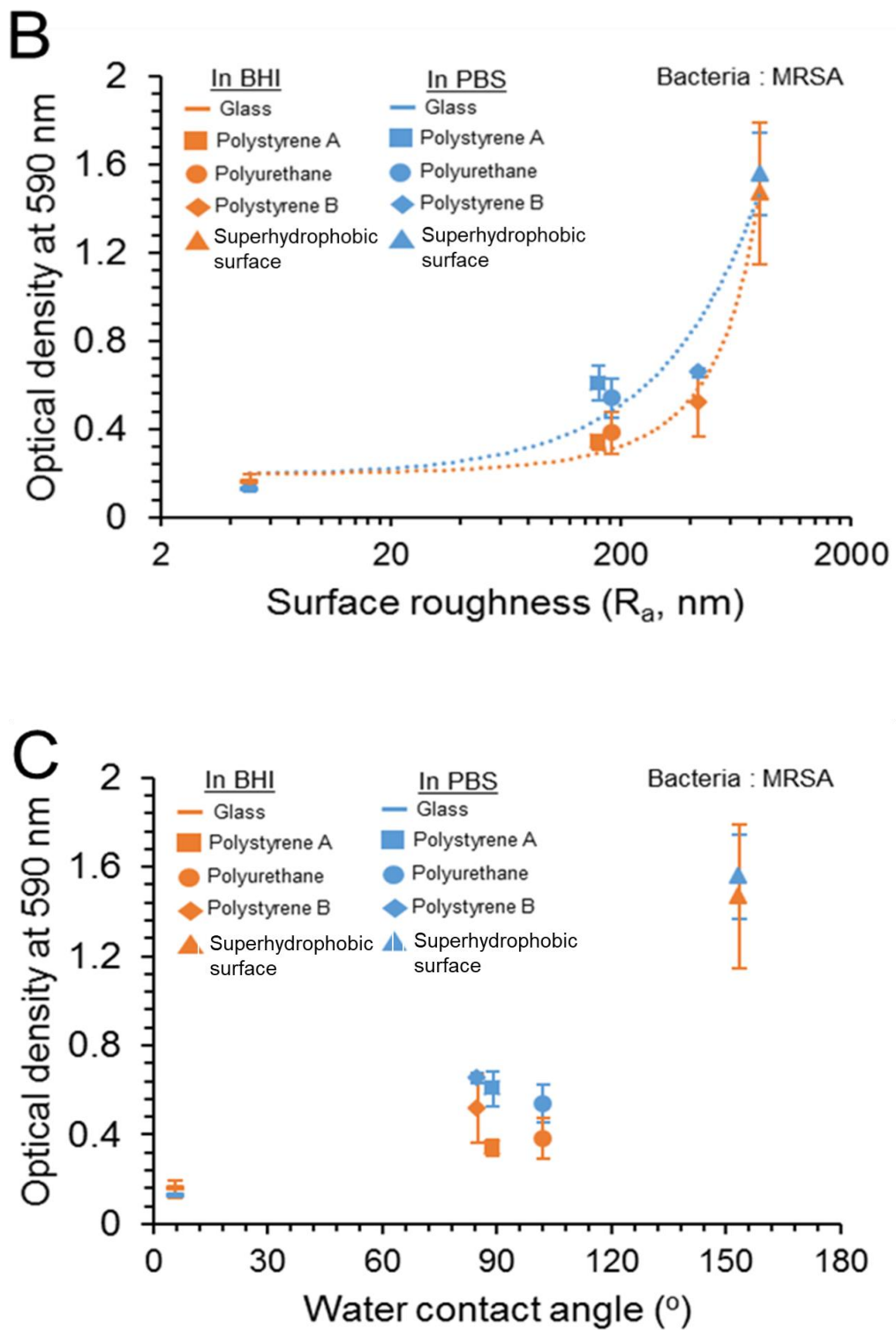
Fig. 2.15 (a) Quantitative comparison of the number of MRSA bacteria attached on samples and correlation of the bacteria number on sample and (b) surface roughness or (c) water contact angle of samples after 24 h exposure in BHI and PBS

Previous research has showed that superhydrophobic surfaces in the Cassie-Baxter

state have less bacteria attachment than glass and other surfaces, and it was speculated that as air-bubbles are entrapped on the superhydrophobic surface when the superhydrophobic surfaces are immersed in bacteria suspension, the bubbles prevent bacteria adhesion on the surface[68,73]. But, the experimental results presented here indicate that over a long period of time, the number of bacteria attached on superhydrophobic surface was greater than the other samples containing glass, polystyrene, and polyurethane. Statistical correlation analyses indicated that the significant increase of bacteria attachment was because of the high roughness of the superhydrophobic surface.

2.3.6 Air-bubble layer on superhydrophobic surface

To determine the reason that bacteria adhesion on the superhydrophobic surface dramatically increased, three different experiments were conducted with respect to mutant bacteria, plastron effect, and air-bubble layer. Figure 2.16 shows adhesion of *S. aureus* and mutant *S. aureus* against superhydrophobic surface after 1 h and 24 h bacteria exposures in BHI and PBS. *S. aureus* (strain JE2) and mutant *S. aureus* (transposon mutant NE679) differ only in that the mutant has an inactivated Δ *pbp4* gene, resulting in a lack of the peptidoglycan cross-linkage[180,181]. Mutant *S. aureus* with defective cell wall structure presents increased deformation of the membrane when it interacts with a surface and a decreased adhesion force indicating that bacterial membrane structure is important for surface recognition. It was hypothesized that the air bubbles were effectively air-cushioned layer and prevented the bacteria from recognizing the adhesion force of the surface[180,181].

After 1 h of the bacteria exposure in BHI or PBS, it was confirmed that both the

number of bacteria attached on the superhydrophobic surface was very low and there was no difference between *S. aureus* and mutant *S. aureus* (*P-value* >0.4 at both BHI and PBS). This indicates that as air-bubbles were entrapped on the superhydrophobic surface, most of the bacteria did not contact the surface, and as a result, they are in the planktonic state. After 24 h exposure, both bacteria attachment significantly increased, and the number of mutant *S. aureus* on the superhydrophobic surface was lower than *S. aureus* (In BHI: *P-value* <0.05, In PBS: *P-value* <0.01), This indicates that physical change occurred to the superhydrophobic surface. It can be explained that the bacteria directly in contact with the superhydrophobic surface as air-bubbles entrapped on superhydrophobic surface disappear, and bacteria begin to colonize the surface. The mutant bacteria, which is less responsive to external force, produce less biofilm than the wild type *S. aureus*.
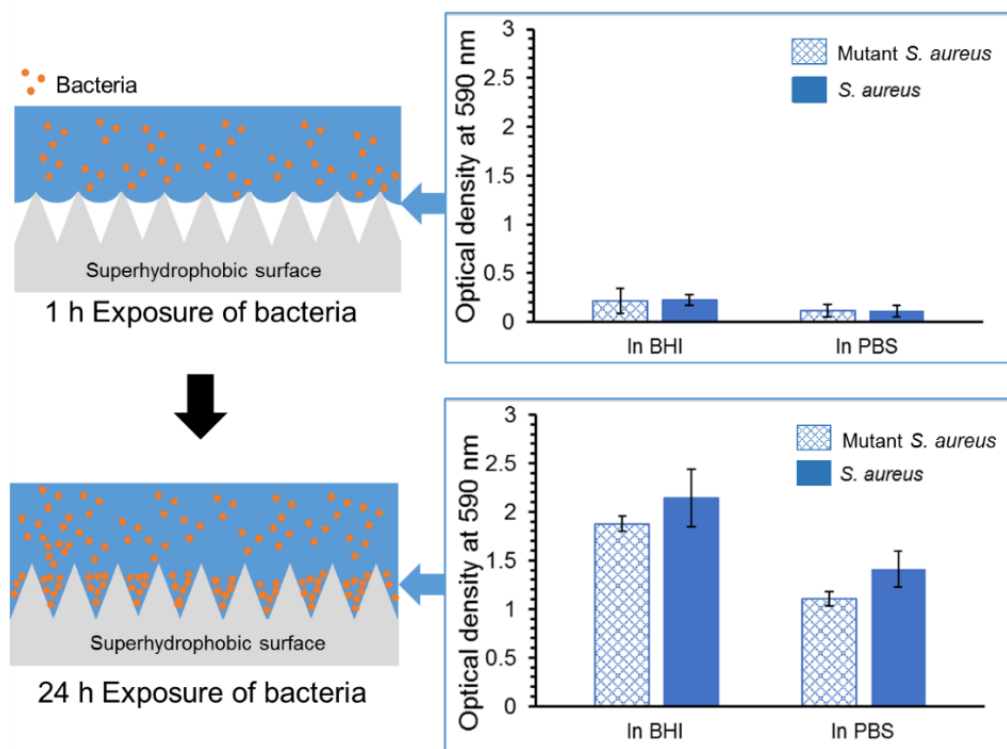
Fig. 2.16 Adhesion of *S. aureus* and mutant *S. aureus* on superhydrophobic surface before and after disappearance of the air-bubble layer

When the superhydrophobic surface, in the Cassie-Baxter state, is vertically placed in water and turned 49 º, a mirror like surface emerges due to light reflection. The effect is produced by the air-bubble layer entrapped between the superhydrophobic surface and water which is known as the plastron effect. As shown in Figure 2.17, the mirror like surface emerged right after being vertically placed and rotated in water and the effect was observed across the superhydrophobic surfaces[171,182]. For 60 min immersion, the mirror like surface was maintained across the surface and after that, it started to disappear. After 120 min in water, the mirror like surface was confirmed around of edge and corner of superhydrophobic surface. After 150 min, the effect totally disappeared from the surface, indicating total disappearance of air-bubbles from the superhydrophobic surface.
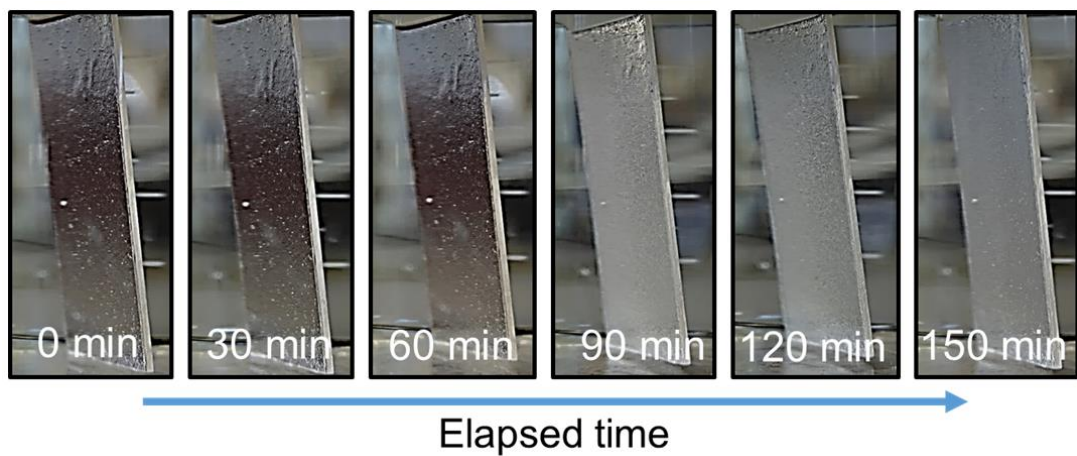
Fig. 2.17 Mirror like surface produced by the plastron effect of an air-bubble layer
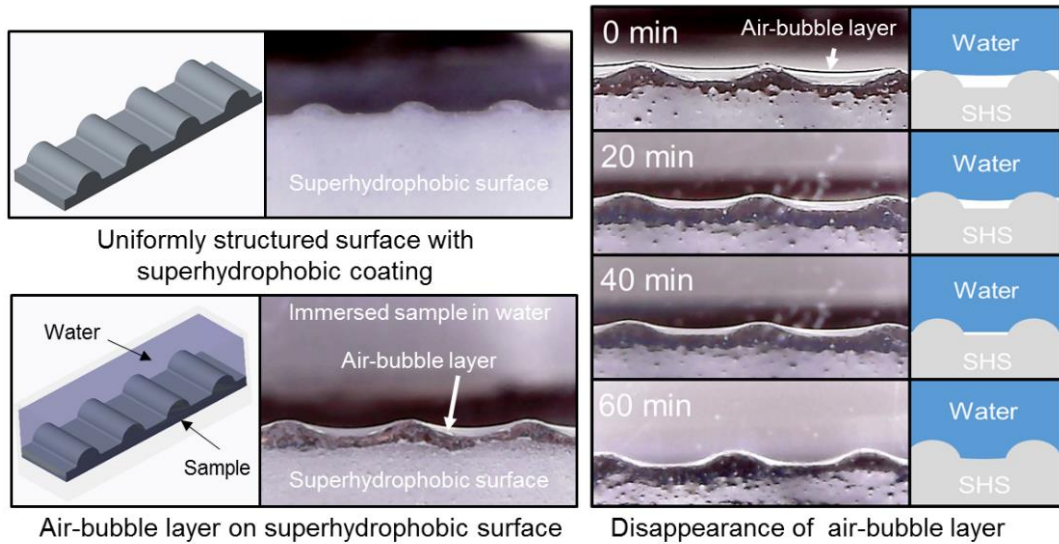
Fig. 2.18 Shape and change of the air-bubble layer entrapped between water and the superhydrophobic surface

Figure 2.18 shows the shape of the air-bubble layer entrapped on the superhydrophobic surface in water. Since air-bubble layer on the superhydrophobic surface which has a surface roughness of about 1 µm was too small, it was impossible to observe the bubble layer on the superhydrophobic surface. Therefore, a superhydrophobic surface, about 139.5 µm in surface roughness (R_a), was used. The sample was horizontally placed in water and then its images were captured side on by optical microscopy. As shown in the Figure, air-bubbles between humps of the surfaces were observed. This explains why superhydrophobic surface has anti-biofouling property over a short period of time. The air-bubble layer entrapped between water and the surface significantly reduced the contact area between bacteria and superhydrophobic surface and the bacteria could not penetrate the air/water interfaces[68]. However, the thickness of the air-bubble layer reduced with increasing immersion time, and it totally disappeared from the surface after 60 min immersion. The loss resulted from air dissolution into water[183,184]. This explains the

reason that bacteria adhesion on superhydrophobic surface significantly increased after 24 h. After disappearance of the air-bubble layer, the high roughness (1.2 µm) of superhydrophobic surface provided a favourable setting to bacteria colonization (*E. coli* (rod shape): ~0.5 µm in diameter and <2 µm in length, and *S. aureus* (spherical shape): <1 µm in diameter)[16,21].

A cleaning experiment against bacteria attached on glass, polystyrene A, polyurethane, polystyrene B, and superhydrophobic surface was conducted. A glove covered finger repeatedly and vigorously wiped the bacteria attached samples. Figure 2.19 showed bacteria numbers on the samples before and after the cleaning process. Of tested samples, the bacteria removal efficiency was the lowest on superhydrophobic surface. This would be due to high roughness of superhydrophobic surface. The wiping does not reach the bacteria settled down inside the groves of the surface. Additionally, after the wiping, the number of remained bacteria was the lowest on glass.

In terms of an anti-biofouling behaviour of the superhydrophobic surface, the Ivanova group reported that in test of bacteria strains, superhydrophobic surface has no anti-biofouling behaviour against *S. aureus* indicating selective anti-biofouling action[185,186]. They speculate that this is attributed to bacteria morphology: different morphology might affect surface contact degree[185,186]. But, researches contradicting the result of Ivanova group have been reported[68,187,188].

S. aureus

A

Legend: Bacteria on samples before finger wiping / Remained bacteria after the wiping

Optical density at 590 nm

Glass | Polystyrene A | Polyurethane | Polystyrene B | Superhydrophobic surface

MRSA

B

Legend: Bacteria on samples before finger wiping / Remained bacteria after the wiping

Optical density at 590 nm

Glass | Polystyrene A | Polyurethane | Polystyrene B | Supehydrophobic surface

Fig. 2.19 The numbers of (a) *S. aureus*, (b) MRSA, (c) *E. coli* and (d) CRE on glass, polystyrene A, polystyrene B, polyurethane, and superhydrophobic surface before and after finger wiping. Samples were immersed in bacterial suspension for 24 h at 37°C and then finger wiping was conducted against bacteria attached samples.

This chapter shows a transformation of a superhydrophobic surface from an anti-biofouling surface to a bacteria reservoir. Contrary to results in previous research[68,71,189], a superhydrophobic surface does not always keep its anti-biofouling property. Even although the air-bubble layer on a superhydrophobic surface prevent bacteria adhesion, the high roughness of the superhydrophobic surface became a favourable condition for bacteria as the bubble layer disappear with time. As a result, bacteria attachment to the superhydrophobic surface was much more than other samples with smooth surfaces such as glass, polyurethane, and polystyrene. Moreover, cleaning tests showed that it was more difficult to remove the bacteria attached to superhydrophobic surface than other sample surfaces.

2.4 Conclusion

In previous researches. Bacterial repellency of superhydrophobic surfaces was reported *via* experiments over a short period of time (<4 h) and they stated that use of superhydrophobic surface can be a useful strategy to control bacteria surface contamination. But, the results in this chapter demonstrated that the anti-biofouling property of superhydrophobic surface is lost with time although it initially has the property resulting in a worse surface than the intact surfaces that have been broadly utilized. This chapter corrects a misunderstanding on anti-biofouling application of certain types of superhydrophobic surfaces.

The use of superhydrophobic surface in air might be useful in the case of removing bacteria and viruses deposited on the surface through water dropping and rolling because the rolling motion takes away the organisms. However, full surface immersion in bacteria contaminated water or permanent exposure of the

contaminated water to the surface can make superhydrophobic surface become a bacteria reservoir which would be a source of HAIs spread. This chapter study clearly shows that it is necessary that hospital surfaces have bactericidal properties to prevent bacteria contaminated surface.

In Chapter 3-5, white light-activated bactericidal polymers, and self-cleaning and bactericidal paints to inhibit the surface contamination were developed, characterised, and tested their bactericidal effect against *E. coli*, and *S. aureus*.

Chapter 3: Silver nanoparticles and toluidine blue O incorporated polyurethane; white light-activated bactericidal polymer

3.1 Introduction

Toluidine blue O (TBO), methylene blue (MB), and crystal violet (CV) are widely known both as biological stains and as light activated bactericidal agents (LABAs) [152,156]. The LABAs are readily soluble in water, ethanol, and acetone, and they generate reactive oxygen species (ROS) when exposed to a visible light source [156,159,190,191]. The ROS produces bacteria cellular injuries including DNA damage, a disruption of membrane integrity, and this induces bacteria death [192,193].

In terms of LABA application to surfaces, a range of studies have been performed. It was reported that LABAs could be encapsulated into polymers, which are widely used in hospitals, by a swell-encapsulated-shrink technique and the polymers

containing LABAs showed bactericidal activity in white light which is a common hospital light source[157,158,194]. It was also reported that gold or zinc oxide nanoparticles addition into the LABA encapsulate polymer significantly enhanced bactericidal activity under light[161,195], and Noimark *et al.* (2014) and (2015) showed that multi-LABAs incorporation into polymer exhibited a potent photobactericidal effect and they also represented bactericidal activity under dark conditions[159,196].

In this chapter, silver nanoparticles and TBO encapsulated polyurethane was produced through a swell-encapsulation-shrink technique, and its bactericidal activity was compared with that of the polymers with TBO and gold nanoparticles or mixture of gold and silver nanoparticles in white light and in the dark. The experimental results showed that silver nanoparticles and TBO encapsulated polyurethane had a stronger photobactericidal activity than the polyurethane with TBO and gold nanoparticles or polyurethane with TBO mixture of the nanoparticles and that it even showed potent bactericidal activity in dark.

3.2 Experimental

3.2.1 Nanoparticle synthesis and characterization

Suspension A: 49.2 mg of Gold (III) chloride trihydrate ($HAuCL_4 \cdot 3H_2O$, Sigma-Aldrich, St. Louis, MO, USA) was dispersed in 25 mL of deionised (DI) water and then sonicated for 5 min to get 5 mM solution.

Suspension B: 45 mg of silver nitrate ($AgNO_3$, Sigma-Aldrich, St. Louis, MO, USA) was dispersed in 50 mL of DI water, and then sonicated for 5 min to produce 5 mM solution.

Suspension C: 294.7 mg of tri-sodium citrate dihydrate ($Na_3C_6H_5O_7 \cdot 2H_2O$, Hopkin & Williams Ltd, London, UK) was dispersed in 50 mL of DI waster and then sonicated to form 20 mM solution.

3.2.1.1 Synthesis of gold (Au) nanoparticles

1 mL of suspension A was mixed with 18 ml of DI water and heated with constant agitation until a boiling point. After that, 1 mL of suspension C was added into the mixture. Under constant agitation, the mixture was boiled for a further 30 min and then it was placed in a dark room to cool down.

3.2.1.2 Synthesis of silver (Ag) nanoparticles

1 mL of suspension B was mixed with 18 mL of DI water and heated with constant agitation until boiling point. After the boiling, 1 mL of suspension C was added into the mixture. Under constant agitation, the mixture was boiled for a further 30 min and then it was placed in a dark room to cool down.

3.2.1.3 Mixture of silver and gold (Ag/Au) nanoparticles

Suspensions of Ag and Au nanoparticles was mixed together and it was agitated for 5 min. The mixing ratio was about 1 to 1.

3.2.1.4 Transmission electron microscopy

In order to determine size, morphology, chemical elements of the synthesized nanoparticles, transmission electron microscopy (TEM) equipped with energy dispersive X-ray spectroscopy (EDS) (JEM-2100, JEOL Inc., Peabody, MA, USA)

was used. A droplet of nanoparticles suspension was dropped on to TEM grid and dried in a dark room for 24 h. The nanoparticles were observed by TEM at an accelerating voltage of 100–200 kV. EDS point analysis and EDS mapping were performed on the particles.

3.2.1.5 Ultraviolet and visible absorbance spectroscopy
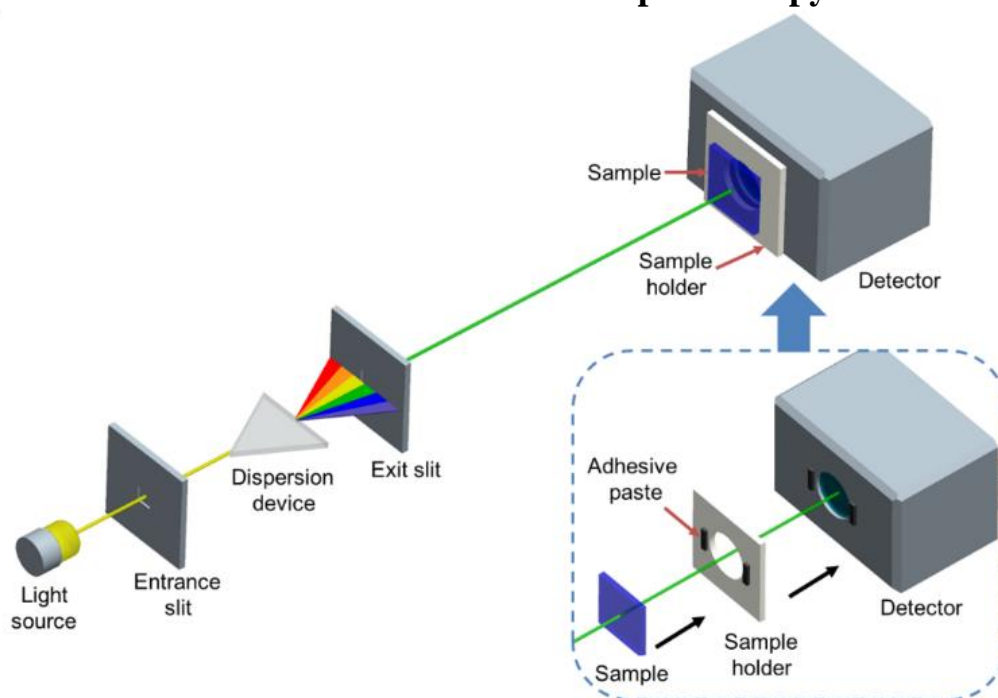
Fig. 3.1 UV/Vis absorption measurement using UV/Vis spectrometer

3 ml of nanoparticle suspension was loaded in a glass cuvette, and the Ultraviolet and Visible (UV/Vis) absorption spectra of the nanoparticles suspension was measured by a UV/Vis spectrometer (Lambda 25, PerkinElmer Inc., Winter St., CT, USA) which has a detection range of wavelengths of 190–1100 nm. As shown in Figure 3.1, the treated sample was loaded on to the light wavelength detector, and then UV/Vis absorption spectra against control, and treated polyurethane were measured at wavelengths of 350–900 nm.

3.2.2 White light-activated bactericidal polyurethane and characterization

3.2.2.1 Production of bactericidal polyurethane
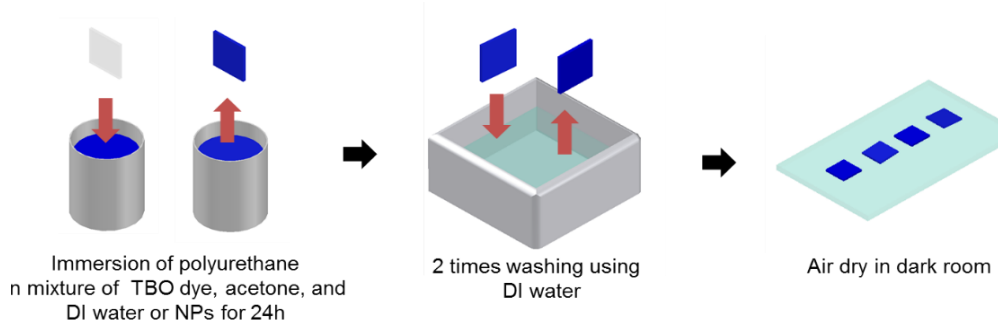
Fig.3.2 Preparation of bactericidal polyurethane

To produce white light-activated bactericidal polyurethane, a swell-encapsulated-shrink process was employed. 60 mg of toluidine blue O powder (TBO, Sigma-Aldrich, St. Louis, MO, USA) was dispersed in to a mixture of acetone (9 mL), and DI water or nanoparticles (1 mL) to obtain 19.6 mM of TBO solution, and then it was sonicated for 5 min in order to get complete dissolution of the TBO powder. As shown in Figure 3.2, polyurethane (1.0 cm ×1.0 cm) was immersed in 10 mL of TBO solution and left in a dark room for 24 h. The polyurethane was collected from the TBO solution, washed by DI water twice and then dried for 24 h in a dark room. Five different samples were produced as follows: control, TBO only, TBO with Au nanoparticles, TBO with Ag nanoparticles and TBO with Au/Ag nanoparticles.

3.2.2.2 Ultraviolet and visible absorbance spectroscopy

To confirm the amount of nanoparticles encapsulated into the polyurethane sample, The UV/Vis absorbance spectra of the nanoparticle suspension were measured before and after the swell-encapsulation-shrink process. The polyurethane was placed in a mixture of acetone (9 mL), and nanoparticles (1 mL) for 24 h. Through comparison of absorbance at 409 nm for (Ag nanoparticles) and 526 nm (Au nanoparticles) or both at 409 and 526 nm (Mixture of Ag and Au nanoparticles), the amount of the nanoparticles encapsulated into polyurethane could be detected.

The uptake ratio of nanoparticles from the suspension to polyurethane was calculated as follow;

$$\text{Uptake ratio} = \frac{\text{AU}_{\text{before}} - \text{AU}_{\text{after}}}{\text{AU}_{\text{before}}}$$

Where $\text{AU}_{\text{before}}$ and AU_{after} represents the absorbance values of nanoparticles suspension before and after polyurethane immersion in the suspension, respectively.

3.2.2.3 Fluorescence microscopy

In order to determine the diffusion of TBO inside polyurethane, the polymer sample was placed in TBO solution for 5, 30, and 60 min, washed by DI water twice, and then followed by drying in a dark room for 24 h. The side section of TBO stained polyurethane was sliced into 400 µm thickness by a scalpel and placed on a glass slide. The images of sample were captured by an inverted fluorescence microscope (Model-IMT-2, Olympus Ltd., Tokyo, Japan) equipped with cooled scientific-grade 16-bit digital CCD camera (Model- PIXIS 512, Roper industries Ltd., Sarasota, FL, USA). The TBO molecules impregnated in the sample was observed

by fluorescence excitation with a 633 nm laser. Fluorescence was detected by a bandpass filter focused at 660 nm (model-660DF30, Omega Optical Inc., Brattleboro, VT, USA). The images were subsequently analysed by WinSpec/32 (Roper industries Ltd., Sarasota, FL, USA) and ImageJ software (\ \http://rsbweb.nih.gov/ij/).

3.2.2.4 Water contact angle

The equilibrium water contact angle was determined on the sample using a contact angle meter (First Ten Angstroms, Inc., Portsmouth, Virginia, USA). A water droplet (volume: 5 µL) was inoculated on the sample, its image was captured side on and analyzed by Surftens 4.5 software.

3.2.2.5 Elastic modulus

Elastic stress of samples was measured using material testing and inspection device (AGS-X, Kyoto, Japan) with 10 kN of load capacity. The tensile action grips were used for sample with size of 0.8 mm (thickness) $\times$ 3 mm (width) $\times$ 55 mm (length). At an initial distance of 30 mm between the grips, the sample was stretched at a speed of 300 mm/min until final sample size increased by 5 times than initial one. The result was analysed by Trapezium Lite X software.

3.2.2.6. Bactericidal test
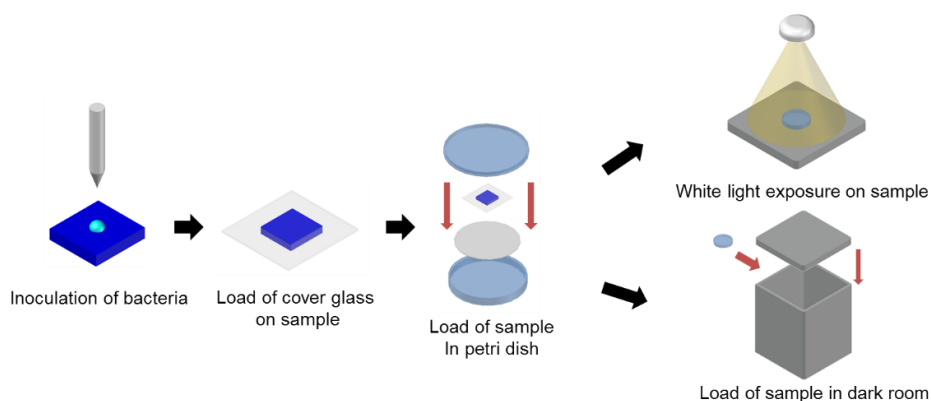
Fig. 3.3 Bactericidal experiment on white light-activated bactericidal polyurethane

The bactericidal activity of the sample was tested against *Escherichia coli* (*E. coli* ATCC 25922) which was stored in Brain-Heart-Infusion broth (Oxoid Ltd., Hampshire, England, UK) containing 20% (v/v) glycerol at -70°C were propagated on MacConkey agar (Oxoid Ltd., Hampshire, England, UK). One bacterial colony was inoculated in 10 mL of BHI broth, and then it was incubated at $37\,^{\circ}$C with shaking at 200 rpm. After 18 h incubation, the bacteria were collected through centrifugation at 5000 rpm for 10 min, and 10 mL of phosphate buffered saline (PBS) was added and vortexed for 1 min. It was centrifuged again in order to get bacteria which re-suspended in 10 mL of PBS, and then it was diluted 1000-fold to obtain ~10^6 colony forming units per mL (CFU/mL). As shown in Figure 3.3, 25 µL of the bacteria suspension was inoculated on to the sample and a sterile glass cover slip (2.2 cm $\times$ 2.2 cm) was placed on it to make a good contact between the bacteria and the sample. The sample was loaded into petri dish with moistened paper to keep humidity and exposed to white light while another sample was kept in a dark room. After light exposure, the sample was placed into 450 µL of PBS, and vortexed for 1 min. The bacterial suspension was serially diluted, plated onto MacConkey agar,

and incubated at $37\,^{\circ}$C for 24 h. The colonies grown on the agar were counted.

3.2.2.7 Statistical analysis

Experimental data were analysed by SPSS (IBM Corporation, Armonk, New York, USA) in terms of Mann–Whitney U test.

3.2.2.8 White light lamp exposure
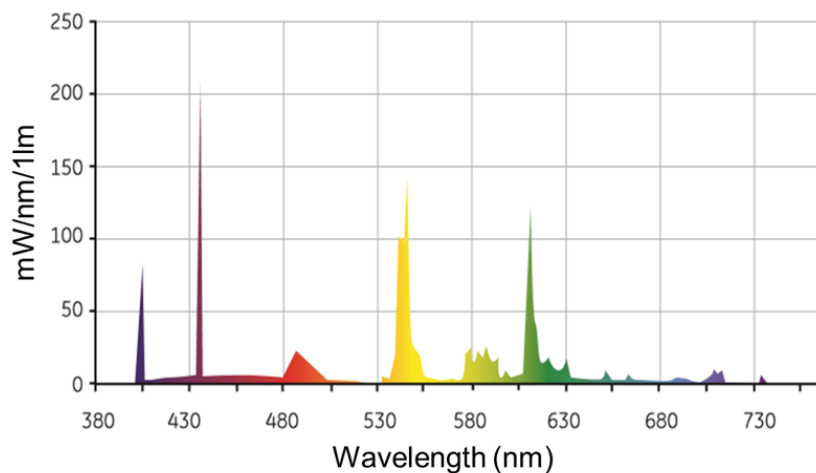
Fig. 3.4 Emission spectrum of white light lamp

The light source selected in present study was 28 W white fluorescent lamp (GE Lighting, East Cleveland, Ohio, USA). This lamp was chosen because it has same characteristic with lamps used in health care facilities of United Kingdom. As shown in Figure 3.4, the emission wavelength of the lamp ranges from 400–730 nm, and it contains peak wavelengths of 405, 495, 545, 588, and 610 nm
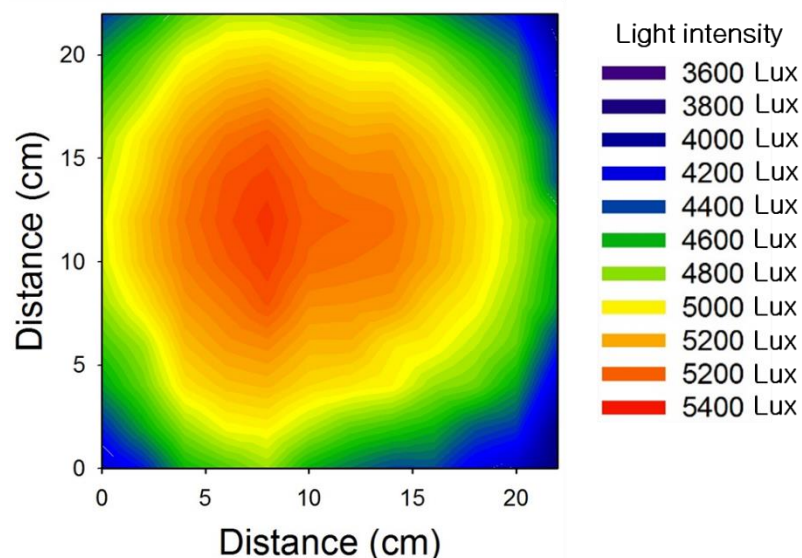
Fig. 3.5 Distribution of light intensity. Colour scale bar corresponds from low (blue) to high light intensity (red)

Figure 3.5 shows that light distribution of the lamp which the painted samples were exposed to. The light intensity was investigated at a distance of 30 cm from the lamp using a lux meter. The light intensity was between 3900 to 5300 lux and the intensity average was 4400 lux. In all experiments, surrounding temperature was kept at 20 $^{\circ}$ C inside an incubator.

3.3. Result and discussion

3.3.1 Synthesis of nanoparticles and their characterization

3.3.1.1 Transmission electron microscopy

To determine the characteristics of synthesized nanoparticles, TEM and EDS was used. The nanoparticles were produced by citrate reduction in solutions of gold (III) chloride trihydrate or silver nitrite at boiling point. Figure 3.6 shows TEM images of silver (Ag) and gold (Au) nanoparticles, and mixtures of Au and Ag nanoparticles (Mix Ag/Au nanoparticles). The size of silver and gold nanoparticles was poly-

dispersed, they were not agglomerated, and they had a wide range of morphology containing spheres, rods, triangles, and ellipses. To determine the size of Ag, Au, and Mix Ag/Au nanoparticles, 20 TEM images at each condition were analysed by ImageJ software. As shown in 3.7 a and b, the average size of silver nanoparticles was 22.4 nm with interquartile range of 24 nm and median of 22 nm, and, average size of gold nanoparticles was 34.4 nm with interquartile range of 12 nm and median of 34 nm. In case of the mixture of Ag and Au nanoparticles, it was observed that most of mixed nanoparticles were aggregated and that the average size of the agglomerations was 252 nm with interquartile range of 200 nm and median of 175 nm (Figure 3.6 c and Figure 3.7 c). As shown in Figure 3.8 a and b, EDS analysis of the nanoparticles showed that all of peaks were assigned to silver and gold, respectively, and the silver and gold elements were uniformly distributed in the particles, respectively. The analysis for the mixture showed that the peaks assigned to both silver and gold (Figure 3.8 c). Additionally, impurities on the nanoparticles were not detected, and peaks on carbon, copper, and silicon were from the TEM grid.
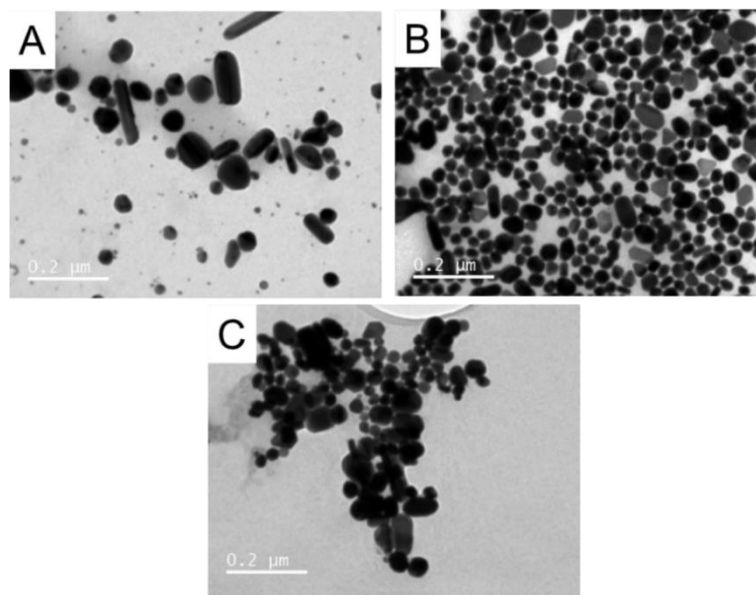
Fig. 3.6 TEM images of (a) Ag, (b) Au, and (c) Mix Ag/Au nanoparticles
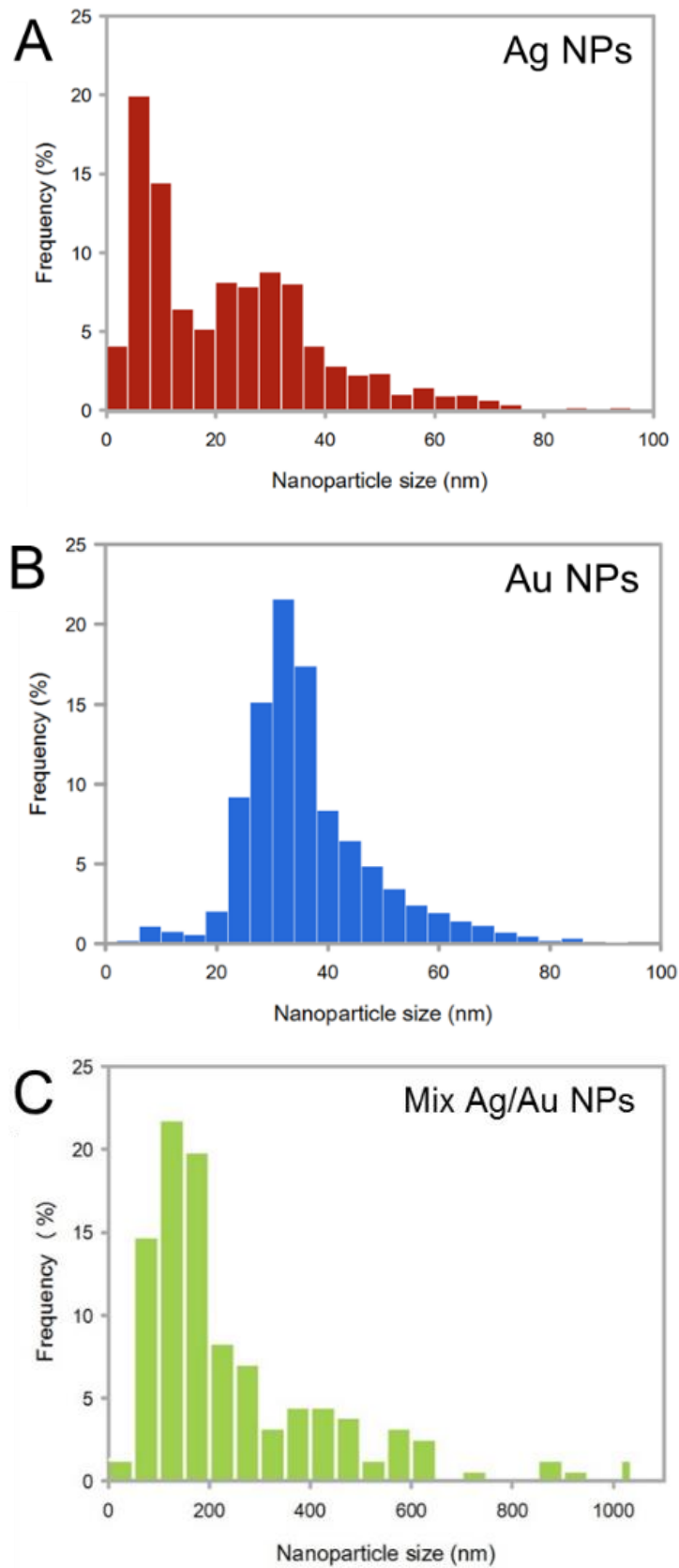
Fig. 3.7 Size distributions of (a) Ag nanoparticles (NPs), (b) Au NPs, and (c) Mix Ag/Au NPs.
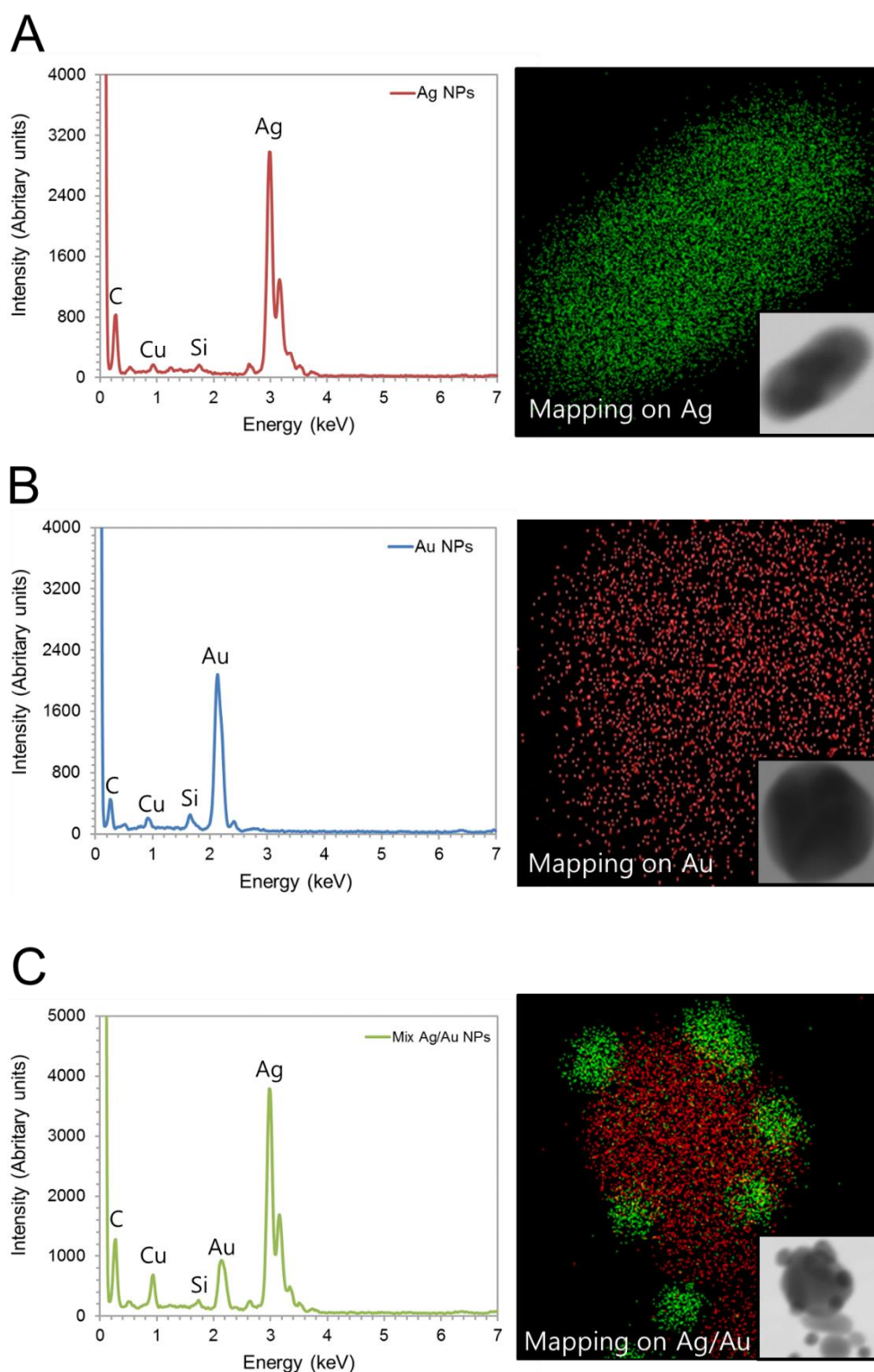
Fig. 3.8 EDS analysis for synthesized (a) Ag nanoparticles, (b) Au nanoparticles, and (c) Mix Ag/Au nanoparticles. Green and red colours on the insets indicate silver and gold elements, respectively.

3.3.1.2 Ultraviolet and visible absorbance spectroscopy

3 mL of the nanoparticles suspension was used at each condition to determine UV/Vis absorbance spectra of the nanoparticles and it was measured at wavelengths of 350–950 nm by UV/Vis spectrometer. As shown in Figure 3.9, the UV/Vis spectra of silver nanoparticles showed a peak at 409 nm and the spectra of gold nanoparticles exhibited a peak at 526 nm. In case of the mixture of both nanoparticles, a dual peak was observed at 412 nm and 530 nm, indicating silver and gold nanoparticles respectively. However, the peaks were slightly shifted right, compared with pure silver or pure gold nanoparticles. This might be that some gold had entered into the Ag nanoparticles or vice versa[197].
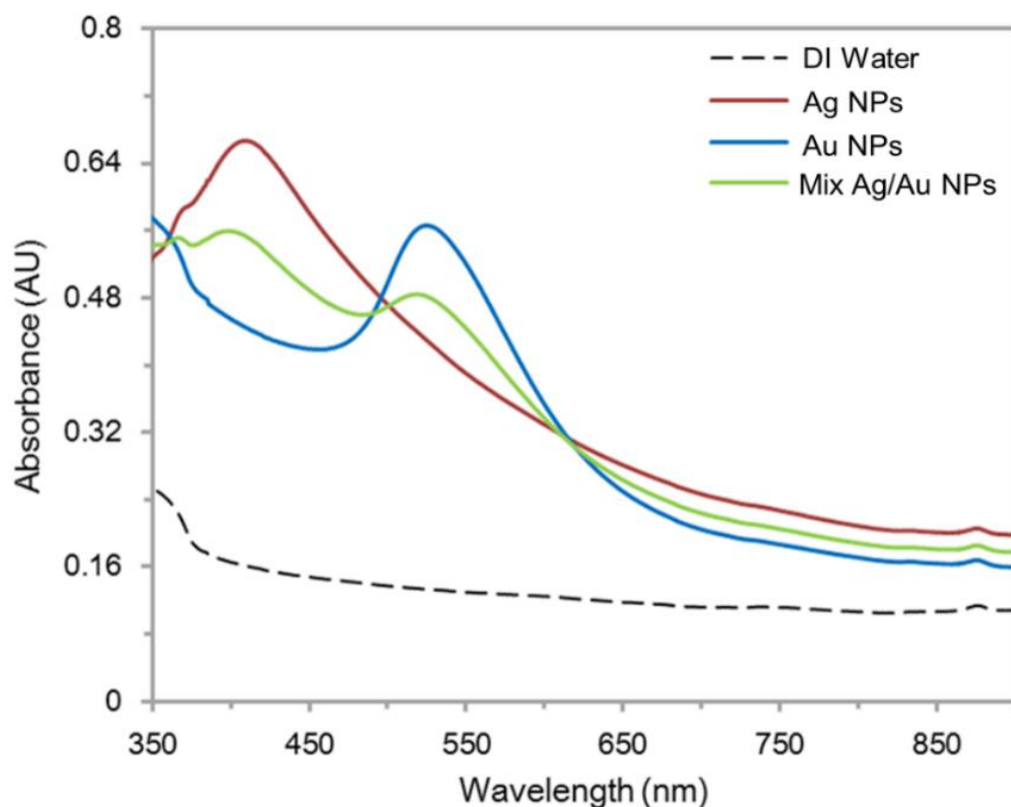
Fig. 3.9 UV/Vis absorption spectra of Ag nanoparticles (NPs), Au NPs, and Mix Ag/Au NPs

3.3.2 White light-activated bactericidal polyurethane and its characterization

A swell-encapsulation-shrink process was used to produce white light activated bactericidal polyurethane. Acetone was employed as a swelling solution. During swell-encapsulation process, as polyurethane swells in acetone, toluidine blue O (TBO) molecules and nanoparticles suspended in acetone were impregnated into the polymer matrix. The polyurethane shrinks when it is collected from acetone and dried in a dark room at normal temperature. After shrinking, the dye molecules and nanoparticles are entrapped inside the polyurethane. White light-activated bactericidal polyurethane was fabricated through the process for 24 h. As shown in Figure 3.10, TBO dye and nanoparticles were incorporated into polyurethane and the colour of the treated polymers was dark blue.
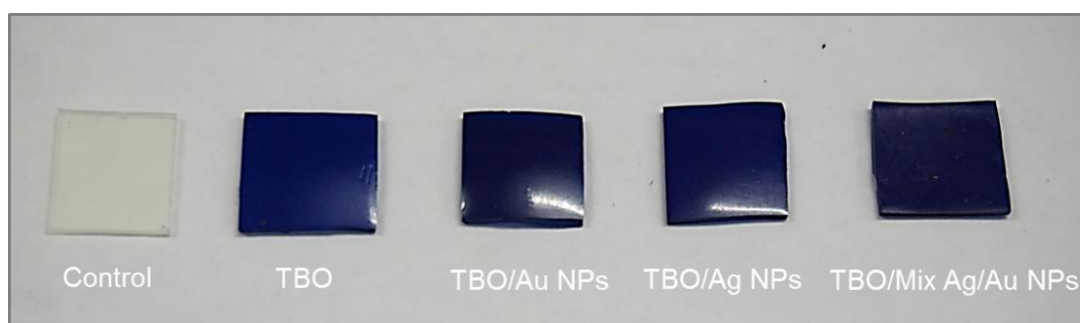
Fig. 3.10 White light-activated bactericidal polyurethane produced by swell-encapsulated-shrink process for 24 h

3.3.2.1 Fluorescence microscopy

To determine TBO dye diffusion within polyurethane, the TBO impregnated polymers for 5, 30, and 60 min were analysed by fluorescence microscopy. The TBO fluorescence on thinly sliced sample side sections were photographed by CCD camera and 633 nm laser and then the image was analysed to determine extension of TBO dye diffusion from the sample surface to inside. Figure 3.11 shows that TBO dye diffusion within the polyurethane increases with immersion time in the TBO solution. Approximately 2/3 of the sliced polymer was observed and it showed the gradient of TBO dye inside the polyurethane. Colour scale bar matches from low (black) to high fluorescence (white). The dye was mostly absorbed into near to the surface of the polyurethane at the beginning. TBO dye diffused inside sample throughout with increase of immersion time and the inside of the polymer was totally saturated with TBO dye, and this trend was also observed in other polymer samples including TBO only, TBO with Au nanoparticles, TBO with Ag nanoparticles and TBO with Mix Au/Ag nanoparticles, and difference in fluorescence between 1 h and 24 h immersed samples was not observed.
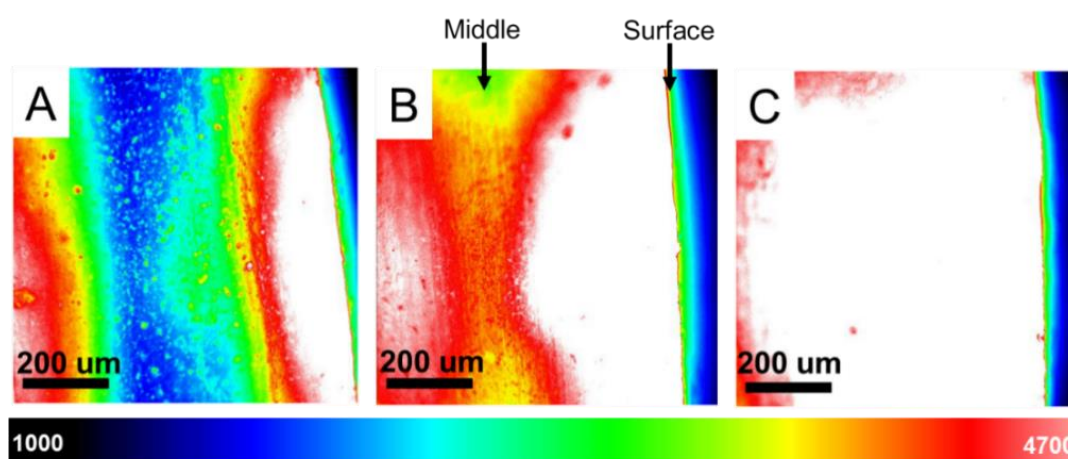
Fig. 3.11 Gradients of TBO dye inside polyurethane after swell encapsulation: (a) 5 min, (b) 30 min, and (c) 60 min. Colour scale bar runs from low (black) to high fluorescence (white). White colour indicates the dye diffusion inside the polymer.

3.3.2.2 Ultraviolet and visible absorbance spectroscopy

3.3.2.2.1 Encapsulation of nanoparticles into polyurethane

In order to determine nanoparticle uptake from the particles suspension to the polyurethane, the UV/Vis absorption spectra of nanoparticles suspension without TBO dye were measured before and after the swell-encapsulation-shrink process. Absorption decreases of Ag and Au nanoparticles suspension were measured at wavelengths of 409 nm and 526 nm, respectively. The decrease of Mix Ag/Au nanoparticles suspension was measured at both 409 nm and 526 nm. As shown Table 3.1, 8 % of Ag nanoparticles in the suspension was encapsulated in to the polymer sample and 32 and 25 % of Au nanoparticles and Mix Ag/Au NPs were absorbed in to the polymer, respectively

Table 3.1 nanoparticles (NP) uptake rate from the NPs suspension to polyurethane sample

Sample	NPs Uptake from NPs suspension to polyurethane sample (%)
Ag NPs	8 ± 0.5
Au NPs	32 ± 7
Mix Ag/Au NPs	25 ± 14

3.3.2.2.2 UV/Vis absorption spectra of white light-activated bactericidal polyurethane

For making the bactericidal polyurethane, the polymer samples were treated by TBO solutions with Ag nanoparticles, Au nanoparticles, and Mix Ag/Au nanoparticles for 24 h, and the UV/Vis absorption spectra of the polymers were measured in the wavelengths of 350–950 nm. Figure 3.12 shows the absorption spectra of control

and treated polymers. All of TBO stained polyurethanes had a main absorbance at 636 nm, and TBO stained sample with the Ag nanoparticles had the highest intensity in absorption. The shoulder peaks of nanoparticles incorporated polymers were affected by the type of nanoparticles (sample with Ag nanoparticles: 595 nm, sample with Au nanoparticles: 590 nm, and sample with Mix Ag/Au nanoparticles: 592 nm), and the absorption spectra of nanoparticles incorporated samples were broader than the TBO stained sample. This means that the addition of Ag or Au nanoparticles affected the position of the spectra feature on TBO stained polyurethane.
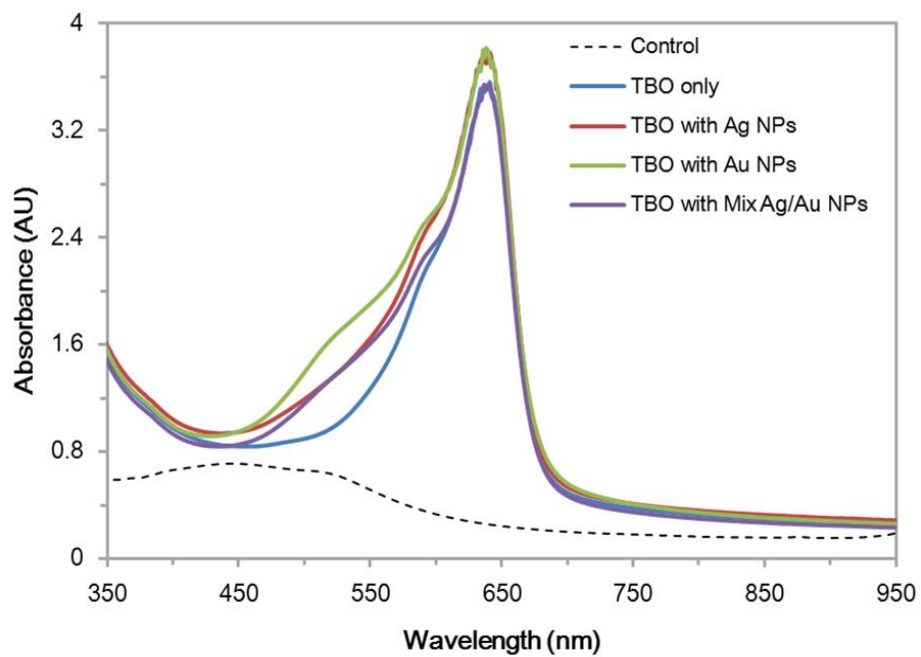
Fig. 3.12 UV/Vis absorption spectra of control, TBO stained polyurethane, and TBO stained polyurethanes with Ag nanoparticles, Au nanoparticles, and Mix Ag/Au nanoparticles.

3.3.2.3 Water contact angle and elastic modulus

Table 3.2 shows the water contact angle and elastic modulus on samples. Water contact angle of intact polyurethane was about 99.9 ° indicating hydrophobicity. However, the contact angles of the polymers reduced after the swell-encapsulation-

shrink process for 24 h. Specifically, the angle reduction of the control was the highest (the reduction: 29 °). the process made the polyurethane changed from hydrophobic to hydrophilic surface, except for the Ag nanoparticle encapsulated incorporated polymer.

Strain-stress experiments were performed in order to investigate a change in mechanical property of polyurethane samples resulted from swell-encapsulation-shrink process. Elastic modulus is a number which measures resistance of an object to being deformed elastically when a stress is applied to it. Swell-encapsulation-shrink process produce a reduction of >5.5 MPa in elastic modulus for all of the treated polymer samples and the maximum reduction was observed on TBO only sample. This indicates that mechanical durability of the treated polyurethane was lower compared to an intact polyurethane, although they are still at a usable range. This trend was similar with previous research[195]. The reduction of mechanical property and water contact angle of the polymers resulted from the swell-encapsulation-shrink process because polyurethane is vulnerable to acetone prolonged or repeated exposure[198]. Additionally, experimental results represented that the nanoparticles addition to polyurethane relieved a reduction of water contact angle and elastic modulus.

Table 3.2 Elastic stress and water contact angle of intact, control, and treated polyurethanes

Sample	Elastic modulus (MPa)	Water contact angle ($^{\circ}$)
Intact[a]	15.1 ± 1.9	99.9 ± 0.7
Control[b]	8.3 ± 0.4	70.5 ± 0.9
TBO only	6.0 ± 0.6	84.4 ± 0.9
TBO with Ag NPs	9.6 ± 0.8	90.6 ± 0.8
TBO with Au NPs	7.6 ± 0.4	88.9 ± 1.1
TBO with Mix Ag/Au NPs	8.7 ± 0.1	89.8 ± 2.1

[a] Untreated polyurethane

[b] Acetone treated polyurethane

3.3.2.4 Bactericidal test

The bactericidal activity of control, TBO stained polyurethane, and TBO stained polyurethane with Ag or Au nanoparticles alone, and Mix Ag/Au nanoparticles was tested against, *Escherichia coli*, which is a representative Gram-negative bacterium and which is a key causative agent of HAI, under white light and dark conditions. 25 µL of *E. coli* suspension (~10^6 CFU/mL) was inoculated onto the surface of control and treated polymer samples, and then they were exposed to white light source at 20°C. Another set of samples were incubated in a dark room at 20°C for the identical period of time. The light intensity of white lamp used in this study ranged from about 3900 to 5300 lux, and in the dark room, the intensity of the light was 0 lux.

Figure 3.13 and Table 3.3 exhibited bactericidal activity of control and treated polyurethanes with nanoparticles and TBO after 3 h and 24 h incubation in a dark
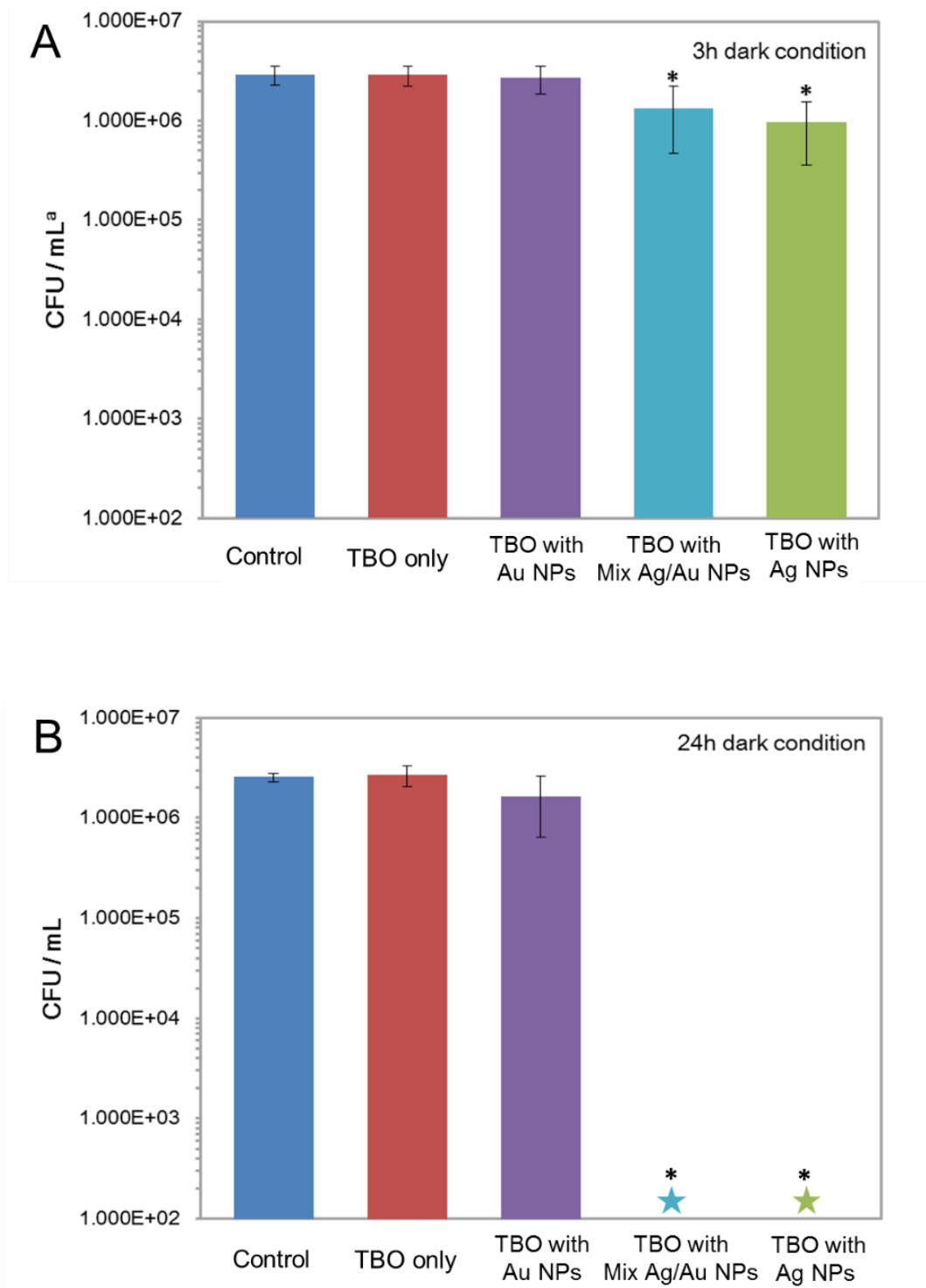
Fig. 3.13 Bactericidal activity of control and treated polyurethane (TBO only, TBO with Au NPs, TBO with Mix Ag/Au NPs, and TBO with Ag NPs) on *E. coli* in a dark room: (a) 3 h and (b) 24 h incubation

[a] Colony forming unit/mL

*P-value < 0.01

☆ lower than detection limit of 10^2 CFU/mL

room. After 3 h in the dark room, there were no decrease in the numbers of viable bacteria on the control, polyurethane with TBO only, and polyurethane with TBO and Au nanoparticles. But, compared to control, a statistically significant (*P-value* <0.01) decrease in the number of viable bacteria were shown on the polymers containing TBO and Mix Ag/Au nanoparticles or TBO with Ag nanoparticles alone: 0.34 and 0.49 log reductions in the number of viable bacteria were confirmed on TBO samples with Mix Ag/Au nanoparticles and Ag nanoparticles, respectively. After 24 h incubation in a dark room, compared to control, the decrease in the number of viable bacteria on polyurethane containing TBO only and the polymer containing TBO and Au nanoparticles was negligible while the polymer containing TBO and Mix Ag/Au nanoparticles or TBO with Ag nanoparticles alone showed a significant reduction in the numbers of bacteria (*P-value* <0.01), falling below detection limit of $<10^2$ CFU/mL.

Figure 3.14 and Table 3.3 show that bactericidal activity of nanoparticle encapsulated polyurethane without TBO in a dark room. There was no reduction in the number of viable bacteria after 3h of incubation in the dark. In contrast, the number of viable bacteria was significantly decreased in Mix Ag/Au nanoparticles encapsulated and Ag nanoparticles encapsulated samples after 24 h incubation in the dark (*P-value* o<0.01): a 2.39 log decrease in the number of bacteria was observed on Mix Ag/Au nanoparticles encapsulated polymer without TBO, and the decrease of bacteria number on Ag nanoparticles encapsulated sample without TBO reached to below detection limit.

AS shown in Table 3.3, it was shown that bactericidal activity of polyurethane containing nanoparticles and TBO was stronger than the polymer
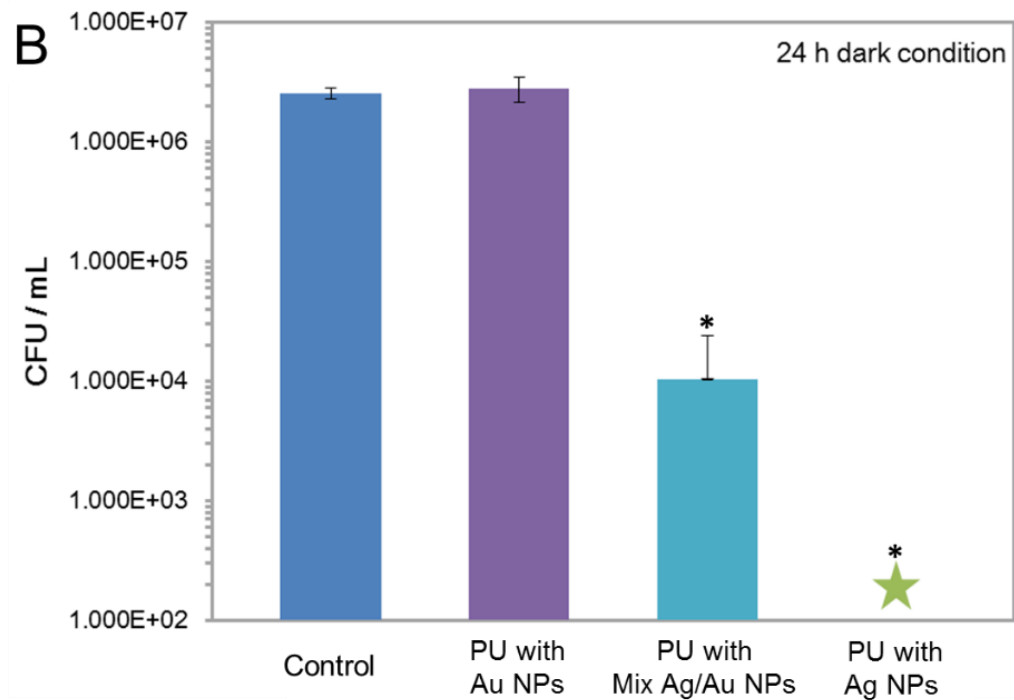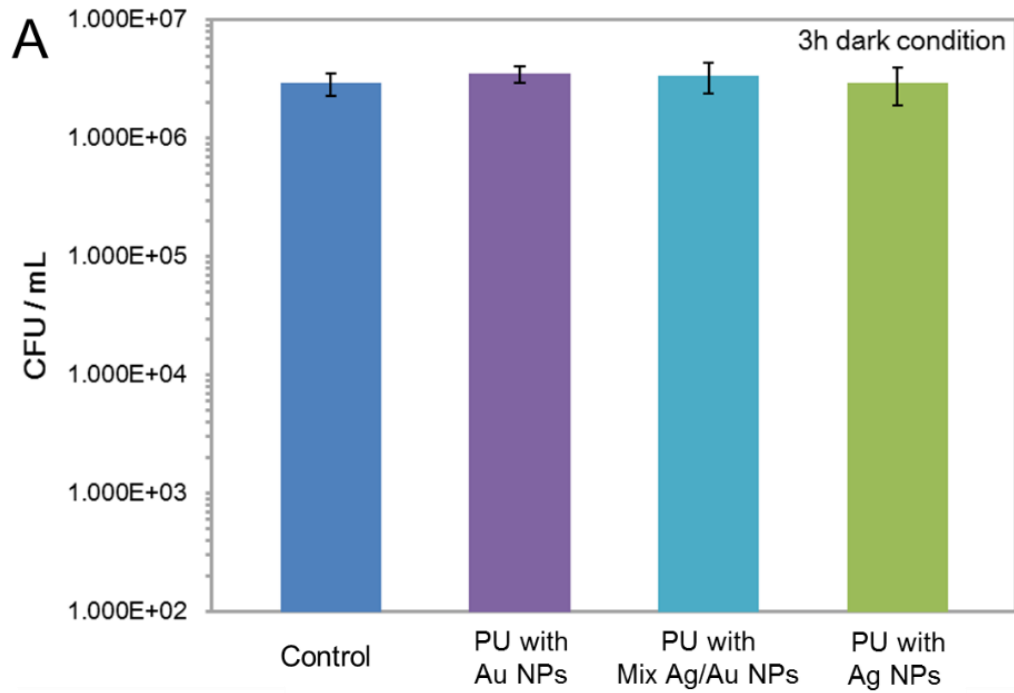
Fig. 3.14 Bactericidal activity of control and nanoparticle encapsulated polyurethane (PU) samples without TBO on *E. coli* in a dark room: (a) 3 h and (b) 24 h incubations

*P-value < 0.01

☆ lower than detection limit of 10^2 CFU/mL

containing nanoparticles only (*P-value* <0.01). This indicated that a combined effect induced by TBO and nanoparticles incorporated into polyurethane produced stronger bactericidal activity than nanoparticles only. Silver and gold nanoparticles are widely known bactericidal agent and they showed a broad bactericidal spectrum[199-201]. But, their bactericidal intensity clearly differs. For example, Ag nanoparticles have stronger bactericidal activity than Au nanoparticles at same concentration of the particle[199]. This trend agreed with our results under dark condition.

Figure 3.15 and Table 3.3 represent the bactericidal activity of control and treated polyurethane with TBO and nanoparticles in white light. In contrast to the treated polymer samples in the dark room, all of the treated polymers showed potent bactericidal activities after 3 h of white light exposure (all treated polymers: *P-value* <0.01). About 0.74 log and 1.9 log decreases in the numbers of viable bacteria were confirmed on polyurethane with TBO only and polyurethane with TBO and Au nanoparticles, respectively. The reductions of viable bacteria on the polymer with TBO and Mix Ag/Au nanoparticles and the polymers with TBO and Ag nanoparticles reached to below the detection limit after 3 h exposure of white light source. As shown in Figure 3.15 a (Table 3.3), difference in bactericidal activity of polyurethane containing Mix Ag/Au nanoparticles and polyurethane containing Ag nanoparticles was not confirmed in the experiment of 3 h white light exposure because the number of viable bacteria was lower than the detection limit. Thus, the experiment of 2 h white light exposure was conducted. As shown in Figure 3.15 b (Table 3.3), the bactericidal activity of polyurethane with Mix Ag/Au nanoparticles showed approximately 1.48 log decrease in viable bacteria number.
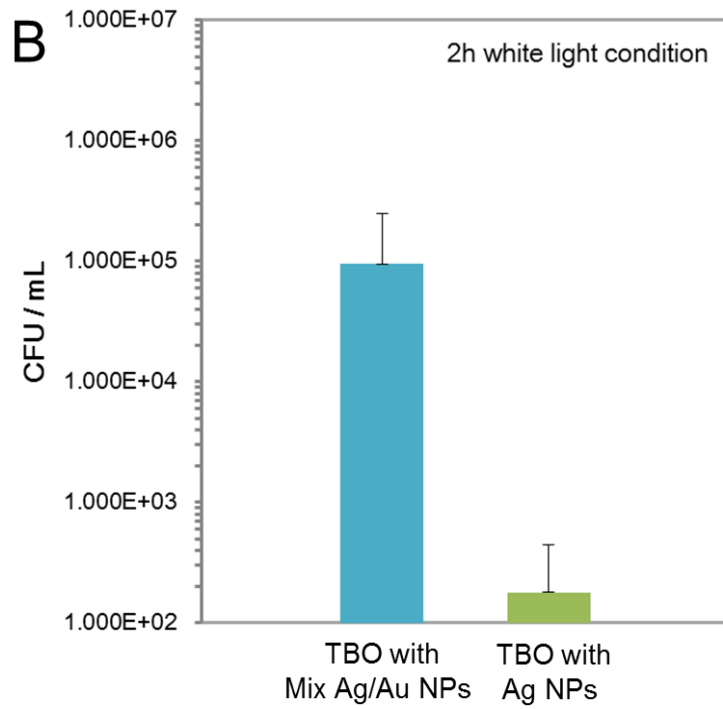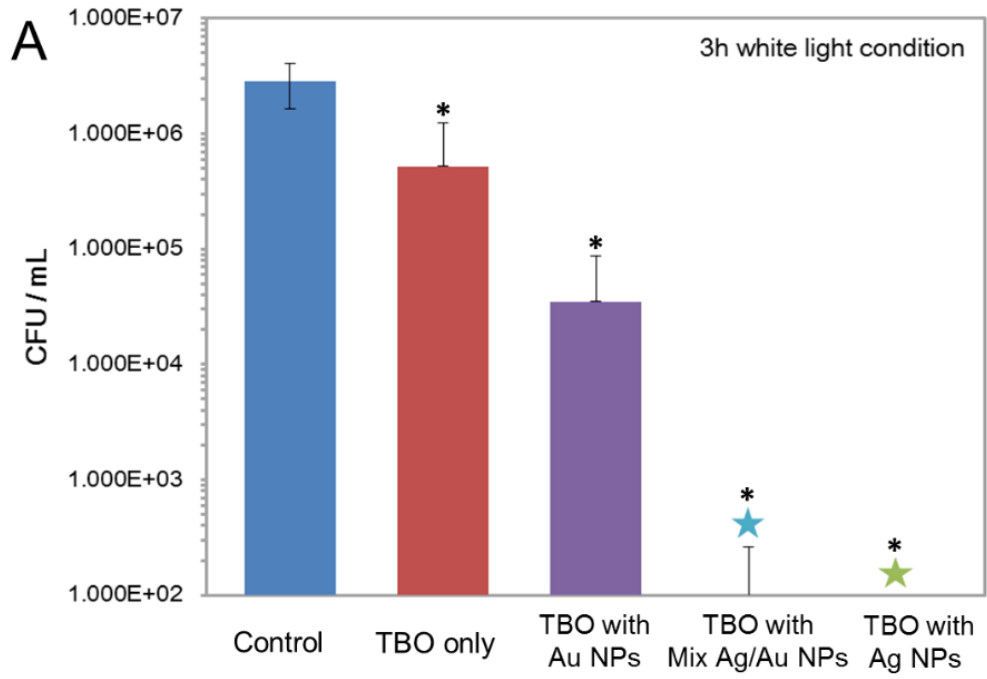
Fig. 3.15 Bactericidal activity of control and nanoparticle encapsulated polyurethane (PU) samples with TBO on *E. coli* in white light: (a) 3 h and (b) 2 h incubations

*P-value < 0.01,

☆ lower than detection limit of 10^2 CFU/mL

This is much lower than that of 3 h white light exposure. In contrast to this, the polyurethane containing Ag nanoparticles still maintained potent bactericidal activity after 2 h of white light exposure, giving a 4.2 log decrease in the number of viable bacteria. The enhanced bactericidal activity exhibited by the polymer containing Ag nanoparticles alone might be due to a higher Ag content than the polymer containing the Mix Ag/Au nanoparticles. Figure 3.16 and Table 3.3 show bactericidal activity of nanoparticles encapsulated polyurethane without TBO after 3 h of white light exposure. Nanoparticles encapsulation into polyurethane without TBO did not enhanced the bactericidal activity. However, as shown in Figure 3.15 a and Table 3.3, addition of nanoparticles into TBO stained polyurethane successfully reinforce the photobactericidal activity, indicating that an interaction of TBO molecules and nanoparticles resulted in an enhancement of photobactericidal activity.
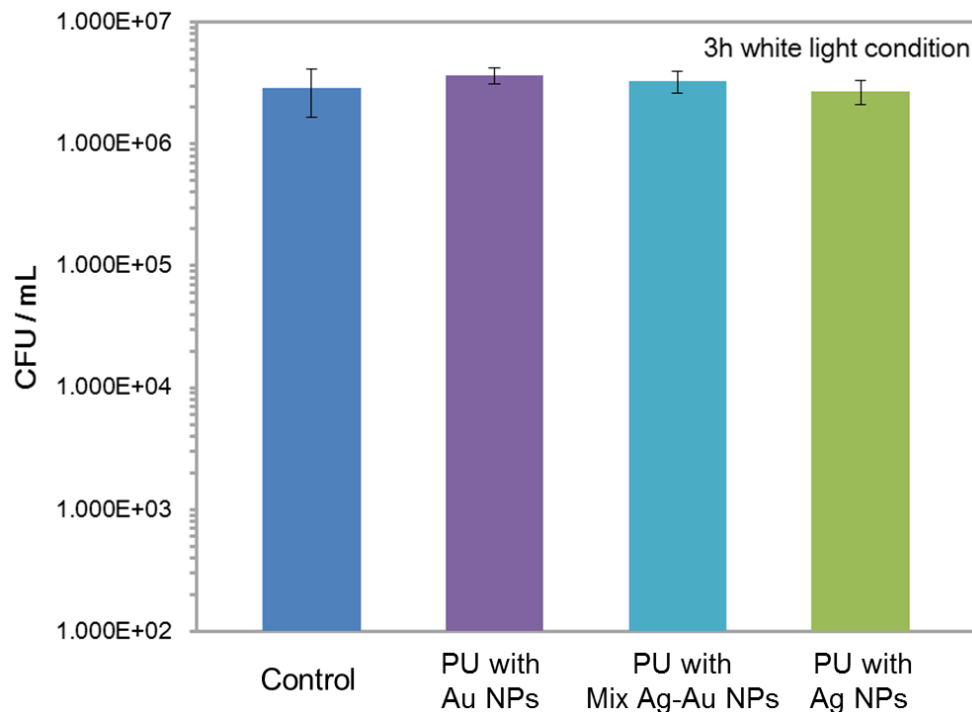
Fig. 3.16 Bactericidal activity of control and nanoparticle encapsulated polyurethane (PU) samples without TBO on *E. coli* after 3 h incubation in white light

Table 3.3 Comparison of bactericidal activity of control and treated samples on *E. coli* under dark and white light conditions

3h in dark conditions		3 h in white light conditions	
Samples	The number of viable bacteria (CFU/mL)	Samples	The number of viable bacteria (CFU/mL)
Control	$2.9 \pm 0.6 \times 10^6$	Control	$2.9 \pm 0.6 \times 10^6$
TBO only	$2.9 \pm 0.6 \times 10^6$	TBO only	$5.2 \pm 7.0 \times 10^5$
TBO with Au NPs	$2.7 \pm 0.8 \times 10^6$	TBO with Au NPs	$3.4 \pm 5.0 \times 10^4$
TBO with Ag/Au NPs	$1.3 \pm 0.9 \times 10^6$	TBO with Ag/Au NPs	$< 10^2$
TBO with Ag NPs	$9.6 \pm 6.0 \times 10^5$	TBO with Ag NPs	$< 10^2$
PU with Au NPs (without TBO)	$3.5 \pm 0.6 \times 10^6$	PU with Au NPs (without TBO)	$3.6 \pm 0.6 \times 10^6$
PU with Ag/Au NPs (without TBO)	$3.4 \pm 1.0 \times 10^6$	PU with Ag/Au NPs (without TBO)	$3.2 \pm 0.7 \times 10^6$
PU with Ag NPs (without TBO)	$2.9 \pm 1.0 \times 10^6$	PU with Ag NPs (without TBO)	$2.7 \pm 0.6 \times 10^6$

24 h in dark conditions		2 h in white light conditions	
Samples	The number of viable bacteria (CFU/mL)	Samples	The number of viable bacteria (CFU/mL)
Control	$2.6 \pm 0.2 \times 10^6$	TBO with Ag/Au NPs	$9.6 \times 10^4 \pm 2.0 \times 10^5$
TBO only	$2.7 \pm 0.6 \times 10^6$	TBO with Ag NPs	$3.4 \pm 0.5 \times 10^4$
TBO with Au NPs	$1.6 \pm 1.0 \times 10^6$		
TBO with Ag/Au NPs	$< 10^2$		
TBO with Ag NPs	$< 10^2$		
PU with Au NPs (without TBO)	$2.8 \pm 0.6 \times 10^6$		
PU with Ag/Au NPs (without TBO)	$1.0 \pm 1.0 \times 10^4$		
PU with Ag NPs (without TBO)	$< 10^2$		

The mechanism of photobactericidal activity could be explained as follows; as being exposed to white light, TBO molecules impregnated polymer are excited from a low ground state to a triplet state[156]. The triplet state molecules undergo via type I (biomolecular reaction) or/and type II (reaction of molecular oxygen) photochemical

reaction to generate ROS which kill bacteria[156]. It was speculated that the addition of nanoparticles reinforced type I and/or type II photochemical reaction of TBO molecules.

The enhancement on bactericidal activity of photoreaction dyes by Au nanoparticles was shown in previous studies[158,160], but that by silver nanoparticles was not reported. Our study showed that Ag nanoparticle encapsulated polymer had >2.54 log higher bactericidal activity than Au nanoparticles after 3 h white light exposure. This means that Ag nanoparticle would be a better material in enhancement of photobactericidal activity than Au nanoparticles.

In previous studies, the research on Ag nanoparticles coated titania film reported that silver addition on titania film could reinforce photobactericidal behaviour of it; under white light condition (5000 lux), the silver added film showed a photobactericidal effect with a 4.4 log reduction in the number of *E. coli* bacteria within 6 h[202]. However, this study confirmed that the combination of Ag nanoparticles and TBO generate stronger photobactericidal activitiy than combination of Ag nanoparticles and titania film. Additionally, in the comparison of dual-dyed polymer with nanoparticles and zinc oxide nanoparticles encapsulated polymer that our group previously reported[159,161,196], Ag nanoparticle and TBO incorporated polymer could decrease the number of viable bacteria to the detection limit in a shorter period of time under comparable white light conditions.

In order to apply the white light-activated bactericidal polymer to the real world, human health effects caused by the polymer must be considered. Because silver nanoparticles have been commonly utilized in medicine, food packing industry, and water disinfection, the toxicity of the particles has been investigated extensively[203-

103

[207], it was reported that their effects are dependent on dosage, exposure time, and size, and in vivo studies on rats showed that silver nanoparticles only had adverse effects after long-term inhalation or ingestion[204,208,209]. According to the Occupational Safety and Health Administration (OSHA) in the USA, toluidine blue O was known to be non-hazardous material although it represented some toxic effect with high concentration inhalation or ingestion[210-212]. In previous researches, long-term leaching tests showed bactericidal polymer produced by a swell-encapsulation-shrink technique is quite stable[159,161]. Thus, it is expected that nanoparticles or toluidine blue O encapsulated into polyurethane would not produce adverse effect on human health. Additionally, long-term photostability of the dye encapsulated into polyurethane is also important for real world applications because it is correlated to a persistence of bactericidal activity. Our previous research showed that after 29 days exposure of white light source with an intensity of ~12,500 lux, which is ~125 times more intense than the lamps in hospital wards and corridors, dye inside the polymer kept its photostability[159]. Thus, it is speculated that the polymers developed in this chapter maintain their photobactericidal activity over a long period of time in the real world.

3.4 Conclusion

In this chapter, silver and gold nanoparticles were synthesized through citrate reduction in $HAuCl_3$ or $AgNO_3$ solution at boiling point, forming polydisperse Ag and Au nanoparticles with 22.4 and 34.4 nm in average size, respectively. The nanoparticles were mixed with TBO solution, and then incorporated into flat polyurethane. Fluorescence microscopy showed that in the swell process, TBO diffused throughout the polymer with time, resulting in its saturation in the polymer,

and UV/Vis spectroscopy showed that the nanoparticles were encapsulated into the polymer during the process.

For the first time, toluidine blue O in combination with silver nanoparticles were encapsulated into a polyurethane which is widely used in healthcare devices. The addition of silver nanoparticles and toluidine blue O into the polymer produce a potent photobactericidal surface; it produced not only a lethal photobactericidal activity on *E. coli* in white light (3 h exposure), but also showed a potent bactericidal activity in the dark (24 h exposure), resulting in that the number of viable *E. coli* bacteria was lower than the detection limit. The bactericidal surface which we developed has potential to keep low bacteria levels and minimise the risk of HAIs transmission in healthcare facilities. In particular, it would be useful to reduce the number of urinary tract infections which are one of the main HAIs. Urinary tract infections are mainly attributed to the use of indwelling urinary catheters: catheter associated infections account for 80 % of urinary tract infections[213]. It is expected that our technique can be easily applied to catheters which is a polymer based material [158]. Additionally, it is also able to be applied to a variety of polymer based medical devices such as covers of keyboards, telephones and tablet PCs.

Chapter 4: Combination of acrylic latex and crystal Violet; white light-activated bactericidal paint

4.1. Introduction

Healthcare-associated infections (HAIs) are a serious issue for healthcare facilities in UK and USA: there were 300,000–718,000 HAI incidents of hospitalized patients annually, and 1–10% of these patients were killed by the infection[4,214,215]. Hospital surface contamination including electronic devices, door handles, food trays, and plates acts as bacteria reservoir contributing to HAIs spread[162,163]. Although a number of HAIs decreased through a variety of schemes including surveillance, disinfection, sterilization, cleaning, and regulation, the infection and death rate is still high, indicating that antimicrobial surfaces are required[4,216,217].

In chapter 3, we introduced novel white light-activated bactericidal surfaces

produced through encapsulation of silver nanoparticles and toluidine blue O into medical grade polyurethane. The results showed that polyurethane based surfaces in hospitals can be transformed into potent photobactericidal polymer through a simple swell-encapsulation-shrink technique. This chapter details white light-activated bactericidal paint which can be readily applied to a range of surfaces. Combination of crystal violet and acrylic latex results in phtobactericidal paints. These novel photobactercidal paints were tested against *E. coli*, a Gram-negative bacterium. The bactericidal paints represented a potent bactericidal activity in dark and it showed significantly enhanced bactericidal activity in white light.

4.2 Experimental

4.2.1 preparation of bactericidal paint
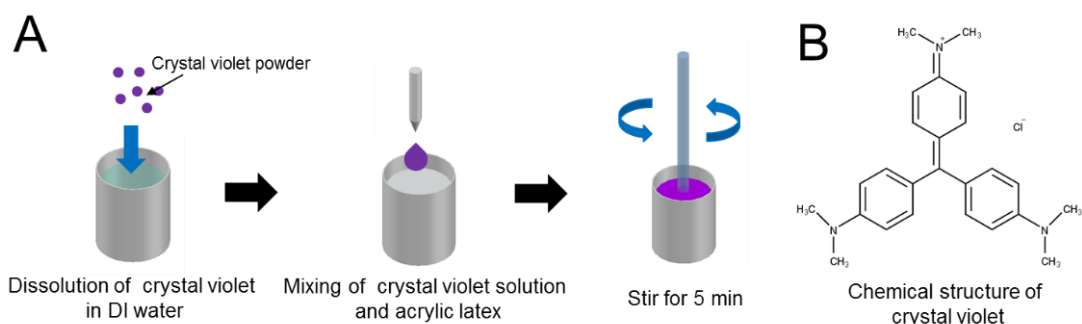
Fig. 4.1 Preparation of light activated bactericidal paint

As shown in Figure 4.1 a, crystal violet (Sigma-Aldrich, St. Louis, MO, USA) was used to produce light activated antimicrobial paint. 100 mg of crystal violet powder which is a triarylmethane dye (Figure 4.1 b) was dispersed in 10 ml of deionized water to make crystal violet solution of 10,000 ppm (24.5 mM), and then it was sonicated for 5 min. The mixture was mixed with acrylic latex (AzkoNovel,

Amsterdam, Netherlands) which is made up of an acrylic resin binder, and water. Bactericidal paints containing crystal violet 250, 500, 750, and 1000 ppm (crystal violet 0.61, 1.23, 1.84, and 2.45 mM) were produced.

4.2.2 Ultraviolet and visible absorbance spectroscopy
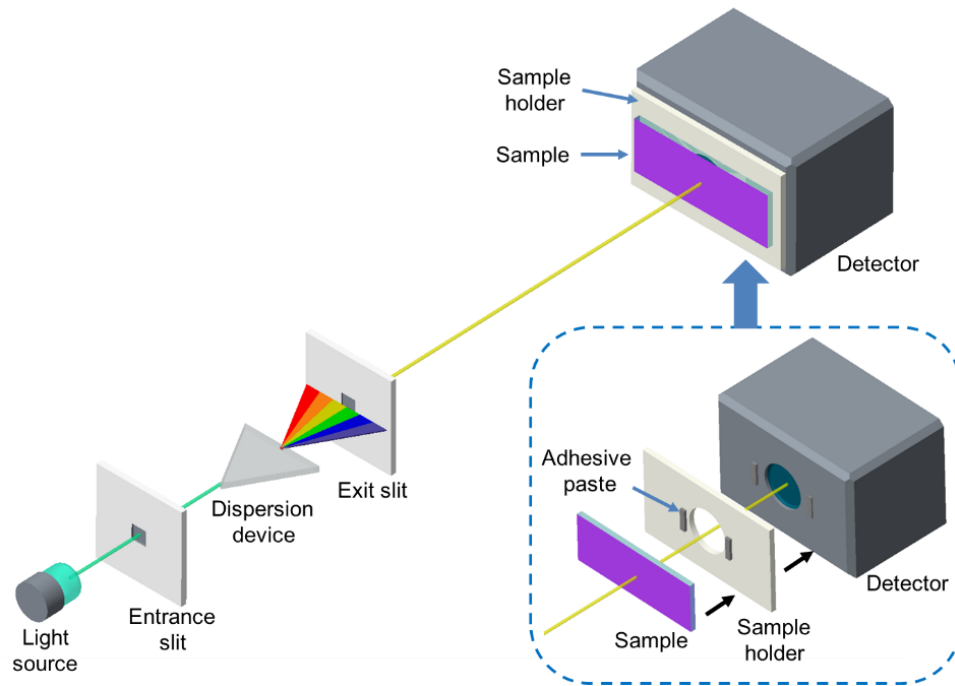
Fig. 4.2 Ultraviolet and visible absorption measurement on samples

For characterising ultraviolet and visible absorption spectrum of light activated bactericidal paint, UV/Vis spectrometer (Lambda 25, PerkinElmer Inc., Winter St., CT, USA) which has a detection range of wavelengths 190–1100 nm, was used. 1.5 mL of light-activated bactericidal paint was injected to the surface of glass slide (2.5 cm $\times$ 7.5 cm), and the surface was tilted for the paint to cover the surface of the glass. After that, it was dried in dark room for 24 h. Absorption spectra of the painted glasses were measured from 400 to 900 nm.

4.2.3 Water contact angle

The equilibrium water contact angle on the painted samples was measured using water contact angle meter (First Ten Angstroms, Inc., Portsmouth, Virginia, United States). A water droplet was dropped onto the samples from a gauge 27 needle, the images of samples were taken side on and they were analyzed using Surftens 4.5 software. The volume of inoculated water droplet (~5 µL) was controlled by the water contact angle meter and software FTA 32 (First Ten Angstroms).

4.2.4. Leaching test

The stability of white light activated bactericidal paint was determined. Thermoplastic polyurethanes (American Polyfilm Inc, Branford, CT, USA) (1.5 cm × 1.5 cm) were coated by 0.6 mL of the bactericidal paint, and they were dried in the dark room for 24 h. The painted samples were placed in 5 mL phosphate buffer saline (PBS) solution at room temperature for 120 h. Ultraviolet and visible absorption spectra of the solutions were periodically measured to determine if crystal violet molecules were leaching from the paint into PBS solution. The PBS absorbance at 590 nm was measured and it was compared with crystal violet calibration curve to determine the concentration of released crystal violet.

4.2.5 Bactericidal test

In order to determine the bactericidal activity of the painted sample, *E. coli* (ATCC 25922) was used in this chapter. *E. coli* bacteria, which were stored in Brain-Heart-Infusion broth (BHI, Oxoid Ltd., Hampshire, England, UK) including 20% (v/v) glycerol at $-70^{\circ}C$, were propagated on MacConkey agar (Oxoid Ltd., Hampshire,

England, UK). One bacteria colony was inoculated into 10 mL of BHI broth and then incubated with shaking of 200 rpm at 37 °C. After 18 h incubation, the bacteria were collected by centrifugation (20 °C, 4000 rpm for 20 min), and washed by 10 mL of PBS. This process was repeated twice. The washed suspension was diluted into 1/1000 to get ~10^6 colony forming units per millilitre (CFU/mL).
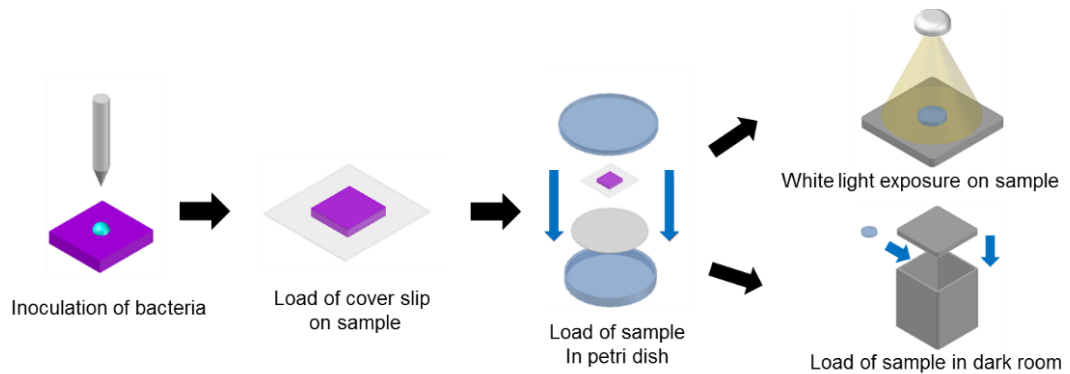
Fig. 4.3 bactericidal test on sample in white light and in dark

As shown in Figure 4.3, 25 µL of bacteria suspension was inoculated on to the sample and a sterile glass cover slip (2.2 cm × 2.2 cm) was placed on to the inoculated sample to get good contact between the surface of the sample and bacteria. The samples were placed into petri dishes with wet paper to keep humidity, and they were exposed to white light. Another set of samples was placed in a dark room. The samples were located into 5 mL of PBS solution after white light irradiation, and vortexed for 1 min to resuspend the bacteria from the sample to the PBS. The bacteria suspension was diluted, and 100 µL of the suspension was plated onto MacConkey agar, and cultured at 37 °C for 24 hours. The colonies grown on the agars were counted.

4.2.6 White light lamp exposure

The light source selected in present study was 28 W white fluorescent lamp (GE Lighting, East Cleveland, Ohio, USA). The light intensity was about 4400 lux in average. Details on information of the light source was stated in Section 3.2.2.8

4.2.7 Statistical analysis

Mann–Whitney U test, linear regression, and Pearson correlation coefficient on results were calculated using the SPSS software (SPSS, Inc., Chicago, IL, USA).

4.3 Result and discussion

4.3.1 Preparation of bactericidal paint

In order to produce white light-activated bactericidal paints, crystal violet powder and acrylic latex were employed in this study. Crystal violet, a triarylmethane dye, is readily dissolved in water, ethanol, and acetone[159,190,191]. Crystal violet is used for classification of bacteria, it is also used as medical first aid because of its disinfection actions containing antibacterial, antifungal, and anthelmintic properties, and it was shown to act as a white light-activated bactericidal agent[149,159,218]. Acrylic latex, mixture of water and acrylic resin, is widely used in a ingradient of household paint. As shown in Figure 4.4 a, bactericidal paints with various concentrations of crystal violet were produced. As crystal violet was added into acrylic latex, the colour of paint changed to bright violet from white, and the violet colour came to be more intense with increasing concentration of crystal violet in the paint. Figure 4.4 b shows the glass slide coated by white light-activated bactericidal paint. Glass slides

were dipped in the bactericidal paint for 5 s, then collected from the paint, followed by that the painted slide was placed in a dark room for 24 h. After the drying process, the colour of the paint without crystal violet changed from white to colourless, and paints containing crystal violet kept their colour. But, contrary to liquid state paints, it was not observed that the colour intensity of bactericidal paints increased with increasing concentration of crystal violet in the paint.
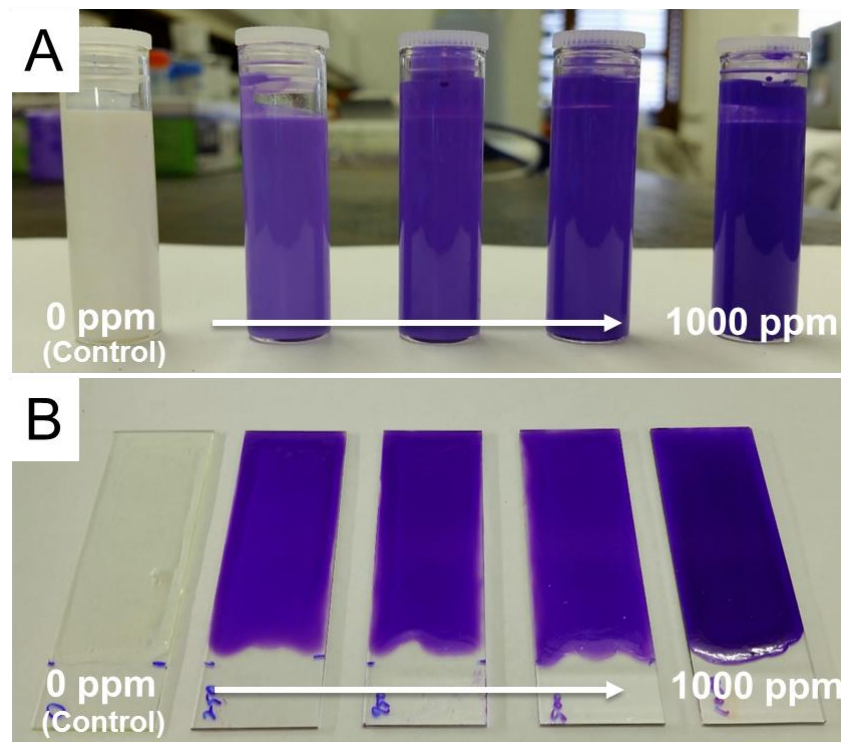
Fig. 4.4 (a) white light-activated bactericidal paints, and (b) the paint coated glass slides

4.3.2 Ultraviolet and visible absorbance spectroscopy

The light absorption spectra of control and the bactericidal paints were measured in the wavelengths of 400–900 nm by UV/Vis Spectrometer. Because the absorption values of paints including >250 ppm (>0.61mM) of crystal violet exceeded the detection limit of the spectrometer, the bactericidal paints were diluted into 1/10 in

order to measure their spectrum features. After dilution, the colour intensity of the bactericidal paints was lower than the original ones. As shown in Figure 4.5, UV/Vis absorption spectra exhibited that all of the bactericidal paints containing crystal violet had a main absorption at 590 nm, and the peak and spectrum range of absorbance increased with the concentration of crystal violet in the paint. The spectrum features of bactericidal paints were different from crystal violet incorporated polymers introduced by previous studies; the absorption spectra of bactericidal paint containing crystal violet had a normal distribution while the spectra of crystal violet incorporated into polymers showed a bimodal distribution[159,196].
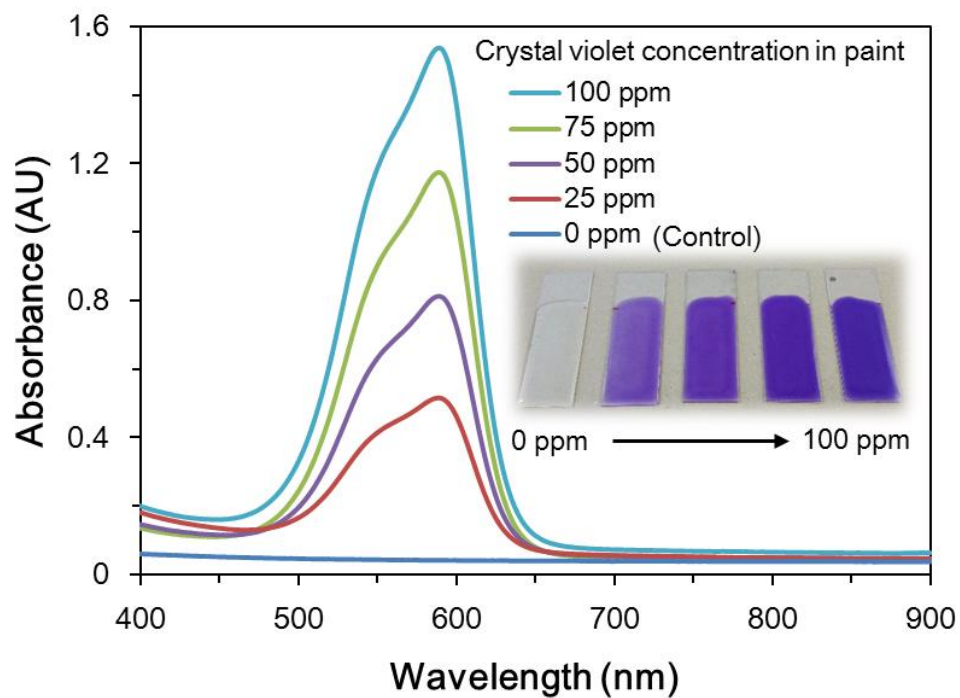
Fig. 4.5 UV/Vis absorption spectra of control and white light-activated bactericidal paints. The bactericidal paint containing 0, 25, 50, 75, and 100 ppm of crystal violet.

In previous studies, a mixture of acetone and water were used as solvent whereas in this chapter acrylic latex and water were used[159,196]. According to previous research, the absorption spectrum feature of crystal violet can be changed by the type of

solvent such as acetone, methanol, and water, and the spectra have different peaks in the wavelengths of 500–650 nm[156,159,160,219]. Thus, it is speculated that the difference of solvent used between them produced the different spectral features of crystal violet. Regardless of the concentration of crystal violet in the paint, all of the bactericidal paints presented comparable spectra.

4.3.3 Water contact angle
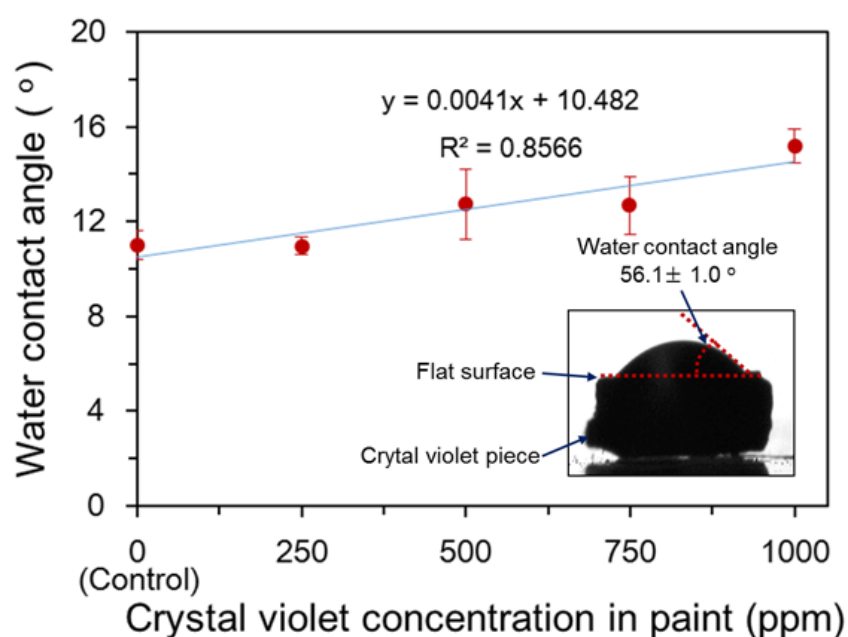
Fig.4.6 Water contact angle on white light-activated bactericidal paints containing 250, 500, 750, and 1000 ppm (0.61, 1.23, 1.84, and 2.45 mM) of crystal violet. To measure water contact angle on crystal violet, a flat crystal violet tablet which was purchased from Sigma-Aldrich was used.

In order to determine the change in water contact angle after mixing of crystal violet and acrylic latex, polyurethane (1.5 cm × 1.5 cm) was coated by white light-activated bactericidal paints through dipping coating and dried in a dark room for 24 h. The equilibrium water contact angle of control and the bactericidal paints was measured using a contact angle meter. As shown in Figure 4.6, the water contact angle of the

control (paint without crystal violet) was approximately 10.9 °, and the angle increased with the concentration of crystal violet ($r^2 = 0.8566$), and the water contact angle was the highest at 1000 ppm of crystal violet. The increase of water contact angle at 1000 ppm was about 4.2 °, compared to the control (*P-value* <0.01). This can be explained because as shown in Figure 4.6 inset, crystal violet is more hydrophobic than the control (acrylic latex), the increase of the amount of crystal violet in acrylic latex made an important contribution to the change in water contact angle.

4.3.4 Leaching test

Crystal violet release from white light-activated bactericidal paints in PBS solution was investigated by a UV/Vis spectrometer. The bactericidal paint coated polyurethanes were placed into 5 mL PBS solution for 120 h (5 days) and the crystal violet release at a wavelength of 590 nm was measured at intervals of 24 h. Figure 4.7 represents crystal violet leaching from the paint coated polymers to PBS solutions for 120 h. It was observed that all of the bactericidal paints released some crystal violet into PBS solution after 24 h and that the concentration of the leached crystal violet was the highest (0.27 ppm) on the bactericidal paint with 1000 ppm of crystal violet: 0.04, 0.07, and 0.14 ppm was leached from the bactericidal paints with 250, 500, and 750 ppm of crystal violet, respectively. Over a period of more than 72 h, additional leaching of crystal violet was not observed in all of the bactericidal paints. The crystal violet leached from the paints in a period of 120 h was quite minor (less than 0.03 %).
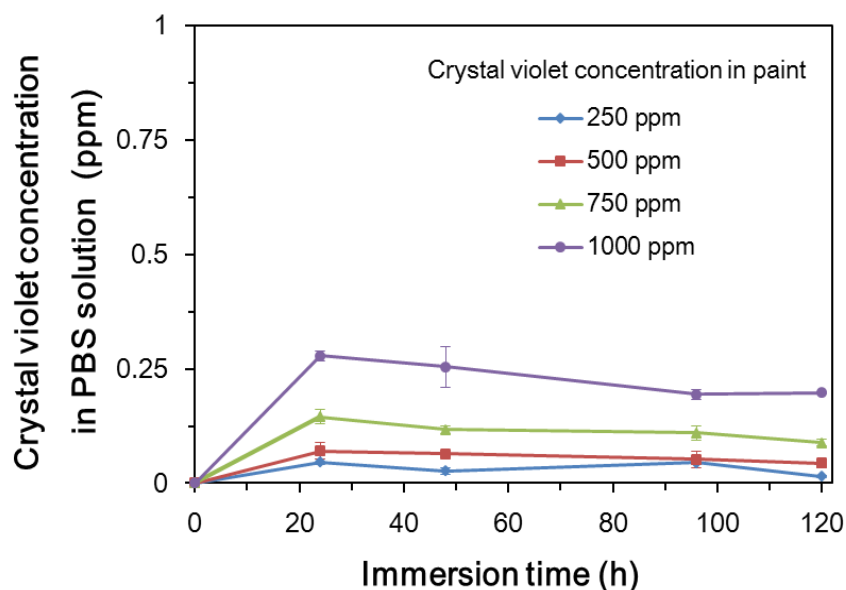
Fig. 4.7 Leaching of crystal violet from white light-activated bactericidal paint coated polyurethane into PBS solution for 120 h

4.3.5 Bactericidal test

For bactericidal test of the paints, polyurethane was coated by the bactericidal paints and dried for 24 h in a dark room. The bactericidal painted polymers were tested on *Escherichia coli*, which is a Gram-negative bacterium under white light and dark conditions. 25 µL of *E. coli* suspension containing ~10^6 CFU/mL was inoculated onto the surface of the painted polyurethane, and they were exposed to white light at 20°C. Another set of the inoculated polymers were incubated in a dark room at 20°C for the identical period of time. The light intensity of white lamp was approximately 4400 lux in average, and in the dark room, the intensity was 0 lux.

Figure 4.8 a shows the bactericidal activity of white light activated bactericidal paints under dark conditions. After 6 h incubation in a dark room, about 0.12 log decrease in the numbers of viable bacteria was confirmed at 250 ppm of crystal violet, compared with the control, and it was observed that the bacteria number

decreased with concentration of crystal violet ($R^2 = 0.996$, *P-value* <0.1) inside the paint. 0.31 and 0.49 log decreases were confirmed at 500 and 750 ppm of crystal violet, respectively, and approximately 1.21 log reduction in the number of viable bacteria was observed at 1000 ppm of crystal violet. Crystal violet used as white light-activated bactericidal agent has its intrinsic bactericidal activity without a light exposure. The dye prevents bacteria growth through interaction between CV^+ ions released from CV and bacteria cell[184,220]. The results of bactericidal paint under dark condition indicate that crystal violet maintained its intrinsic bactericidal behaviour after combination with acrylic latex.

Figure 4.8 b shows the bactericidal activity of the bactericidal paints under white light condition. As that under the dark condition, it was observed that the decrease in the numbers of viable bacteria increased with increasing concentration of crystal violet after 6 h of white light exposure ($R^2 = 0.811$, *P-value* <0.1). But, a statistically significant difference in bactericidal activity of the samples under the white light condition compared to the dark condition was confirmed (comparison of all conditions under white light and dark conditions: *P-value* <0.05). After 6 h white light exposure, compared with the control, 0.36, 0.43, and 0.86 log decreases in the viable bacteria number were shown at 250, 500, and 750 ppm of crystal violet, respectively and the reduction of viable bacteria number reached to below the detection limit (<10^3 CFU/mL) at 1000 ppm of crystal violet. Further, the difference in bactericidal activity between the paints in the light and dark conditions increased with concentration of crystal violet inside the paint. The difference was 0.48 log at 250 ppm of crystal violet and it increased by 0.43 log at each increment of 250 ppm of crystal violet.
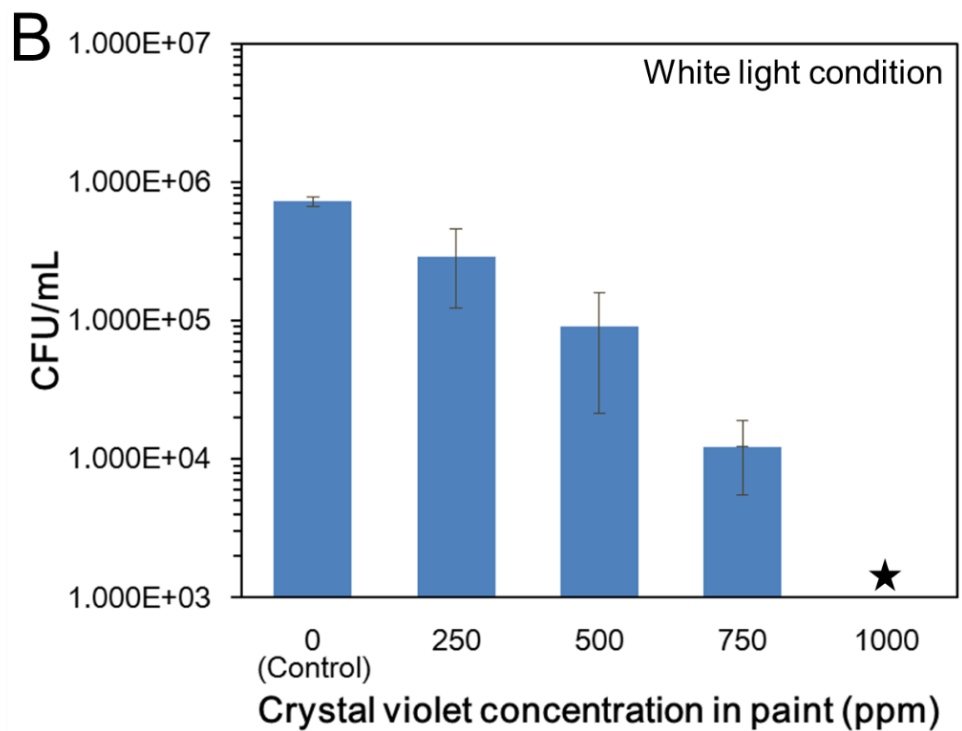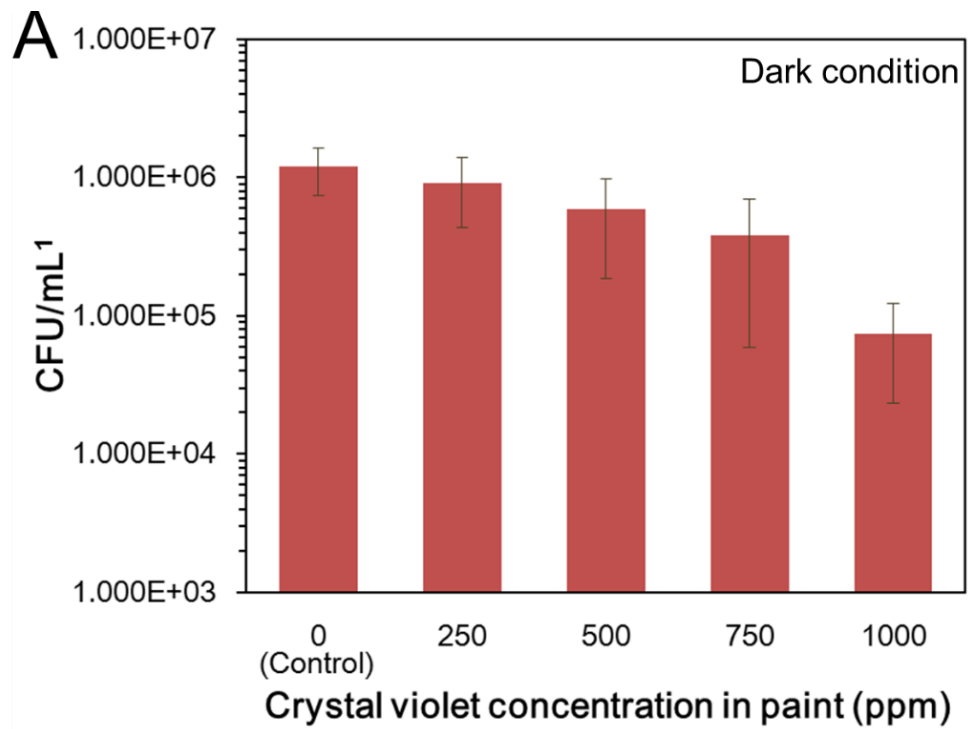
Fig. 4.8 Batericidal activity of the paints against *E. coli*: (a) 6 h incubation under the dark condition, and (b) 6 h incubation under white light condition.

[1] Colony forming unit/ mL

★ Below detection limit of 1000 CFU

The variation between white light and dark conditions was the highest (>1.8 log) at 1000 ppm of crystal violet.

The mechanism of bactericidal activity of the paint in white light condition can be explained as follows: on being exposed to white light, crystal violet molecules inside the paint are excited *via* an intersystem crossing from a low ground state to a triplet state. Crystal violet molecules in the triplet state undergo one or both of two photochemical action pathways[158]; type I (biomolecular reaction) and type II (reaction of molecular oxygen) photochemical reactions. Through the process, reactive oxygen species (ROS) and singlet oxygen ($^1O_2$) are produced. The produced ROS and $^1O_2$ can initiate multi-site attacks on bacteria leading to the cell death[156].

Since the first synthesis of crystal violet in 1883, it has been applied to a wide range of fields[221,222]. Crystal violet has been used as a gradient of black or blue ink for printing, printer and ball pen, and to colourise products containing leather, and fertilizer and it has been medically used for marking surgical site, treating bacterial and fungal infections, and controlling burn wounds or inflammations. However, several studies reported that crystal violet may have dosage-related carcinogenic potential and prolonged or repeated ingestion and skin exposure may cause a mild irritation, peritonitis, and weight loss[222-224]. Additionally, The Food and Drug Administration in US (FDA) concluded that there is not enough scientific data to prove that use of crystal violet in animal feed is safe[225]. In this chapter, the stability experiment showed that the amount of crystal violet leached out from the photobacterial paints was quite minor (<0.27 ppm) indicating that the paint was stable. Thus, we believe that the paints will have minor effects on human health.

4.4 Conclusion

In this chapter, crystal violet was mixed with acrylic latex which is widely utilized in commercial paints to make a white light-activated bactericidal paint. UV/Vis spectroscopy showed that the paints have main light absorption at a wavelength of 590 nm, indicating that paints can produce a photoreaction by visible light. Bactericidal experiments showed that the bactericidal paints not only showed a potent photobactericidal activity but also represented bactericidal activity in the dark; the number of viable bacteria was below detection limit on the paint containing 1000 ppm of crystal violet after 6 h of white light exposure and the number of viable bacteria reduced by 1.21 log on the paint after 6 h in dark. Additionally, in the leaching test for 120 h, a minor leaching of crystal violet was observed from the paint into PBS solution indicating that the paint is stable.

Techniques introduced by previous studies showed a good bactericidal activity. However, most of them including physiochemical modification, swell-encapsulation-shrink, and chemical vapor deposit cannot be applied to all substrates. As shown in Figure 4.9, the bactericidal paints that we developed in this study can be readily applied to various substrates such as metal, paper, glass, and hard and soft polymers. Additionally, our paint is easy to fabricate and the surface coating using the paint is simple and easy to prepare. It is predicted that white light-activated antimicrobial paint could be used in healthcare facilities including surgery room, dialysis room, and nursing room and it can be also applied in the home for decoration.
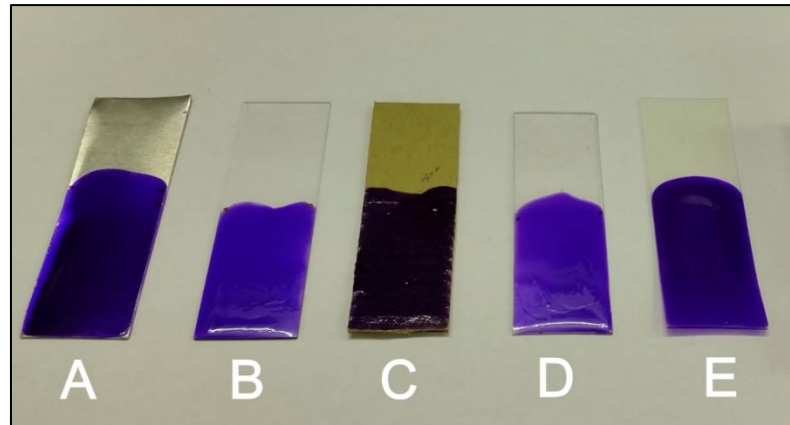
Fig. 4.9 White light-activated bactericidal paint coated (a) aluminum, (b) glass, (c) paper (d) polystyrene, and (e) polyurethane

Chapter 5: Combination of TiO$_2$ nanoparticles, 1H, 1H, 2H, 2H-perfluorooctyltriethoxysilane, and white light-bactericidal agents to produce a dual-functional surface; superhydrophobic and photobactericidal paints

5.1 Introduction

It is a good strategy to develop antimicrobial surfaces containing superhydrophobic and bactericidal properties because killing bacteria while keeping inhibition of bacteria adhesion can effectively minimize biofilm formation on surfaces[226]. Many attempts have been performed to develop the dual functional surfaces. Chung *et al.* (2012) showed that silver and 1H,1H,2H,2H-perfluorodecanethiol doped surface had superhydrophobic and bactericidal activities: compared to polystyrene, 77% inactivation of *Pseudomonas aeruginosa* and less bacteria surface coverage (85% reduction) was observed on the dual functional surface[169], and Berendjchi *et al.* (2011) showed that 0.5% copper doped silica surface had a high water contact angle

and bactericidal activity (92–99% reduction in the number of viable *E. coli and S. aureus*), but its anti-biofouling behavior was not shown[227]. Yamauchi *et al.* (2011) showed that combination of polytetrafluoroethylene (PTFE) which is widely used to produce superhydrophobic surface and N-doped TiO$_2$ did not achieved superhydrophobicity but it showed photobactericidal activity under visible light[228].

Chapter 3 and 4 focused on developing photobactericidal surfaces using nanoparticles, polymer, and crystal violet or TBO. This chapter introduces superhydrophobic and photobactericidal paints, which resulted from chemical combination of TiO$_2$ nanoparticle, 1H, 1H, 2H, 2H-perfluorooctyltriethoxysilane, crystal violet and toluidine blue O. Superhydrophobic and anti-biofouling properties were observed from the dual functional paint coated slides. In the bactericidal test of *E. coli and S. aureus*, the painted slide represented a potent photosterilization in white light and even it showed strong bactericidal activity in the dark. Moreover, the treated slides worked even after hexadecane oil contamination. The techniques introduced in this chapter can be readily used in a variety of substrates containing plastic, paper, and glass.

5.2 Experimental

5.2.1 Preparation of the dual functional paint

Solution A: 1.0 g (2×10^{-3} mole) of 1H, 1H, 2H, 2H-perfluorooctyltriethoxysilane (PFOTES, C$_8$F$_{13}$H$_4$Si(OCH$_2$CH$_3$)$_3$, Sigma-Aldrich, St. Louis, MO, USA) and 99.0 g of pure ethanol (EDM Millipore Co., Billerica, MA, USA) were mixed together and then it was stirred for 1 min

TiO₂ paint: 4.0 g (50 × 10⁻³ mole) of TiO₂ nanoparticles (P 25, Thermo fisher scienctific, Waltham, MA, USA) and 40 mL of solution A was mixed together under constant agitation, and then, it was sonicated for 5 min and agitated for 5 min.

Toluidine blue O paint: 4.0 g of TiO₂ nanoparticles (P 25, Thermo fisher scienctific, Waltham, MA, USA), and 40 mg (130 × 10⁻⁶ moles) of toluidine blue O (Sigma-Aldrich, St. Louis, MO, USA) were mixed in 40 mL of solution A under constant agitation, and then, it was sonicated for 5 min and agitated for 5 min.

Crystal violet paint: 4.0 g of TiO₂ nanoparticles (P 25, Thermo fisher scienctific, Waltham, MA, USA), and 40 mg (98 × 10⁻⁶ moles) of crystal violet (Sigma-Aldrich, St. Louis, MO, USA) were mixed in 40 mL of solution A under constant agitation, and then, it was sonicated for 5 min and agitated for 5 min.

5.2.2 Ultraviolet and visible spectroscopy
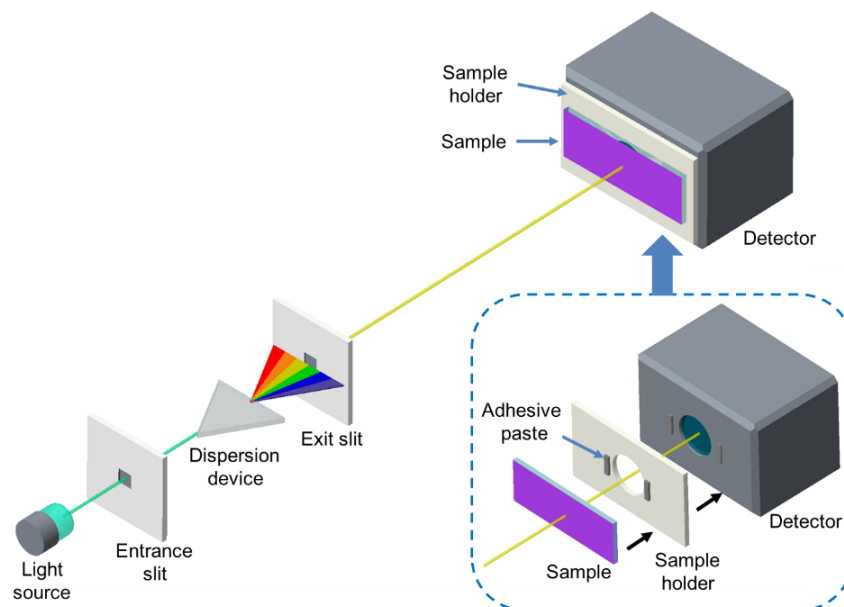
Fig. 5.1 Measurement on water contact angle of the painted surfaces

As shown Figure 5.1, UV/Vis spectrometer (Lambda 25, PerkinElmer Inc., Winter St., CT, USA) which has a detection range of wavelength 190–1100 nm, and a wavelength accuracy of ± 0.1 nm, was used to characterize ultraviolet and visible absorption spectra of intact glass (control), and painted glass slide. Absorption spectra of the samples were measured in wavelength of 400–900 nm.

5.2.3 Water contact angle in air

Equilibrium water contact angle was determined on the painted surface using a contact angle meter (First Ten Angstroms, Inc., Portsmouth, Virginia, USA). A water droplet (volume: 5 µL) was inoculated on the sample surface, its image was captured side on, and analyzed by Surftens 4.5 software. The contact angle hysteresis (CAH) was determined by "add and remove volume" method[170]. Advanced and receding angles were measured and then the difference between them was used to calculated the CAH.

5.2.4 Self-cleaning and water repellent properties of the painted surfaces in air

To make dual functional surfaces, glass slide (2.5 cm × 7.5 cm) was coated 450 µL of paint, then dried for 3 h in a dark room. After 3 h of the drying, the treated surface was washed by deionized (DI) water for removing non-combined toluidine blue or crystal violet. In water repellent test, 0.5 mL of water was dropped on the painted surface at a height of ~ 20 mm. For self-cleaning test, iron oxide nanoparticles were placed on the painted surface, and then from a pipette, 1 ml of water was dropped on to the surface. The results of self-cleaning and water repellent experiments were

filmed by a mobile camera (Galaxy S5, Samsung Electronics Co., Ltd, Suwon, South Korea)

5.2.5 Water contact angle in hexadecane

The painted sample was placed in hexadecane oil and droplets of Congo red dye (Sigma-Aldrich, St. Louis, MO, USA) dissolved water were inoculated on the unpainted (control) and painted glass slides. It was captured side on, and then analysed by Surftens 4.5 software.

5.2.6 Self-cleaning and water repellent properties after hexadecane contamination

In order to produce an oil contaminated surface, the painted glass was dipped in hexadecane oil for 3 min. For water repellent test on the oil contaminated sample, from a pipette, 0.5 mL of Congo red dye dissolved water was dropped on the sample which was titled at an angle of 20 $^{\circ}$

For self-cleaning experiment on the contaminated sample, vanadium oxide powder was loaded on to the sample. From a pipette, 0.5 ml of DI water was dropped on to the contaminated sample which were inclined at an angle of 20 $^{\circ}$.

5.2.7 SEM analysis

In order to determine the surface morphology of the painted sample, Scanning electron microscopy (SEM, JEOL Inc., Peabody, MA, USA) was employed. To prevent surface charging. The sample was coated by gold crystals for 60 s through

a sputter coating process, and then the surface morphology was observed by SEM at an accelerating voltage of 5 kV. Images of the sample was taken by SEMAfore software.

5.2.8 AFM analysis

To determined topography and roughness of the painted surface, Atomic force microscopy (AFM, EeasyScan 2 AFM, Nanosurf, Liestal, Switzerland) was employed. For the tapping mode, non-contacting mode and dynamic force mode was applied, and the resonant frequent of the cantilever ranged from 150 to 200 kHz. Scanning area of AFM on the surface was about 50 µm × 50 µm.

5.2.9 Anti-biofouling test

For an anti-biofouling test of the painted sample, the glass slide was dipped into paint solution, and then dried for 3 h in a dark room. After drying, the sample was washed by DI water. In an anti-biofouling test, *Escherichia* coli (ATCC 25922) and *Staphylococcus aureus* (NCTC 13143) bacteria were used. *E. coli* and *S. aureus* which were stored in brain-heart-infusion broth (BHI broth, Oxoid Ltd., Hampshire, England, UK) including 20% glycerol at -70°C were propagated on MacConkey agar (Oxoid Ltd., Hampshire, England, UK) and Mannitol salt agar (Oxoid Ltd.), respectively. One bacteria colony was inoculated into 10 mL of BHI broth and then incubated with shaking of 200 rpm at 37 °C. After 18 h incubation, the bacteria were collected by centrifugation (21 °C, 4000 rpm for 10 min), and washed by 10 mL of PBS. This process was repeated twice. The washed suspension was diluted into 1/10 to get ~10^8 colony forming units per millilitre (CFU/mL). The painted glass was

dipped vertically in 30 mL of bacterial suspension with ~10^{10} CFU for 3 min, located into 30 ml of PBS solution, and then vortexed for 1 min to recover bacteria from sample to the solution. The bacteria suspension was concentrated into 450 µL through centrifugation at 5000 rpm for 20 min, and it was serially diluted and 100 µL of the suspension was plated on to agar. After 24 h incubation at 37 $^{\circ}$C, the bacteria colonies grown on the agar were counted.

5.2.10 Bactericidal test
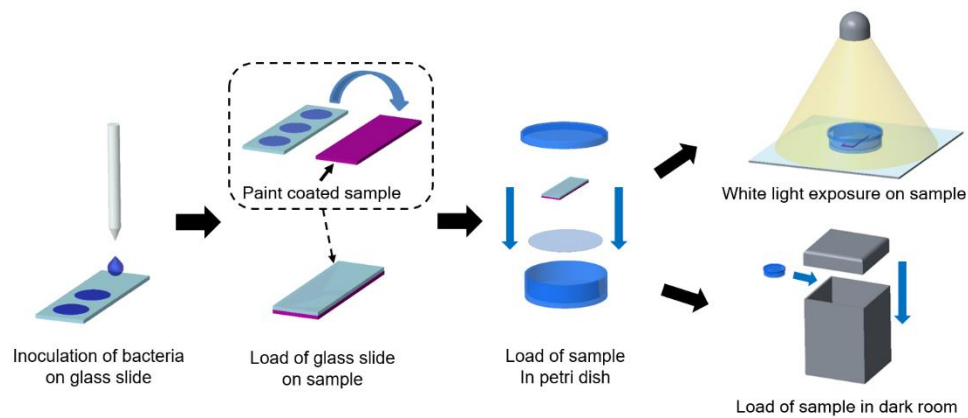
Fig. 5.2 Bactericidal test on paint coated surface

The washed bacteria suspension was diluted into 1/1000 to achieve ~10^6 colony forming units per millilitre (CFU/mL). As shown in Figure 5.2, 75 µL of bacteria suspension was inoculated onto sterilized glass slide (2.5 cm $\times$ 7.5 cm). The bacteria inoculated slide was overturned and placed on the paint coated sample. The sample was placed in petri dishes with wet paper to keep humidity, and it was exposed to white light source. Another set of samples was placed in the dark room. After white light exposure, the sample was placed into 40 mL of PBS, and vortexed for 1 min. The bacterial suspension was concentrated into 450 µL through centrifugation at

5000 rpm (at 21 °C for 20 min), serially diluted, and plated onto agar; (MacConkey agar for *E. coli*, and mannitol salt agar for *S. aureus*). After 24 h incubation at 37 ° C, the bacteria colonies on the agar were counted.

5.2.11 White light lamp exposure

28 W white fluorescent lamp (GE Lighting, East Cleveland, Ohio, USA) was selected as light source. The light intensity ranged from 3900 to 5300 lux and the intensity average was 4400 lux. Detail on information of light source was stated in Section 3.2.2.8.

5.2.12 Abrasion test of painted surface
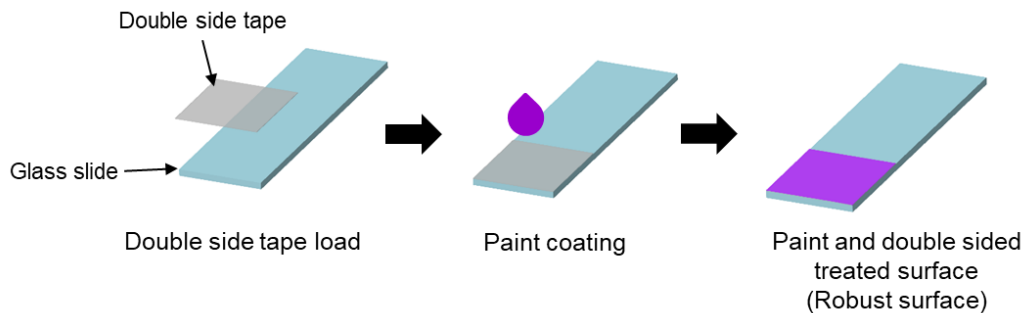
Fig. 5.3 Double sided tape and paint treated glass slides

Figure 5.3 shows the procedure to produce robust superhydrophobic and bactericidal surface. Sellotape double sided tape (Düsseldorf, Germany) was attached onto glass slide, and then the tape attached slide was painted. The painted slide was located in a dark room for 6 h.

Figure 5.4 shows the abrasion test of sand paper on paint and double sided tape treated slide. The slide was placed face down to sandpaper (CAMI grit no. 150) and

weight of 40 g was loaded on the slide. The painted slide moved back and forth for

8 cm along ruler. This process defined as one cycle. The water contact angle of the

treated slide was examined after each cycle.
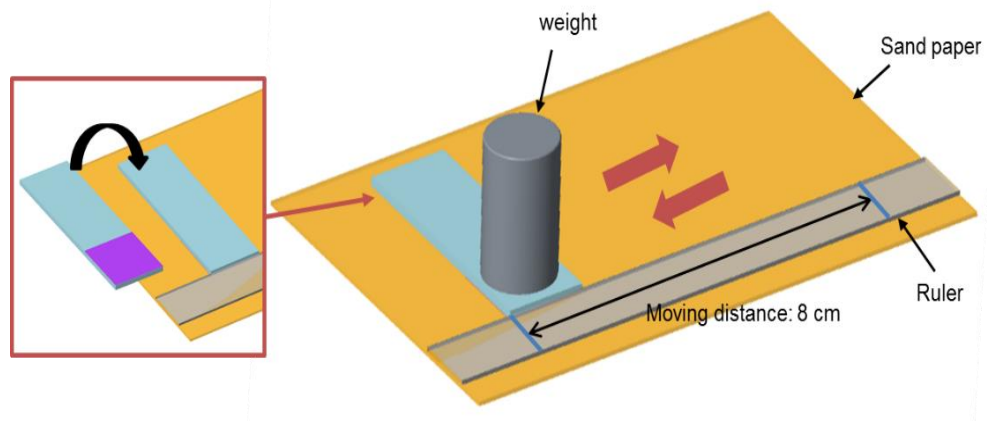
Fig. 5.4 Abrasion test on paint and double sided tape treated surface

5.2.13 Statistical analysis

Experimental data were analysed by SPSS (IBM Corporation, Armonk, New York,

USA) in terms of Mann–Whitney U test.

5.3 Result and discussion

5.3.1 Preparation of the dual functional paint

According to previous studies, the PFOTES molecules covalently bond to the surface of oxide nanoparticles including TiO_2, $CaCO_3$. and SiO_2 nanoparticles[229-231]. Based on these facts, superhydrophobic and antimicrobial paints were produced using toluidine blue O (TBO), crystal violet (CV), TiO_2 nanoparticles, and PFOTES, and ethanol. Figure 5.5 shows three different paints. To make TiO_2 paint, ethanol, PFOTES, and TiO_2 nanoparticles were mixed, and CV and TBO were added into TiO_2 paint in order to produce TBO and CV paints, respectively. After mixing, the paints were placed in a dark room for 2 days. Figure 5.6 shows AFM topography and SEM images of the painted glass slide. Glass slides were coated by TiO_2, TBO, and CV paints and then dried for 3 h in the dark room. The coated slides were washed by deionized (DI) water to eliminate non-combined CV or TBO to TiO_2 nanoparticles and PFOTES after the drying. AFM analysis showed that the paint coating on smooth glass had a rough surface: a surface roughness change from ~5.1 to ~1000 nm (Table 5.1). SEM analysis showed that a high roughness of the painted surface was due to agglomeration of approximately 21 nm TiO_2 nanoparticles[175].
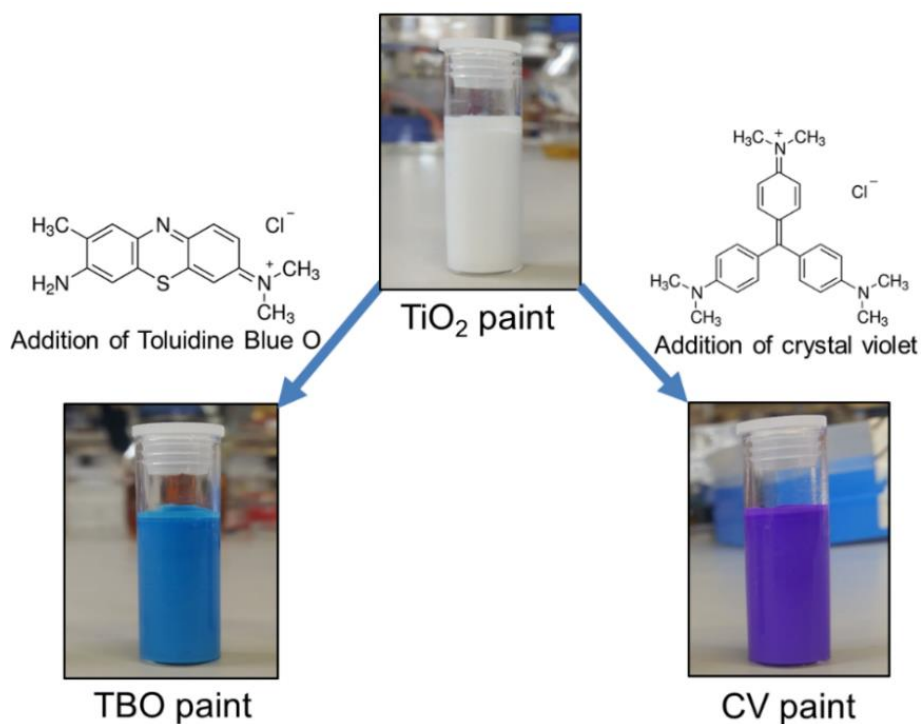
Fig. 5.5 TiO$_2$, toluidine blue O (TBO), and crystal violet (CV) paint solutions

Table 5.1 Water contact angle, rolling off angle, contact angle hysteresis, surface roughness of control, TiO$_2$ paint, TBO paint, CV paint

Sample	Water contact angle (^{o})	Rolling off angle (^{o})	Contact angle hysteresis (^{o})	Surface roughness (Sa, nm)
Glass slide (Control)	5.9 ± 0.6	n/a	n/a	5.1 ± 0.8
TiO$_2$ painted surface	164.4 ± 2.2	<1	0.4 ± 0.5	1150.7 ± 610.5
TBO painted surface	163.6 ± 1.6	<1	0.8 ± 0.6	1046.1 ± 757.6
CV painted surface	163.1 ± 1.8	<1	0.9 ± 1.0	1027.8 ± 61.9
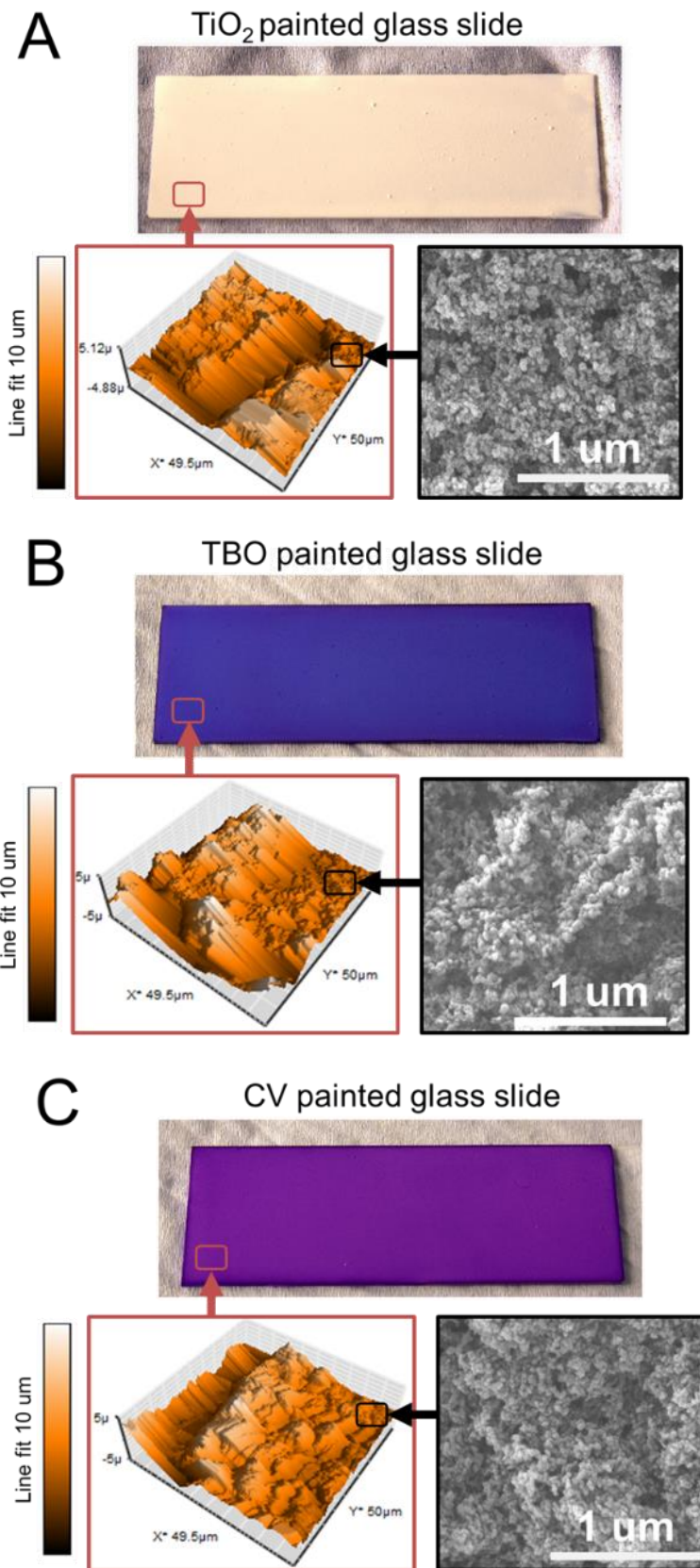
Fig.5.6 AFM and SEM images of (a) TiO$_2$, (b) TBO, and (c) CV painted glass slides

5.3.2 Ultraviolet and visible spectroscopy

UV/Vis absorption spectra of the control, TiO₂, TBO, and CV painted glass slides were measured from 400–900 nm by a UV/Vis spectrometer. Figure 5.7 shows the spectra of the samples. Because TiO₂ is UV induced catalyst: TiO₂ mainly absorbs radiation with wavelengths of <400 nm[232], a main absorbance on TiO₂ paint was not observed at the wavelengths of 400–900 nm whereas the main absorption peaks in TBO and CV paints were confirmed at 589 and 590 nm, respectively, corresponding to the peaks of toluidine blue O and crystal violet. The absorbance spectrum characteristics of CV and TBO between 400–750 nm would explain their role in photobactericidal activity.
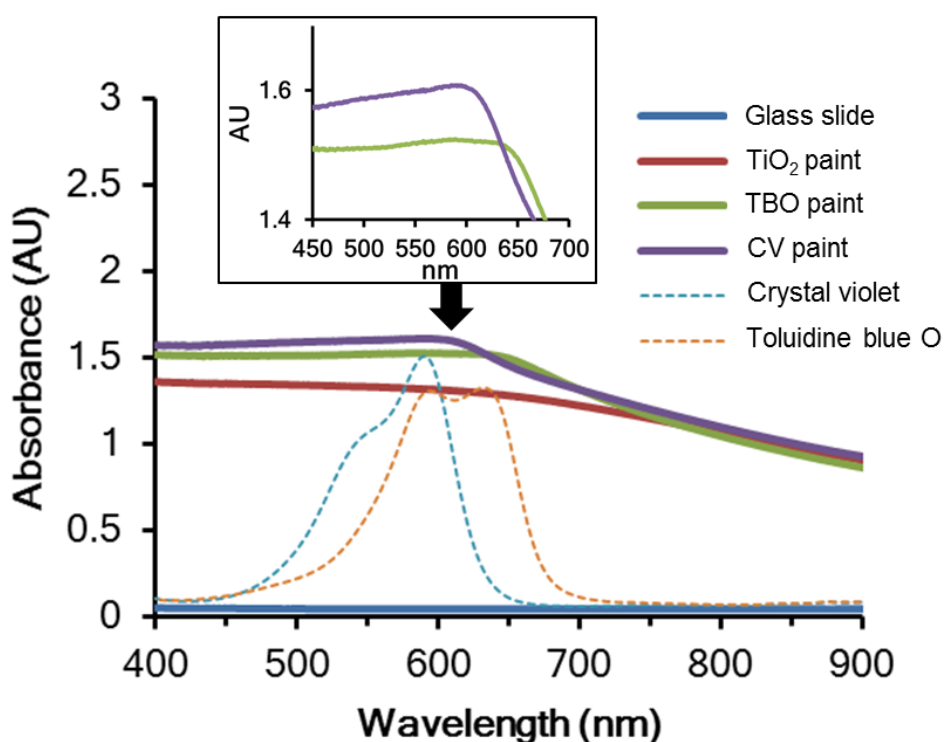
Fig. 5.7 Ultraviolet and visible (UV/Vis) absorption spectra of glass slide (control), white, blue, and violet painted glass slides. Absorption spectra were measured over wavelengths of 400–900 nm.

5.3.3 Water contact angle in air

The equilibrium water contact angle of the intact glass slide, TiO$_2$, TBO, and CV painted glass slides was measured using a water angle meter. As shown in Figure 5.8, the water contact angle of intact glass slide was approximately 5.9 °, indicating superhydrophilicity. The water contact angles of painted glass slides were >160 ° meaning that they were superhydrophobic (TiO$_2$ painted surface: 164.4 °, TBO painted surface: 163.6 °, CV painted surface: 163.1 °) (Table 5.1)[233].
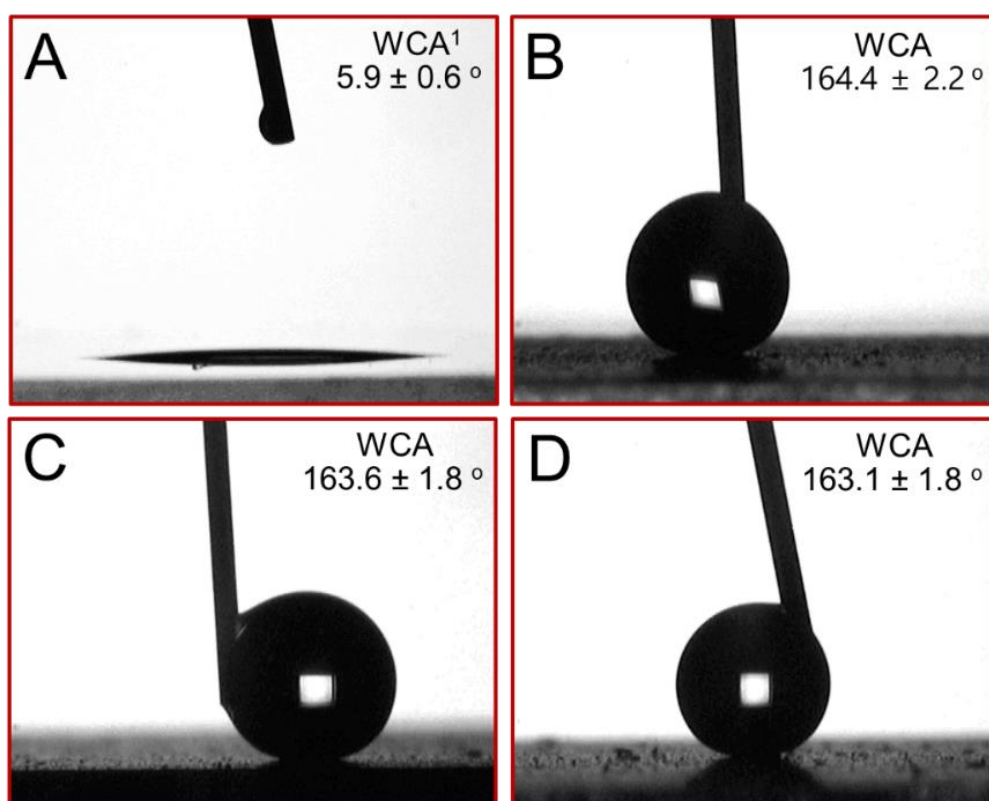
Fig. 5.8 Water contact angle of (a) glass slide (control), (b) TiO$_2$, (c) TBO, and (d) CV painted glass slides in air

[1]WCA: Water Contact Angle

5.3.4 Self-cleaning and water repellent properties in air

To determine the water repellent characteristic of the painted surfaces, 0.5 mL of water was dropped on to the surface. As shown in Figure 5.9, water droplets were

trapped on the surface of intact glass slide while the water droplets rolled off on the painted surfaces without wetting. The water rolling phenomena on the treated surfaces is due to superhydrophobicity of the paints giving a high water contact angle with low contact angle hysteresis (<1 °) and low roll off angle (<1 °) (Table 5.1).

Figure 5.10 shows the self-cleaning test on TiO_2, TBO, and CV painted glass slides. after water was dropped on the surface of the intact glass slide, the powder sustained within the water remained on the glass slide whereas the water droplets rolled off on the painted surface, the powder was carried away by the water droplets. PFOTES molecules bonding on the rough surface significantly reduce the surface energy, resulting in significant reduction in the water attraction to the surface[234]. This considerably decreases the contact area between water droplet and the surface as the water droplet forms a sphere on the surface, leading to reduction of water adhesion force on the surface. Thus, because the adhesion force to the rough surface is weaker than that of the droplet to the powder, it was washed away by water droplets which rolled on the surface[186].
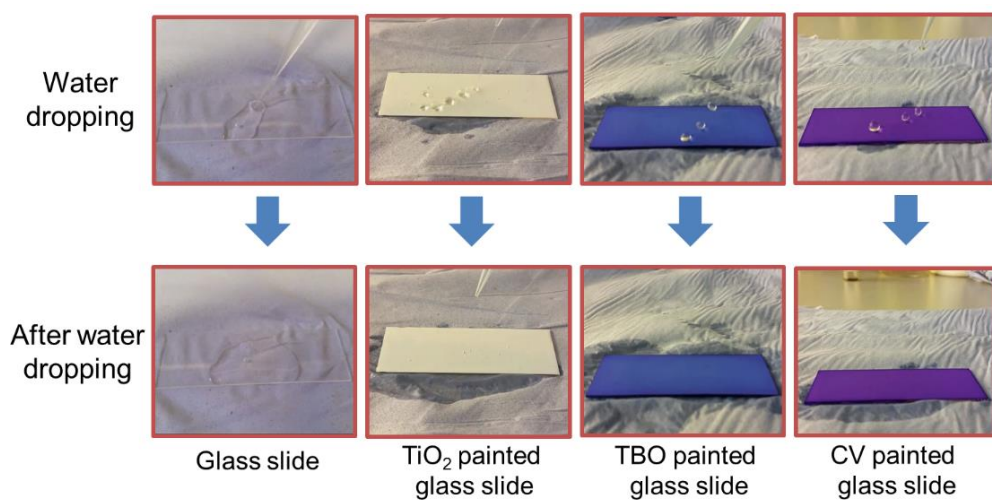
Fig. 5.9 Water repellent property of glass slide, TiO_2, TBO, and CV painted glass slides in air
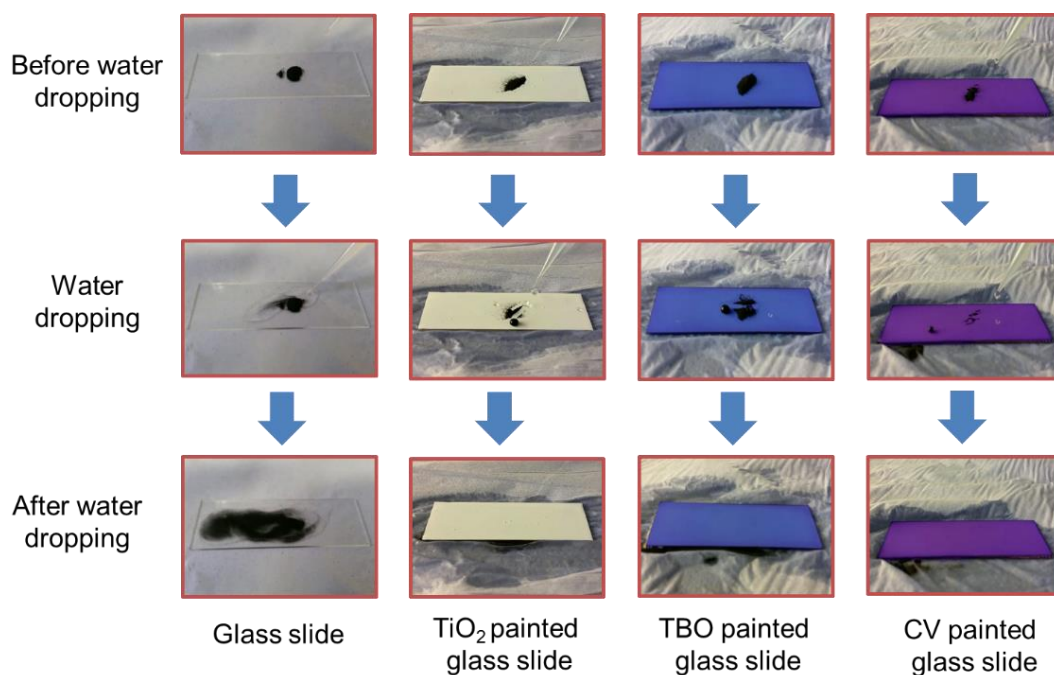
Fig. 5.10 Self-cleaning property of glass slide, TiO$_2$, TBO, and CV painted glass slides in air

In order to produce the treated TiO$_2$, TBO and CV particles, paint solutions were dried by ethanol evaporation and the particle were obtained by a top-down process. As shown in Figure 5.11, the particles kept their individual colours and the experiment of the water contact angle showed that the particles still maintained superhydrophobicity. Crystal violet and toluidine blue O powders used in this chapter are soluble in water[156,159,190,191]. Water stability test of the particles showed that crystal violet and toluidine blue O did not leach out from particles in water. This would be because PFOTES attached onto the surface of TiO$_2$ prevents water from contacting the dye molecules. As shown in Figure 5.12, it was expected that the dye molecules dissolved in ethanol are entrapped into the surface of P25 TiO$_2$ which is hydrophilic. After evaporation of ethanol, the dye molecules remain on the surface of the TiO$_2$ which has a high roughness, and then PFOTES is covalently attached

onto the TiO$_2$ with the dye molecules [229-231,235]. As a result, the property of the particles changes from hydrophilic to hydrophobic and they obtain photobactericidal activity under visible light because of the absorbed dye.
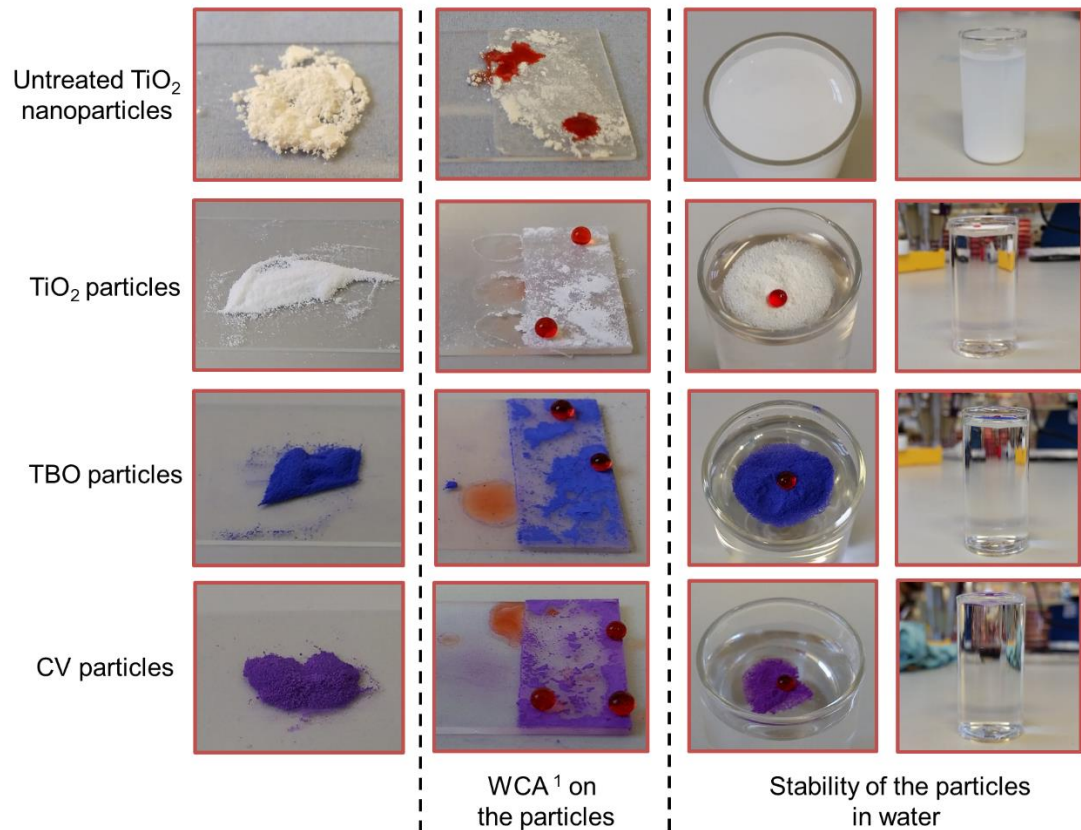
Fig. 5.11 Water repellent and stable tests of intact TiO$_2$, treated TiO$_2$, TBO, and CV particles

WCA[1] : Water Contact Angle
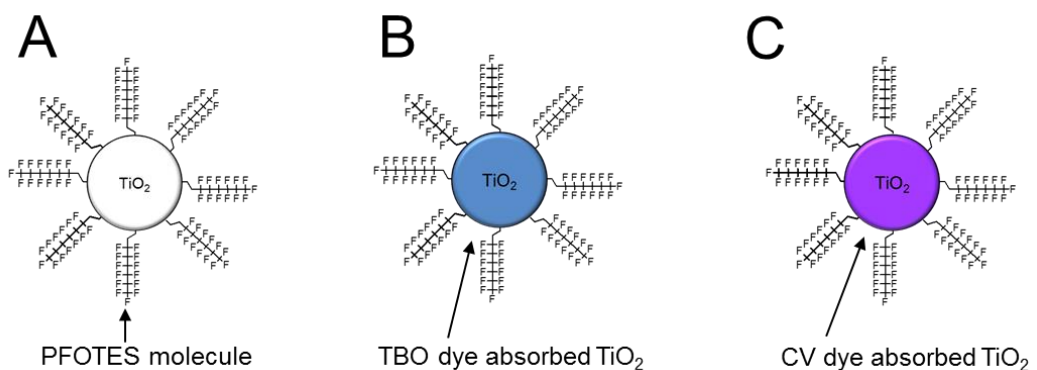
Fig. 5.12 Chemical structures on the combinations of (a) TiO$_2$ nanoparticle and PFOTES, (b) TiO$_2$ nanoparticle, PFOTES and toluidine blue O (TBO), (c) TiO$_2$ nanoparticle, PFOTES and crystal violet (CV)

5.3.5 Water contact angle in hexadecane

To determine if the painted surfaces sustain the water repellency in hexadecane, water droplets were placed on the unpainted and painted surfaces. Figure 5.13 shows the test of the water repellency of the painted surfaces immersed in hexadecane oil. After that, water diffused on the unpainted surface (glass slide) whereas on the painted surface, droplets still formed a spherical shape, and the water contact angle was >160 $^{\circ}$. As the painted surface was immersed into hexadecane, the oil penetrated inside of the surface. Thus, it was speculated that the water droplets were supported by hexadecane and the rough surface, and kept their spherical shape.
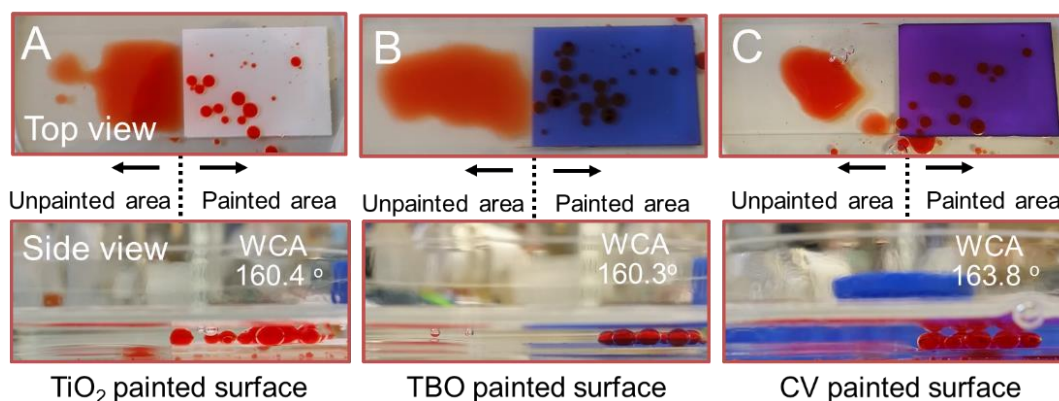
Fig. 5.13 Water contact angles of TiO$_2$, TBO, and CV painted glass slides in hexadecane oil

5.3.6 Self-cleaning and water repellent properties after hexadecane contamination

The painted surfaces were immersed into hexadecane for 1 min to determine water repellency and self-cleaning properties of the surfaces after oil contamination. As shown in Figure 5.14 and 5.15, water droplets slid off on the painted surfaces at 20 $^{\circ}$ tilt angle and the self-cleaning behaviour was maintained at that angle. It is speculated that the oil penetration inside the painted surface produces a lubricant

139

layer on the surface, resulting in slippery surfaces when the surface was exposed to

hexadecane oil[72,236].
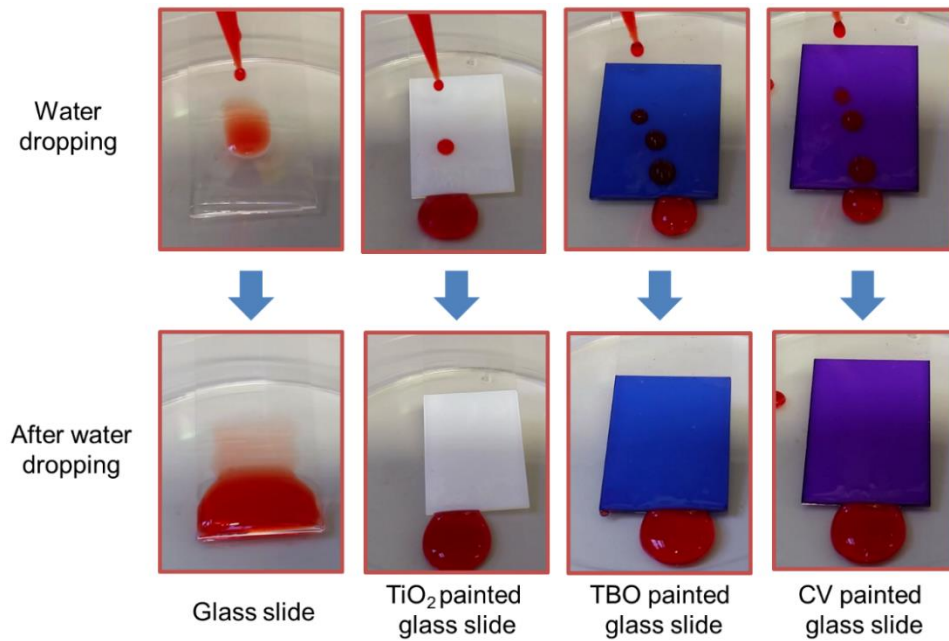
Fig. 5.14 Water repellency of TiO$_2$, TBO, and CV painted glass slides after the oil contamination
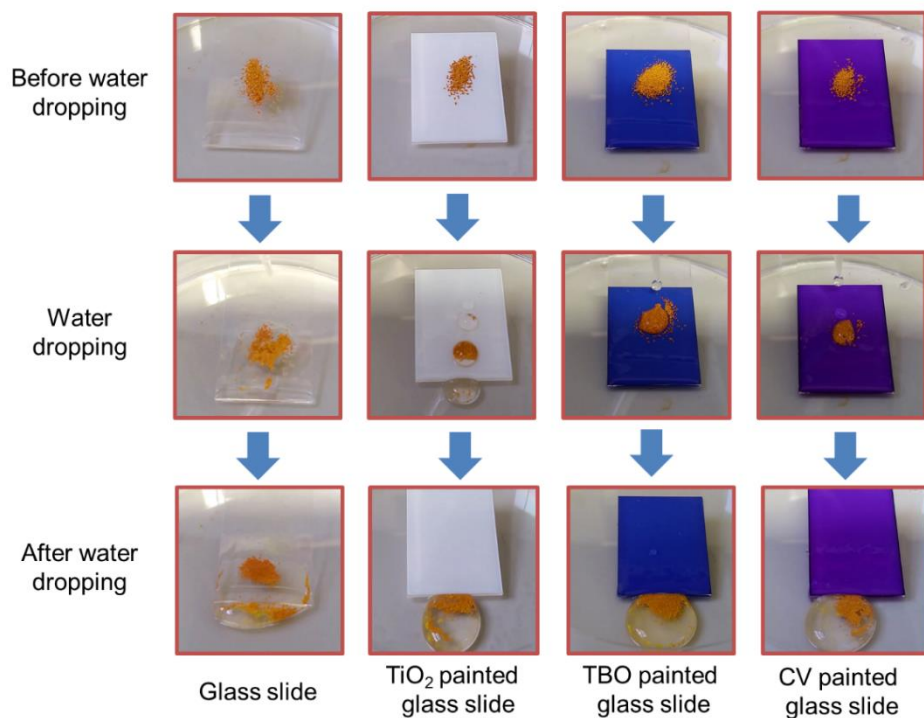
Fig. 5.15 Self-cleaning property of TiO$_2$, TBO, and CV painted glass slides after the oil contamination

5.3.7 Anti-biofouling test

In order to determine anti-biofouling property of the paint coated surfaces, suspensions of *S. aureus* (NCTC 13143, total number: ~10^{10} CFU) and *E. coli* (ATCC 25922, total number: ~10^{10} CFU) were used. The painted surfaces were dipped in the bacterial suspension for 3 min and then the number of bacteria attached on the surface was investigated. Figure 5.16 shows the number of bacteria attached to intact glass slide and the painted coated slide glass. The number of *S. aureus* attached to intact glass slide was approximately 4.5×10^7 CFU, and after paint coating on the slide, the number of the attached bacteria significantly decreased by >99.9 % (*P-value* <0.01); the numbers on TiO_2, TBO, and CV painted surfaces were 3.2×10^4 CFU, 1.9×10^4 CFU, and 1.6×10^4 CFU, respectively. In the test against *E. coli*, a significant reduction in bacteria adhesion was also observed on all three painted surfaces (*P-value* <0.01 at all of painted glass slides compared to intact glass slide). The number of *E. coli* attached to intact glass slide was about 2.0×10^7 CFU, and the bacteria numbers to the TiO_2, TBO, and CV painted slides were approximately 4.9×10^3, 2.4×10^5, and 5.7×10^4 CFU, respectively. The significant reduction of bacteria attachment is due to the superhydrophobicity of treated surfaces. Fine air bubbles are entrapped on the superhydrophobic surface when it is immersed in water, and the air bubble layer reduces a contact area of bacteria and the surface, and bacteria could not cross the air/water interfaces because of the surface tension of water[186].
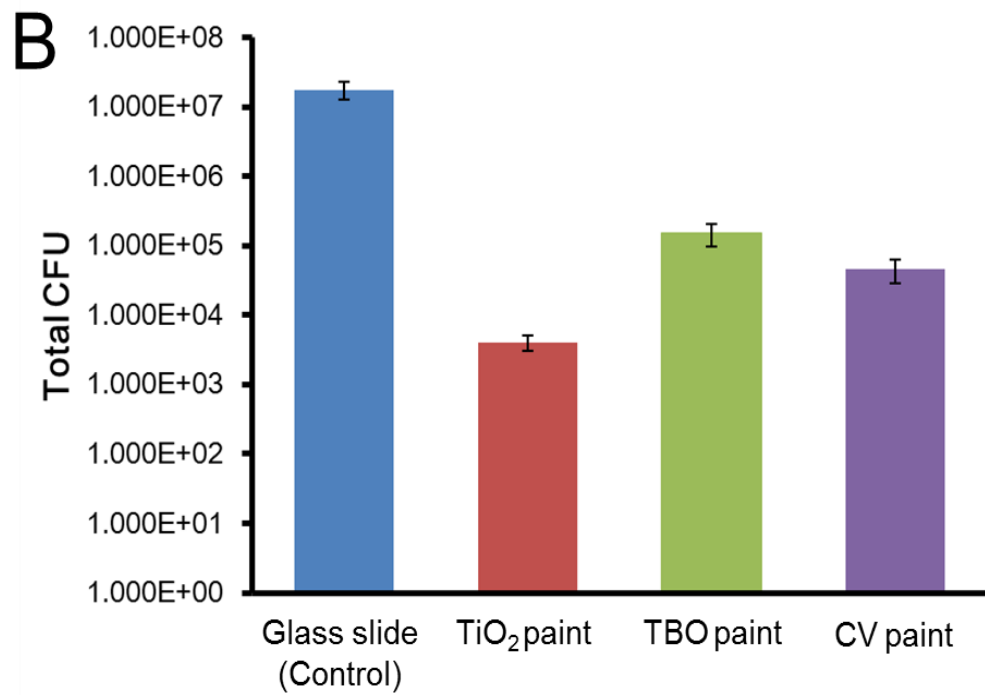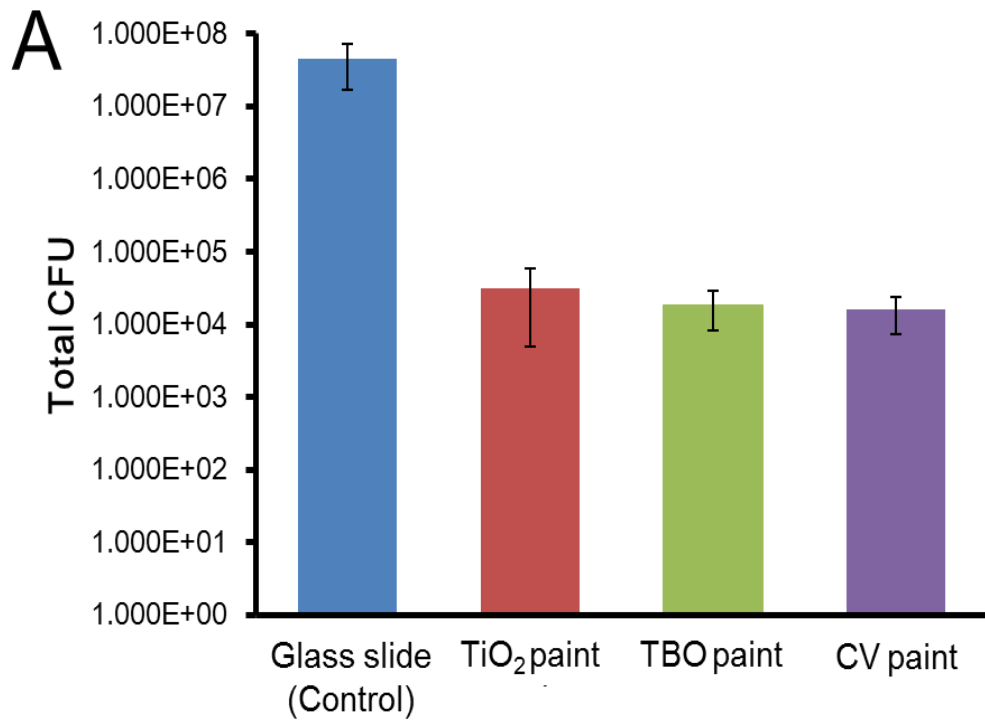
Fig. 5.16 Numbers of (a) *S. aureus* and (b) *E. coli* bacteria attached to glass slide (control), TiO_2, TBO, and CV painted glass slides

5.3.8 Bactericidal test

For the bactericidal test, *S. aureus*, a representative Gram-positive bacterium, and *E. coli*, a representative Gram-negative bacterium, were used in this chapter, and both species are key hospital pathogen. 75 µL of bacteria suspension was used for each sample. The bacteria inoculated samples were incubated in a dark room, and another set of the samples were exposed to white light source. The light intensity of white lamp used in this chapter was approximately 4400 lux in average, and the light intensity in the dark room was near zero lux.

Figure 5.17 shows the bactericidal activity of painted glass slide on *S. aureus* in the dark and in white light. It was observed that the number of viable bacteria reduced on the TiO_2, TBO, and CV painted glass slides, after 3h incubation in dark (*P-value* <0.05), and the CV painted slide showed the best bactericidal activity: compared to the intact glass slide (control), 0.3, 0.9, and 1.1 log reductions in the number of viable bacteria was observed for TiO_2, TBO, and CV painted surfaces, respectively. In white light, the painted glass slides showed enhanced bactericidal activity, compared to the identical samples in the dark. Compared to intact glass slide, 2.3 log and 3.2 log decreases in the numbers of viable bacteria were confirmed on TiO_2 and TBO painted slides after 3h of white light exposure, and in case of CV painted slide, the number of viable bacteria was dropped to below the detection limit (<10 CFU/mL). All of the painted slides showed stronger bactericidal activity in the light than that in the dark: 0.7, 2.4 and 3.4 log differences in the number of bacteria between in dark and in white light was confirmed for the TiO_2, TBO, and CV painted slides, respectively.
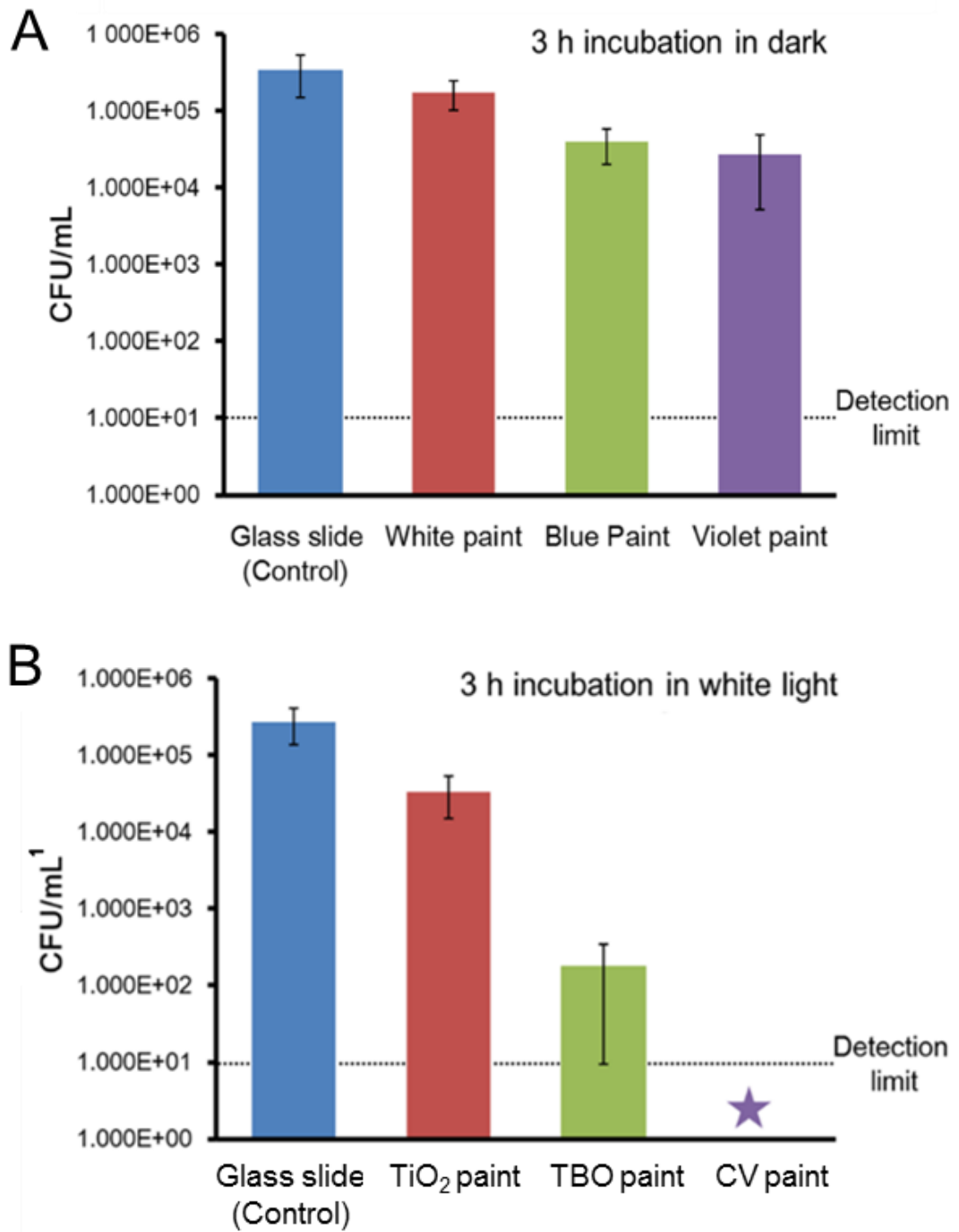
Fig. 5.17 Bactericidal activity of glass slide (control) and TiO$_2$, TBO, and CV painted glass slides on *S. aureus* in (a) dark and in (b) white light

[1] Colony forming unit/mL

★ Detection limit: <10 CFU/mL

Figure 5.18 exhibits the bactericidal activity against *E. coli* after 4h incubation in dark and in the white light. In the dark, bactericidal activity was not observed on all of the painted glass slides (*P-value* >0.1), and in white light, bactericidal activity was negligible on TiO_2 painted glass slide; statistical significance was not observed (*P-value* >0.1). However, it was shown that the number of viable bacteria significantly decreased on the TBO and CV painted slides (*P-value* <0.01); Compared to the intact glass slide, about 2.6 log decrease in the viable bacteria number were observed on the TBO painted slide, and for CV painted surface, the number of viable bacteria had dropped to below the detection limit (viable bacteria reduction: >5 log). It was reported that crystal violet, toluidine blue O, and titanium dioxide used in this chapter have some intrinsic antibacterial activity[125,131,134,157,184,220,237]. Ur dark conditions, the bactericidal experiment of our samples on *S. aureus* showed that crystal violet, toluidine blue O, and titanium dioxide maintained their intrinsic bactericidal activity after incorporation in the paint. But, despite longer time in the dark than that of *S. aureus*, a decrease in the number of viable *E. coli* bacteria was not detected on all of the painted glass slides, and even in white light, *E. coli* was less vulnerable. This might be due to their different membrane structure; as shown Figure 5.19, the cell wall of Gram-positive strain is made up of plasma membrane, and peptidoglycan while Gram-negative strain has a more complex membrane containing layers of peptidoglycan plasma membrane, periplasmic space, outer membrane consisting of lipopolysaccharide and protein[238]. The outer membrane of Gram-negative strain reduces the penetration of many molecules and it is often responsible for resistance to chemical materials[238,239]. Compared to that of the slides in dark, the painted slides exhibited increased

bactericidal activity in white light. But, TiO$_2$ painted slide showed weaker
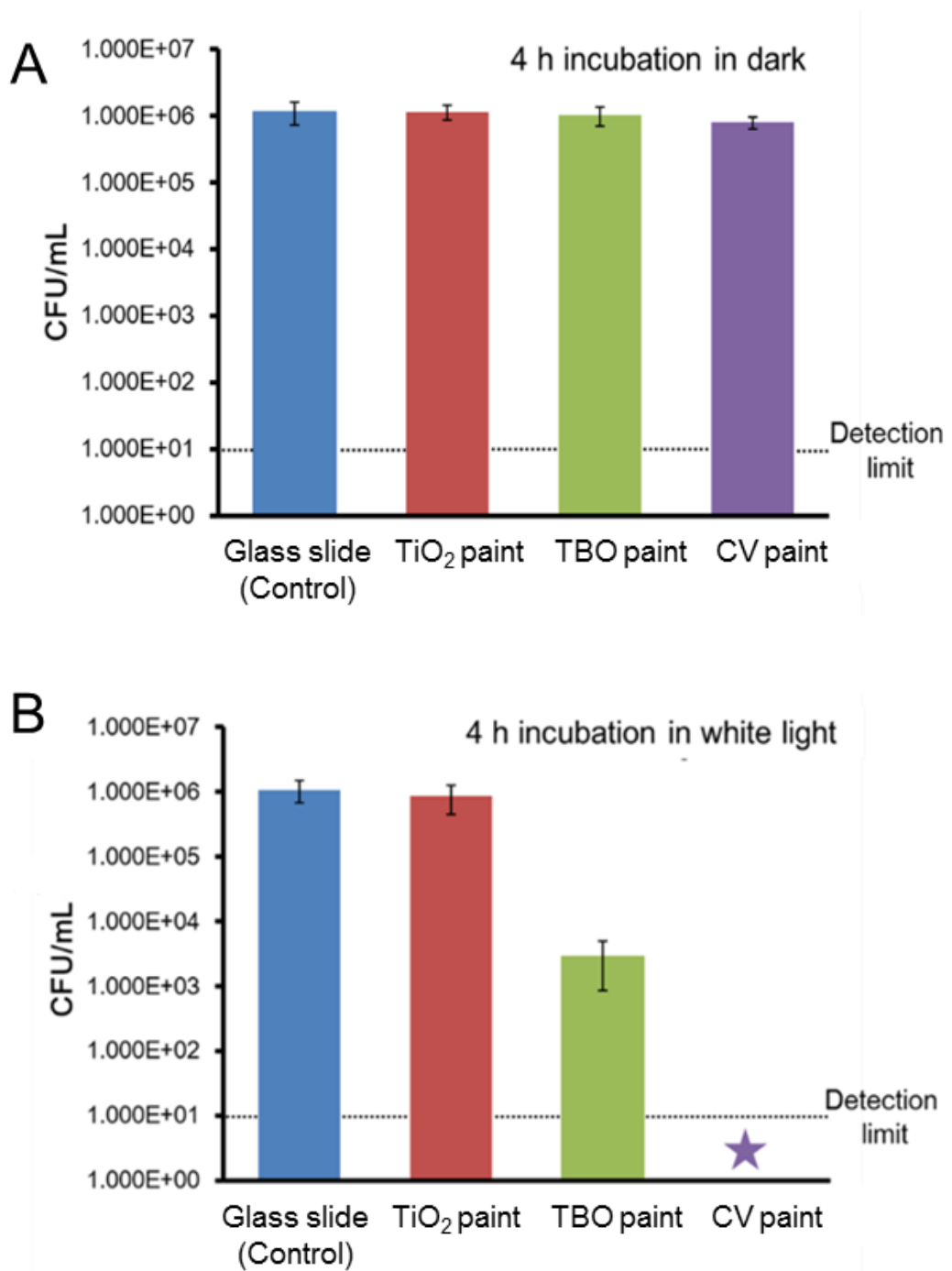
Fig. 5.18 Bactericidal activity of glass slide (control) and TiO$_2$, TBO, and CV painted glass slides on *E. coli* in (a) dark and in (b) white light

★ Detection limit: <10 CFU/mL
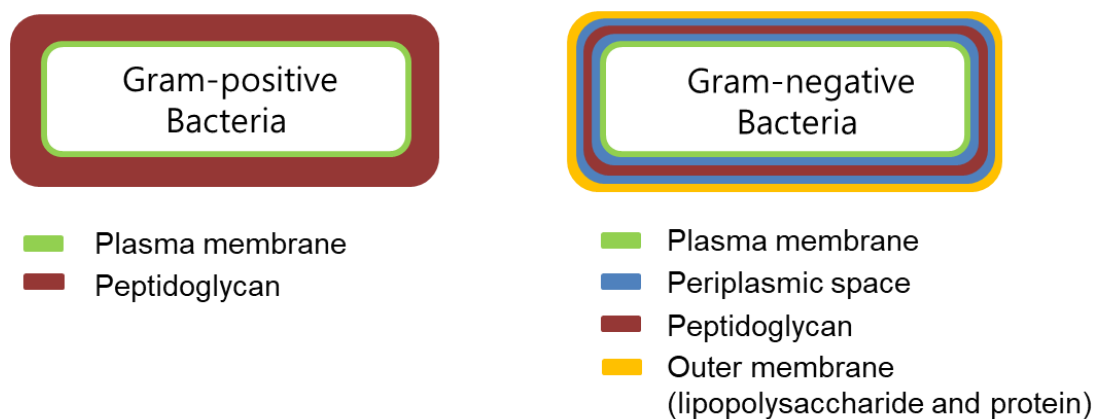
Fig. 5.19 Membrane structure of Gram-positive and- negative bacteria

photobactericidal activity than TBO and CV painted slides. Titanium dioxide nanoparticles used in this chapter are a UV light induced-bactericidal agent, and their photobactericidal activity is mainly due to hydroxly radicals (•OH) and other reactive oxygen species (ROS) driven by the UV irradiation[166,239-241]. Because UV light accounts for a very small portion of total irradiation of the white lamp, this can explain the reason that the TiO_2 paint showed weaker photobactericidal activity than the TBO and CV paints. The potent photobactericial activity of TBO and CV paints is attributed to toluidine blue O and crystal violet dyes. Figure 5.20 and equation (5-1) to (5-5) show the mechansim of phtobactrericidal activity induced by CV and TBO paints[242]. The dyes impreged into TiO_2 nanoparticles acted as a sensitizer for TiO_2[243]. As the dyes absorbed visible photons, they were pomoted into an excited electronic state CV^* or TBO^* and then electron was transferred into the conduction band of TiO_2 through interfaces between dye and TiO_2[242,243]. As a result, the photogenerated electron drived production of reactive oxygen species (ROS) [242,243]. The generated ROS kills bacteria by oxidative damage to cellular membranes, intracellular proteins and DNA [159,244].
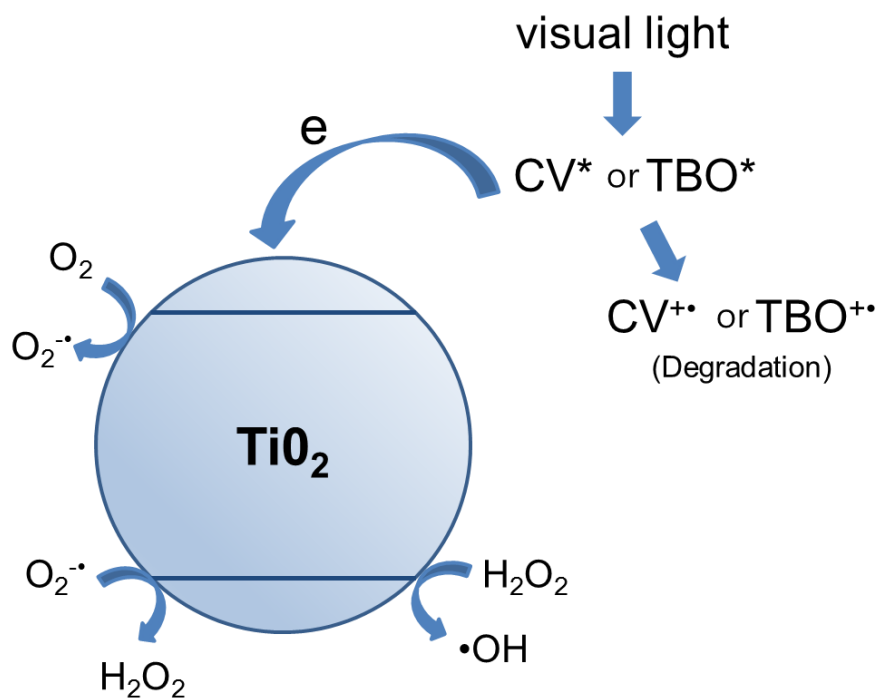
Fig. 5.20 Schematic illustration of the mechanism for reactive oxygen species generation through photoreaction between crystal violet (CV) or toluidine Blue O (TBO) and TiO_2

$$CV \text{ or } TBO + hv \ \longrightarrow CV^* \ or \ TBO^* \qquad\qquad (5-1)$$

$$CV^* or \ TBO^* + TiO_2 \ \longrightarrow CV^{+\bullet} \ or \ TBO^{+\bullet} + TiO_2 \ (e) \quad (5-2)$$

$$TiO_2 \ (e) \ + \ O_2 \ \longrightarrow \ TiO_2 \ + \ O_2^{-\bullet} \qquad\qquad (5-3)$$

$$O_2^{-\bullet} \ + \ TiO_2 \ (e) \ + \ 2H^+ \ \longrightarrow H_2O_2 \qquad\qquad (5-4)$$

$$H_2O_2 + \ TiO_2 \ (e) \ \longrightarrow \bullet OH + \ OH^- \qquad\qquad (5-5)$$
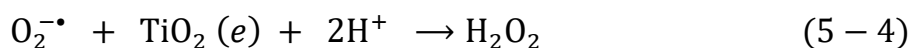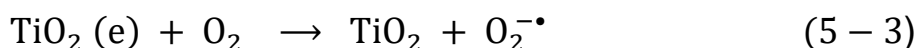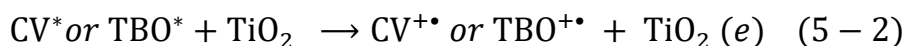
Despite use of the same amount of the light activated bactericidal agents (toluidine blue O: 40 mg, crystal violet: 40 mg), the bactericidal activity of TBO and CV paints was different; The reduction of viable bacteria by CV painted surface was > 1.2 log higher than the reduction by TBO painted surface. This result indicates that the

148

crystal violet and TiO_2 combination may generate more ROS than toluidine blue O and TiO_2.

Producing robust superhydrophobic surface is a challenge because nano or micro sized structures made by superhydrophobic coating are readily destroyed by external forces, resulting in loss of superhydrophobicity. In this chapter, and the bactericidal paint and double sided tape (Sellotape, Cheshire, UK) were used to produce robust superhydrophobic and bactericidal surfaces and their robustness was investigated though sand paper abrasion test. The paint and double sided tape treated glass slide was loaded onto sand paper coated by particles with ~92 µm in size (CAMI grit no. 150) and then 40 g of weight was placed on to the slide. The slide then moved back and forth for 8 cm. One back and forth movement was considered as one cycle.

Figure 5.21 shows the water contact angle, rolling off angle, contact angle hysteresis of painted glass slides after the sand paper abrasion test. The 10 cycles experiment represented that after the abrasion, the painted slides maintained a water contact angles of >158 $^\circ$, a rolling off angle of <0.5 $^\circ$ and a contact angle hysteresis of <3.4 $^\circ$. The colours and the coating thickness (55 µm) of paint were also maintained (Figure 5.21 insets and Figure 5.22).

In previous studies, it was shown that combination of superhydrophobic agents and bactericidal substances caused reduced or no bactericidal activities although it kept superhydrophobicity[65,71,168,169,227,228,233,245]. This might be mainly due to reduction of contact area between bacteria and bactericidal substances by the superhydrophobic polymer coating. In this chapter, the problem was addressed through the combination of TiO_2 particles, light activated bactericidal agent, and PFOTES. As a result, bacteria are killed by ROS generated from the painted surface in white light.
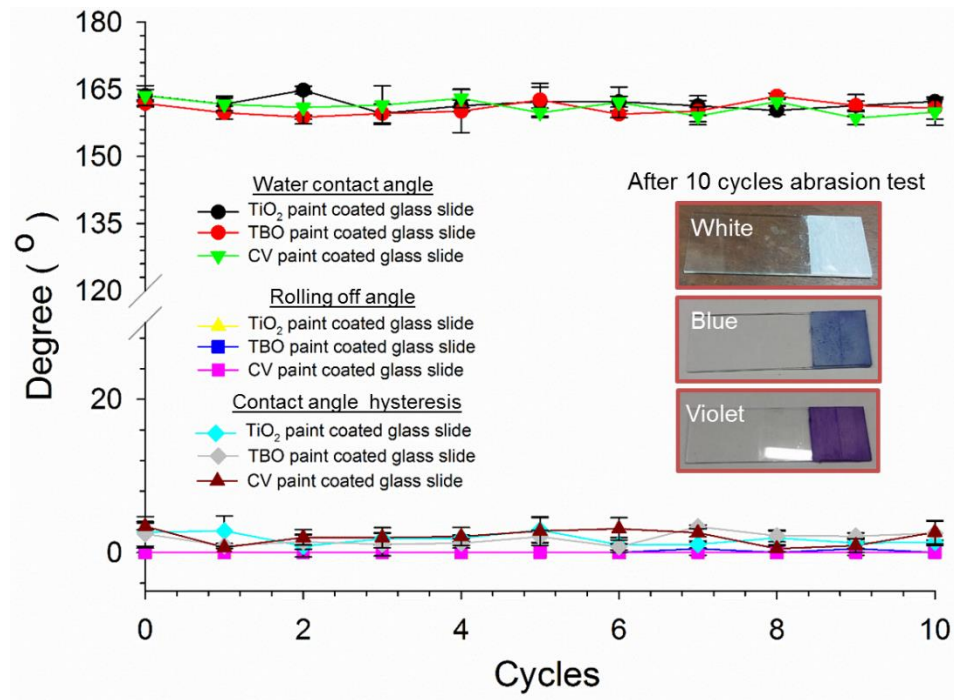
Fig. 5.21 Water contact angle, rolling off angle, contact angle hysteresis of robust treated surface after sand paper abrasion test
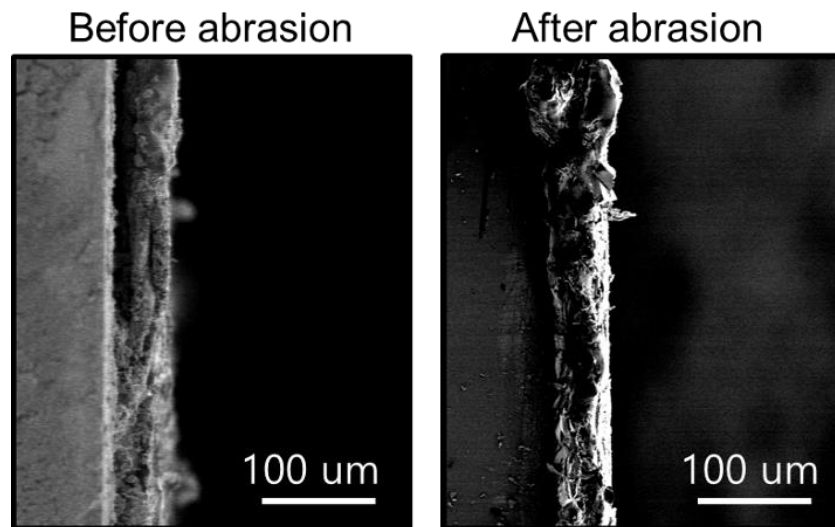
Fig. 5.22 Variation of coating thickness before and after abrasion test.

Perfluorinated chemicals (PFOs) including perfluorooctanoic acid (PFOA), perfluorooctane sulfonate (PFOS), perfluorobutane sulfonate (PFBS), and

perfluorodecanoic acid (PFDA) are widely used to make commercial products resistant to stains, grease, and water[246]. In recent years, many studies reported that PFOs have a potential to be a health concern because some PFOs persist in the environment and stay in the human body for a long period of time[247-249]. Currently, human health effect from exposure to a low amount of PFOs is unknown but, lab animal testing given a large amount of PFOs showed that some PFCs may affect growth and development, reproduction, and injure the liver[250]. Thus, more research to evaluate human health effect of exposure to PFOs are necessary. The International Agency for Research on Cancer (IARC) has classified PFOA as "possibly carcinogenic to humans" (Group 2B)[251], and US Food & Drug Administration (FDA) regulated the use of PFOA to minimize exposure to PFOA (treated paper or paperboard: ≤ 0.17 lb/1000ft^2, and coating solids: ≤ 2 % in weight) [252]. Although PFOTES used in this study contains perfluorinated C8 moiety, the quantity (0.14 lb/1000ft^2) met FDA requirement. Thus, we believe that the paints developed in this study has minor effects on human health.

5.4 Conclusion

This chapter details a simple and easy one step technique to produce superhydrophobic and photobactericidal properties. TiO$_2$ nanoparticles, PFOTES, and light activated bactericidal agents containing crystal violet, and toluidine blue O, and ethanol were combined together to fabricated TiO$_2$, CV, and TBO paints. The painted slides exhibited superhydrophobic and self-cleaning properties and even after hexadecane oil contamination, they maintained their properties. A bacterial adhesion assay showed that the surface bacteria adhesion was significantly reduced

on the painted slides (bacteria adhesion reduction: >99.8% at all of TiO_2, CV, and TBO paints). In the bactericidal experiment, the painted slides showed not only dark kill of *E. coli* and *S. aureus* but also represented very strong photobactericidal activity in white light.

In this chapter, the technique that we developed has several advantages: firstly, that fabrication of the paints is easy; secondly, its treatment on surfaces is simple like commercial paint; thirdly, through one simple treatment, a dual functional surface is produced; finally, the paints can coat a variety of surfaces such as plastic, paper (Figure 5.23) and glass (Figure 5.6) It is expected that these dual functional paints may be useful for healthcare facilities to prevent HAIs transmission.

Fig. 5.23 TiO_2, CV, and TBO paints coated plastics (plastic toys) and papers

Chapter 6: Conclusion

With an increase in pathogen resistance to antibiotics, healthcare-associated infections are a big problem in UK hospitals and worldwide. Although vigorous schemes including mandatory surveillance, legislation, inspection and disinfection to prevent the spread of healthcare-associated infection have been performed and they reduce somewhat the incidence of HAI, the rate of the infection is still high. Bactericidal surfaces are a promising approach to significantly decrease the number of healthcare associated infections because they can minimize transmissions of pathogens by preventing bacterial contamination on a surface which healthcare workers and patients frequently touch. This thesis has shown a previously unknown limitation of superhydrophobic surfaces which are well known anti-biofouling surfaces, and white light-activated bactericidal polyurethane and paints which have very potent bactericidal activity in white light.

In Chapter 2 which is the first experimental chapter, the anti-biofouling property of a superhydrophobic surface was tested for 1, 4, 8, 16, and 24 h using representative hospital-associated pathogens (*E. coli*, *S. aureus*, MRSA, and CRE) and compared with glass, polyurethane, and polystyrenes. After 1 h bacteria exposure, the superhydrophobic surface had significantly less adhesion than the other samples. However, with increasing exposure time, the numbers of adherent bacteria increased on superhydrophobic surface. After 24 h bacteria exposure, the number of bacteria attached on superhydrophobic surface was greater than the other surfaces. The results showed that as the air-bubble layer entrapped on a superhydrophobic surface, which reduces the contact area between bacteria and the surface, was dissolved in the water, the layer disappeared from the surface and the high roughness of a

superhydrophobic surface became a favourable setting to bacteria, resulting in a significant increase in bacteria attachment on superhydrophobic surface

Chapter 3 introduced a white light-activated bactericidal polymer produced by a simple swell-encapsulation shrink process. Toluidine blue O and silver nanoparticles were encapsulated into polyurethane which is widely used in medical devices in hospitals. The encapsulation induced a potent photobactericidal activity on *E. coli* within 3 h of white light exposure, and even showed strong bactericidal behaviour after 24 h of incubation in the dark. In both cases, the bacterial numbers decreased to below the detection limit indicating that the reduction in the number of viable *E. coli* bacteria was > 4 log.

In chapter 4 and 5, photobatericidal paints were introduced for the first time. Crystal violet and commercial acrylic latex were mixed together to produce bactericidal paint. The combination of crystal violet and acrylic latex resulted in white light-activated bactericidal paint. In bactericidal tests, the bactericidal paint with 1000 ppm of crystal violet showed not only strong bactericidal activity with 1.21 log reduction of viable *E. coli* at 6 h incubation in the dark but also exhibited very potent photobactericidal activity indicating that the reduction is > 3 log after 6 h of white light exposure. Stability tests in PBS over 120 h showed that after drying, crystal violet molecules hardly leached out from the paint, indicating that the paint is quite stable.

Crystal violet, toluidine blue O, P25 TiO_2 nanoparticles, and 1H, 1H, 2H, 2H-perfluorooctyltriethoxysilane were employed in order to make dual functional paints with superhydrophobic and bactericidal properties, and TiO_2, TBO, and CV paints

were produce through physical and chemical reaction. The dual functional paint coated slide showed a strong water repellence and self-cleaning properties, and it showed good anti-biofouling property with a reduction in the number of bacteria attached to the samples by >99.8%. A bactericidal experiment with *E. coli* and *S. aureus* showed that the coated slide had some bactericidal activity in the dark and under white light, they had very potent photosterilisation. Among the paints, CV paint showed the strongest at activity with >5 log reduction of viable bacteria.

As an alternative strategy for preventing surface contaminations, anti-biofouling and bactericidal surfaces have been considered as a promising technique. This thesis showed that surfaces with only anti-biofouling property can be a bacterial reservoir through experiments with superhydrophobic surfaces which is well known anti-biofouling surface, and from that result, it was concluded that bactericidal surface would be better strategy to prevent surface contamination by bacteria. Various types of surfaces in hospital environment exist such as polymer, glass, and wood, metal, and paper. Photobacterial polymer and paints in this thesis can be readily applied to many hospital surfaces and they can render the surface with potent bactericidal properties.

6.1 Future work

Although the bacterial killing mechanism of photobactericidal materials was not investigated, it is speculated that reactive oxygen species induced by photoreactions kill bacteria on the materials. Sehmi *et al.* (2015) showed that photobactericidal polymers generate reactive oxygen species[161], but the identity of the reactive oxygen species and the mechanism on photosterilisation enhancement by nanoparticles were

not extensively determined. In future work, determining the identity of reactive oxygen species *via* chemical entrap method (fufuryl alchohol for singlet oxygen; XTT assays for superoxide anion; *p*-Chlorobezoic acid for hydroxyl radical) would be useful to understand the mechanism.

For real world application, it is key to determine stability of the photobactericidal materials under a variety of environmental settings. Although the materials in this work showed potent bactericidal activities, environmental factors affect their performance. Thus, it is crucial to investigate how efficiently the materials work with or without routine cleanings in hospital setting. Further tests in hospital setting would provide valuable information to developed bactericidal surface to reduce the number of hospital associated infections.

Publication arising from this work

Gi Byoung Hwang, Kristopher Page, Adnan Patir, Sean P. Nair, Elaine Allan and Ivan P. Parkin, Short-lived anti-biofouling property of superhydrophobic surfaces and their transformation into bacteria reservoir, under review

Gi Byoung Hwang, adnan Patir, Elaine Allan, Sean P. Nair, and Ivan P. Parkin. Superhydrophobic and white light-activated bactericidal surface through a simple coating, ***ACS Appl. Mater. Interfaces***, **2017,** online publication, DOI: 10.1021/acsami.7b05977

Gi Byoung Hwang, Elaine Allan, and Ivan P. Parkin, White light-activated antimicrobial paint using crystal violet, ***ACS Appl. Mater. Interfaces***, **2016, 8, 15033-15039.**

Gi Byoung Hwang, Sacha Noimark, Kristopher Page, Sandeep Sehmi, Alexander J. Macrobert, Elaine Allan and Ivan P. Parkin, White light-activated antimicrobial surfaces: effect of nanoparticles type on activity, ***J. Mater. Chem. B***, **2016, 4, 2199-2207.**

References

1. Office for National Statistics. Deaths involving *Clostridium difficile* : England and Wales 2003–07. *Health Stat. Q.* **39**, 67-76 (2008).

2. Office for National Statistics. Deaths involving MRSA: England and Wales. *Health Stat. Q.* **39**, 56-66 (2008).

3. Garner, J. S., Jarvis, W. R., Emori, T. G., Horan, T. C. & Hughes, J. M. CDC definitions for nosocomial infections, 1988. *AJIC* **16**, 128-140, doi:10.1016/0196-6553(88)90053-3 (1988).

4. National Audit Office. Reducing healthcare associated infection in hospitals in England. (2009).
<http://www.publications.parliament.uk/pa/cm200809/cmselect/cmpubacc/812/81 2.pdf>

5. National Audit Office. Improving patient care by reducing the risk of hospital acquired infection: A progress report. (2004).

6. Rai, M., Yadav, A. & Gade, A. Silver nanoparticles as a new generation of antimicrobials. *Biotechnol. Adv.* **27**, 76-83, doi:10.1016/j.biotechadv.2008.09.002 (2009).

7. National Institutes of Health (US).Biological sciences curriculum study. NIH curriculum supplement series [Internet]. Bethesda (MD): national institutes of health (US); 2007. Understanding emerging and re-emerging infectious diseases. (2007).

8. Public Health England. Mandatory health care associated infection surveillance: Data quality bstatement. (Public Health England 2017).
 <https://www.gov.uk/government/publications/mandatory-healthcare-associatedinfection-hcai-surveillance-data-quality-statement>

9. Department of Health. The Health and Social Care Act 2008: Code of Practice on the prevention and control of infections and related guidance.(2015). <https://www.gov.uk/government/publications/the-health-and-social-care-act2008-code-of-practice-on-the-prevention-and-control-of-infections-and-relatedguidance>

10. Gurusamy, K. S., Koti, R., Toon, C. D., Wilson, P. & Davidson, B. R. Antibiotic therapy for the treatment of methicillin-resistant *Staphylococcus aureus* (MRSA) infections in surgical wounds. *Cochrane Database Syst. Rev.*, CD009726, doi:10.1002/14651858.CD009726.pub2 (2013).

11. Boucher, H. W. & Corey, G. R. Epidemiology of methicillin-resistant *Staphylococcus aureus*. *Clin. Infect. Dis.* **46 Suppl 5**, S344-349, doi:10.1086/533590 (2008).

12. Moellering, R. C., Jr. MRSA: the first half century. *J. Antimicrob. Chemother.* **67**, 4-11, doi:10.1093/jac/dkr437 (2012).

13. Kuehnert, M. J. *et al.* Methicillin-resistant-*Staphylococcus aureus* hospitalizations, United States. *Emerg. Infect. Dis.* **11**, 868-872, doi:10.3201/eid1106.040831 (2005).

14. Hospital Infection Society. The third prevalence survey of healthcare associated infections in acute hospitals (Hospital Infection Society 2006).

15. Public Health England. Annual Epidemiological Commentary Mandatory MRSA, MSSA and *E. coli* bacteraemia and *C. difficile* infection data 2016/17. (Public Health England 2017).
<https://www.gov.uk/government/uploads/system/uploads/attachment_data/file/634675/Annual_epidemiological_commentary_2017.pdf>

16. Monteiro, J. M. *et al.* Cell shape dynamics during the *staphylococcal* cell cycle. *Nat. Commun.* **6**, 8055, doi:10.1038/ncomms9055 (2015).

17. Rehm, S. J. & Tice, A. *Staphylococcus aureus*: methicillin-susceptible *S. aureus* to methicillin-resistant *S. aureus* and vancomycin-resistant *S. aureus*. *Clin. Infect. Dis.* **51 Suppl 2**, S176-182, doi:10.1086/653518 (2010).

18. National Health Service (NHS). *Staphylococcal* infections. (2015).<https://www.nhs.uk/conditions/staphylococcal-infections/>

19. Public Health England. *Staphylococcus aureus*: guidance, data and analysis.

(2014).
<https://www.gov.uk/government/collections/staphylococcus-aureus-guidancedata-and-analysis>

20. Public Health England. Annual epidemiological commentary: Mandatory MRSA, MSSA, and *E. coli* bacteriaemia and *C. difficile* infection data 2013/14. Public Health England (2014).
<https://www.gov.uk/government/uploads/system/uploads/attachment_data/file/330529/HCAI_mandatory_surveillance_annual_epidemiological_commentary_2013_14.pdf>

21. Rogers, K. & Kadner, R. J. Facts about *E. coli*: dimensions, as discussed in bacteria: diversity of structure of bacteria: – Britannica Online Encyclopedi. (2015).
<https://www.britannica.com/science/bacteria/Diversity-of-structure-of-bacteria>

22. US Centers for Disease Control and Prevention (CDC). *Escherichia coli* (E. coli). <https://www.cdc.gov/ecoli/general/index.html>

23. House of commons Committe of Public Account, Reducing healthcare associated infection in hospitals in England, <http://www.publications.parliament.uk/pa/cm200809/cmselect/cmpubacc/812/812.pdf>

24. Viljanen, M. K. *et al.* Outbreak of diarrhoea due to *Escherichia coli* 0111:B4 in school children and adults: association of Vi antigen-like reactivity. *The Lancet* **336**, 831-834, doi:10.1016/0140-6736(90)92337-h (1990).

25. Nataro, J. P. & Kaper, J. B. Diarrheagenic *Escherichia coli*. *Clin. Microbiol. Rev.* **11** 142-201 (1998).

26. Moreno, M. A., Furtner, F. & Rivara, F. P. *Clostridium difficile*: a cause of diarrhea in children. *JAMA Pediatr* **167**, 592, doi:10.1001/jamapediatrics.2013.2551 (2013).

27. Ryan, K. J. & Ray, C. G. Sherris Medical Microbiology. 322-324 (McGraw Hill., 2004).

28. Loo, V. G. *et al.* A predominantly clonal multi-institutional outbreak of *Clostridium difficile*-associated diarrhea with high morbidity and mortality. *N. Engl.*

J. Med. **353**, 2442-2449, doi:10.1056/NEJMoa051639 (2005).

29. Paredes-Sabj, D., Shen, A. & Sorg, J. A. *Clostridium difficile* spore biology: sporulation, germination, and spore structural proteins. *Trends Microbiol.* **22**, 406-416, doi:10.1016/j.tim.2014.04.003 (2014).

30. Edwards, A. N. *et al.* Chemical and Stress Resistances of *Clostridium difficile* spores and vegetative cells. *Front, Microbiol,* **7**, 1698, doi:10.3389/fmicb.2016.01698 (2016).

31. National Health Survice (NHS). *Clostridium difficile* (2016). <https://www.nhs.uk/conditions/c-difficile/>

32. Takeya, K. & Amako, K. A rod-shaped *pseudomonas* phage. *Virology* **28**, 163-165, doi:10.1016/0042-6822(66)90317-5 (1966).

33. Yayan, J., Ghebremedhin, B. & Rasche, K. Antibiotic resistance of *Pseudomonas aeruginosa* in pneumonia at a single university hospital center in germany over a 10-year period. *PLoS One* **10**, e0139836, doi:10.1371/journal.pone.0139836 (2015).

34. Public Health England. *Pseudomonas aeruginosa*: guidance, data and analysis. (Public Health England, 2017).

35. National Audit Office. The management and control of hospital acquired infection in acute NHS trusts in England. (National Audit Office, 2000). <https://www.nao.org.uk/report/the-management-and-control-of-hospital-acquiredinfection-in-acute-nhs-trusts-in-england/>

36. National Audit Office. Report 2004/05 Improving patient care by reducing the risks of hospital acquired infection: a progress report <https://www.nao.org.uk/report/improving-patient-care-by-reducing-the-risk-ofhospital-acquired-infection-a-progress-report/>

37. Health Protection Agency. Health care associated infection operational guidance and standards for health protection units (2012).

38. Public Health England. Annual Epidemiological Commentary: Mandatory

MRSA, MSSA and *E. coli* bacteraemia and *C. difficile* infection data, 2014/15. (Public Health England 2015). <https://www.gov.uk/government/uploads/system/uploads/attachment_data/file/442952/Annual_Epidemiological_Commentary_FY_2014_2015.pdf>

39. Bunn, S. UK Trends in infectious disease. *POST Note* **545**, 1-5 (2017).

40. Otter, J. A., Yezli, S., Salkeld, J. A. & French, G. L. Evidence that contaminated surfaces contribute to the transmission of hospital pathogens and an overview of strategies to address contaminated surfaces in hospital settings. *Am. J. Infect. Control* **41**, S6-11, doi:10.1016/j.ajic.2012.12.004 (2013).

41. Boyce, J. M. *et al.* Outbreak of multidrug-resistant *Enterococcus faecium* with transferable vanB class vancomycin resistance. *J. Clin. Microbiol.* **32**, 1148-1153 (1994).

42. Boyce, J. M., Potter-Bynoe, G., Chenevert, C. & King, T. Environmental contamination due to methicillin-resistant *Staphylococcus aureus*: Possible infection control implications. *Infect. Control Hosp. Epidemiol.* **18**, 622-627, doi:10.2307/30141488 (1997).

43. Huslage, K., Rutala, W. A., Sickbert-Bennett, E. & Weber, D. J. A quantitative approach to defining "high-touch" surfaces in hospitals. *Infect. Control Hosp. Epidemiol.* **31**, 850-853, doi:10.1086/655016 (2010).

44. Yezli, S. & Otter, J. A. Minimum infective dose of the major human respiratory and enteric viruses transmitted through food and the environment. *Food Environ Virol* **3**, 1-30, doi:10.1007/s12560-011-9056-7 (2011).

45. Hayden, M. K., Blom, D. W., Lyle, E. A., Moore, C. G. & Weinstein, R. A. Risk of hand or glove contamination after contact with patients colonized with vancomycin-resistant *enterococcus* or the colonized patients' environment. *Infect. Control Hosp. Epidemiol.* **29**, 149-154, doi:10.1086/524331 (2008).

46. Kramer, A., Schwebke, I. & Kampf, G. How long do nosocomial pathogens persist on inanimate surfaces? A systematic review. *BMC Infect. Dis.* **6**, 130,

doi:10.1186/1471-2334-6-130 (2006).

47. Wagenvoort, J. H., Sluijsmans, W. & Penders, R. J. Better environmental survival of outbreak vs. sporadic MRSA isolates. *J. Hosp. Infect.* **45**, 231-234, doi:10.1053/jhin.2000.0757 (2000).

48. Wagenvoort, J. H. *et al.* Environmental survival of vancomycin-resistant *Enterococcus faecium*. *J. Hosp. Infect.* **77**, 282-283, doi:10.1016/j.jhin.2010.11.008 (2011).

49. Yezli, S. & Otter, J. A. Does the discovery of biofilms on dry hospital environmental surfaces change the way we think about hospital disinfection? *J. Hosp. Infect.* **81**, 293-294, doi:10.1016/j.jhin.2012.05.012 (2012).

50. Vickery, K. *et al.* Presence of biofilm containing viable multiresistant organisms despite terminal cleaning on clinical surfaces in an intensive care unit. *J. Hosp. Infect.* **80**, 52-55, doi:10.1016/j.jhin.2011.07.007 (2012).

51. Page, K., Wilson, M. & Parkin, I. P. Antimicrobial surfaces and their potential in reducing the role of the inanimate environment in the incidence of hospital-acquired infections. *J. Mater. Chem.* **19**, 3819-3831, doi:10.1039/b818698g (2009).

52. Quinn, M. M. *et al.* Cleaning and disinfecting environmental surfaces in health care: Toward an integrated framework for infection and occupational illness prevention. *Am. J. Infect. Control* **43**, 424-434, doi:10.1016/j.ajic.2015.01.029 (2015).

53. Morter, S. *et al.* Norovirus in the hospital setting: virus introduction and spread within the hospital environment. *J. Hosp. Infect.* **77**, 106-112, doi:10.1016/j.jhin.2010.09.035 (2011).

54. Manian, F. A. *et al.* Isolation of Acinetobacter baumannii complex and methicillin-resistant *Staphylococcus aureus* from hospital rooms following terminal cleaning and disinfection: can we do better? *Infect. Control Hosp. Epidemiol.* **32**, 667-672, doi:10.1086/660357 (2011).

55. Byers, K. E. *et al.* Disinfection of hospital rooms contaminated with vancomycin-resistant *Enterococcus faecium*. *Infect. Control Hosp. Epidemiol.* **19**, 261-264 (1998).

56. E., Z. C. & C., A. E. The significance of marine bacteria in the fouling of submerged surfaces. *J. Bacteriol.* **29**, 239-251 (1935).

57. Hasan, J., Crawford, R. J. & Ivanova, E. P. Antibacterial surfaces: the quest for a new generation of biomaterials. *Trends Biotechnol.* **31**, 295-304, doi:10.1016/j.tibtech.2013.01.017 (2013).

58. Chung, K. K. *et al.* Impact of engineered surface microtopography on biofilm formation of *Staphylococcus aureus*. *Biointerphases* **2**, 89-94, doi:10.1116/1.2751405 (2007).

59. Tiller, J. C., Liao, C. J., Lewis, K. & Klibanov, A. M. Designing surfaces that kill bacteria on contact. *PNAS* **98**, 5981-5985, doi:DOI 10.1073/pnas.111143098 (2001).

60. Ivanova, E. P. *et al.* Natural bactericidal surfaces: mechanical rupture of *Pseudomonas aeruginosa* cells by cicada wings. *Small* **8**, 2489-2494, doi:10.1002/smll.201200528 (2012).

61. Law, K. Y. Definitions for hydrophilicity, hydrophobicity, and superhydrophobicity: getting the basics right. *J. Phys. Chem. Lett.* **5**, 686-688, doi:10.1021/jz402762h (2014).

62. Chang, F.-M., Hong, S.-J., Sheng, Y.-J. & Tsao, H.-K. High contact angle hysteresis of superhydrophobic surfaces: hydrophobic defects. *Appl. Phys. Lett.* **95**, 064102, doi:10.1063/1.3204006 (2009).

63. Ma, M. & Hill, R. M. Superhydrophobic surfaces. *Curr. Opin. in Colloid Interface Sci.* **11**, 193-202, doi:10.1016/j.cocis.2006.06.002 (2006).

64. Li, X. M., Reinhoudt, D. & Crego-Calama, M. What do we need for a superhydrophobic surface? A review on the recent progress in the preparation of

superhydrophobic surfaces. *Chem. Soc. Rev.* **36**, 1350-1368, doi:10.1039/b602486f (2007).

65. Privett, B. J. *et al.* Antibacterial fluorinated silica colloid superhydrophobic surfaces. *Langmuir* **27**, 9597-9601, doi:10.1021/la201801e (2011).

66. Liu, K. & Jiang, L. Bio-inspired design of multiscale structures for function integration. *Nano Today* **6**, 155-175, doi:10.1016/j.nantod.2011.02.002 (2011).

67. Ma, J., Sun, Y., Gleichauf, K., Lou, J. & Li, Q. Nanostructure on taro leaves resists fouling by colloids and bacteria under submerged conditions. *Langmuir* **27**, 10035-10040, doi:10.1021/la2010024 (2011).

68. Crick, C. R., Ismail, S., Pratten, J. & Parkin, I. P. An investigation into bacterial attachment to an elastomeric superhydrophobic surface prepared via aerosol assisted deposition. *Thin Solid Films* **519**, 3722-3727, doi:10.1016/j.tsf.2011.01.282 (2011).

69. Freschauf, L. R., McLane, J., Sharma, H. & Khine, M. Shrink-induced superhydrophobic and antibacterial surfaces in consumer plastics. *PLoS One* **7**, e40987, doi:10.1371/journal.pone.0040987 (2012).

70. Tang, P. F. *et al.* Effect of superhydrophobic surface of titanium on *Staphylococcus aureus* Adhesion. *J. Nanomater.*, doi:Artn 17892110.1155/2011/178921 (2011).

71. Ozkan, E., Crick, C. C., Taylor, A., Allan, E. & Parkin, I. P. Copper-based water repellent and antibacterial coatings by aerosol assisted chemical vapour deposition. *Chem. Sci.* **7**, 5126-5131, doi:10.1039/c6sc01150k (2016).

72. Wong, T. S. *et al.* Bioinspired self-repairing slippery surfaces with pressure-stable omniphobicity. *Nature* **477**, 443-447, doi:10.1038/nature10447 (2011).

73. Epstein, A. K., Wong, T. S., Belisle, R. A., Boggs, E. M. & Aizenberg, J. Liquid-infused structured surfaces with exceptional anti-biofouling performance. *PNAS* **109**, 13182-13187, doi:10.1073/pnas.1201973109 (2012).

74. Leslie, D. C. *et al.* A bioinspired omniphobic surface coating on medical devices

prevents thrombosis and biofouling. *Nat. Biotechnol.* **32**, 1134-1140, doi:10.1038/nbt.3020 (2014).

75. Yao, X. *et al.* Adaptive fluid-infused porous films with tunable transparency and wettability. *Nat. Mater.* **12**, 529-534, doi:10.1038/nmat3598 (2013).

76. Kim, P., Kreder, M. J., Alvarenga, J. & Aizenberg, J. Hierarchical or not? Effect of the length scale and hierarchy of the surface roughness on omniphobicity of lubricant-infused substrates. *Nano Lett.* **13**, 1793-1799, doi:10.1021/nl4003969 (2013).

77. Howell, C. *et al.* Stability of surface-immobilized lubricant interfaces under flow. *Chem Mater* **27**, 1792-1800, doi:10.1021/cm504652g (2015).

78. Vogel, N., Belisle, R. A., Hatton, B., Wong, T. S. & Aizenberg, J. Transparency and damage tolerance of patternable omniphobic lubricated surfaces based on inverse colloidal monolayers. *Nat. Commun.* **4**, 2167, doi:10.1038/ncomms3176 (2013).

79. Amini, S. *et al.* Preventing mussel adhesion using lubricant-infused materials. *Science* **357**, 668-+, doi:10.1126/science.aai8977 (2017).

80. MacCallum, N. *et al.* Liquid-infused silicone as a biofouling-free medical material. *ACS Biomater. Sci. Eng.* **1**, 43-51, doi:10.1021/ab5000578 (2015).

81. Howell, C. *et al.* Self-replenishing vascularized fouling-release surfaces. *ACS Appl. Mater. Interfaces* **6**, 13299-13307, doi:10.1021/am503150y (2014).

82. Allen, M. J., Tung, V. C. & Kaner, R. B. Honeycomb carbon: a review of graphene. *Chem. Rev.* **110**, 132-145, doi:10.1021/cr900070d (2010).

83. Novoselov, K. S. *et al.* Electric field effect in atomically thin carbon films. *Science* **306**, 666-669, doi:10.1126/science.1102896 (2004).

84. Discovery of graphen. APS News Vol. 18   2 (American Physical Society, New Yorks, 2009).

85. Frank, I. W., Tanenbaum, D. M., van der Zande, A. M. & McEuen, P. L. Mechanical properties of suspended graphene sheets. *J. Vac. Sci. Technol.* **25**, 2558, doi:10.1116/1.2789446 (2007).

86. Falkovsky, L. A. Optical properties of graphene. *J. phys. Conf. Ser.* **129**, 012004, doi:10.1088/1742-6596/129/1/012004 (2008).

87. Shao, Y. *et al.* Graphene based electrochemical sensors and biosensors: A review. *Electroanalysis* **22**, 1027-1036, doi:10.1002/elan.200900571 (2010).

88. Martínez-Pérez, M., Puértolas, J. A., González-Pallarés, I. & Esteban, J. Bacterial adhesion studies on graphene layers obtained by chemical vapour deposition. *DIAM Conference.*(Elsvier).

89. Parra, C. *et al.* A nanomolecular approach to decrease adhesion of biofouling-producing bacteria to graphene-coated material. *J. Nanobiotech.* **13**, 82, doi:10.1186/s12951-015-0137-x (2015).

90. Rai, M., Yadav, A. & Gade, A. Silver nanoparticles as a new generation of antimicrobials. *Biotechnol. Adv.* **27**, 76-83 (2009).

91. Castellano, J. J. *et al.* Comparative evaluation of silver-containing antimicrobial dressings and drugs. *Int. Wound J.* **4**, 114-122 (2007).

92. Heggers, J. P. *et al.* Acticoat versus silverlon: The truth. *J. Burn Care Rehabil.* **23**, S115, doi:10.1097/00004630-200203002-00146 (2002).

93. Landsdown, A. B. G. Silver I: its antibacterial properties and mechanism of action. *J. Wound Care* **11**, 125-138 (2002).

94. Klasen, H. J. Historical review of the use of silver in the treatment of burns. Part I early uses. *Burns* **30**, 1-9 (2000).

95. Feng, Q. L. *et al.* A mechanistic study of the antibacterial effect of silver ions on *Escherichia coli* and *Staphylococcus aureus*. *J. Biomed. Mater. Res.* **52**, 662-668, doi:DOI: 10.1002/1097-4636(20001215)52:4<662::AID-JBM10>3.0.CO;2- (2000).

96. Matsumura, Y., Yoshikata, K., Kunisaki, S. i. & Tsuchido, T. Mode of bactericidal action of silver zeolite and its comparison with that of silver nitrate. *Appl. Environ. Microbiol.* **69**, 4278-4281, doi:10.1128/aem.69.7.4278-4281.2003 (2003).

97. Furno, F. *et al.* Silver nanoparticles and polymeric medical devices: a new approach to prevention of infection? *J. Antimicrob. Chemother.* **54**, 1019-1024, doi:10.1093/jac/dkh478 (2004).

98. Li, Y., Leung, P., Yao, L., Song, Q. W. & Newton, E. Antimicrobial effect of surgical masks coated with nanoparticles. *J. Hosp. Infect.* **62**, 58-63, doi:10.1016/j.jhin.2005.04.015 (2006).

99. Durán, N., Marcato, P. D., De Souza, G. I. H., Alves, O. L. & Esposito, E. Antibacterial effect of silver nanoparticles produced by fungal process on textile fabrics and their effluent treatment. *J. Biomed. Nanotech.* **3**, 203-208, doi:10.1166/jbn.2007.022 (2007).

100. Chopra, I. The increasing use of silver-based products as antimicrobial agents: a useful development or a cause for concern? *J. Antimicrob. Chemother.* **59**, 587-590, doi:10.1093/jac/dkm006 (2007).

101. Fox, C. L., Jr. & Modak, S. M. Mechanism of silver sulfadiazine action on burn wound infections. *Antimicrob. Agents Chemother.* **5**, 582-588 (1974).

102. Jung, J. H., Hwang, G. B., Lee, J. E. & Bae, G. N. Preparation of airborne Ag/CNT hybrid nanoparticles using an aerosol process and their application to antimicrobial air filtration. *Langmuir* **27**, 10256-10264 (2011).

103. Jain, P. & Pradeep, T. Potential of silver nanoparticle-coated polyurethane foam as an antibacterial water filter. *Biotechnol. Bioeng.* **90**, 59-63, doi:10.1002/bit.20368 (2005).

104. Braydich-Stolle, L., Hussain, S., Schlager, J. J. & Hofmann, M. C. In vitro cytotoxicity of nanoparticles in mammalian germline stem cells. *Toxicol. Sci.* **88**, 412-419, doi:10.1093/toxsci/kfi256 (2005).

105. Borkow, G. & Gabbay, J. Copper, an ancient remedy returning to fight microbial, fungal and viral infections. *Curr. Chem. Biol.* **3**, 272-278, doi:10.2174/187231309789054887 (2009).

106. Ingle, A. P., Duran, N. & Rai, M. Bioactivity, mechanism of action, and cytotoxicity of copper-based nanoparticles: a review. *Appl. Microbiol. Biotechnol.* **98**, 1001-1009, doi:10.1007/s00253-013-5422-8 (2014).

107. Noyce, J. O., Michels, H. & Keevil, C. W. Potential use of copper surfaces to reduce survival of epidemic meticillin-resistant *Staphylococcus aureus* in the healthcare environment. *J. Hosp. Infect.* **63**, 289-297, doi:10.1016/j.jhin.2005.12.008 (2006).

108. Wilks, S. A., Michels, H. & Keevil, C. W. The survival of *Escherichia coli* O157 on a range of metal surfaces. *Int. J. Food Microbiol.* **105**, 445-454, doi:10.1016/j.ijfoodmicro.2005.04.021 (2005).

109. Wilks, S. A., Michels, H. T. & Keevil, C. W. Survival of *Listeria monocytogenes* Scott A on metal surfaces: implications for cross-contamination. *Int. J. Food Microbiol.* **111**, 93-98, doi:10.1016/j.ijfoodmicro.2006.04.037 (2006).

110. Weaver, L., Michels, H. T. & Keevil, C. W. Survival of *Clostridium difficile* on copper and steel: futuristic options for hospital hygiene. *J. Hosp. Infect.* **68**, 145-151, doi:10.1016/j.jhin.2007.11.011 (2008).

111. Sehmi, S. K. *et al.* Potent antibacterial activity of copper embedded into silicone and polyurethane. *ACS Appl. Mater. Interfaces* **7**, 22807-22813, doi:10.1021/acsami.5b08665 (2015).

112. Mao, S., Pu, H. & Chen, J. Graphene oxide and its reduction: modeling and experimental progress. *RSC Adv.* **2**, 2643, doi:10.1039/c2ra00663d (2012).

113. Dreyer, D. R., Park, S., Bielawski, C. W. & Ruoff, R. S. The chemistry of graphene oxide. *Chem. Soc. Rev.* **39**, 228-240, doi:10.1039/b917103g (2010).

114. Compton, O. C. & Nguyen, S. T. Graphene oxide, highly reduced graphene

oxide, and graphene: versatile building blocks for carbon-based materials. *Small* **6**, 711-723, doi:10.1002/smll.200901934 (2010).

115. Perreault, F., de Faria, A. F., Nejati, S. & Elimelech, M. Antimicrobial properties of graphene oxide nanosheets: Why size matters. *ACS Nano* **9**, 7226-7236, doi:10.1021/acsnano.5b02067 (2015).

116. Gurunathan, S., Han, J. W., Dayem, A. A., Eppakayala, V. & Kim, J. H. Oxidative stress-mediated antibacterial activity of graphene oxide and reduced graphene oxide in *Pseudomonas aeruginosa*. *Int. J. Nanomedicine* **7**, 5901-5914, doi:10.2147/IJN.S37397 (2012).

117. Chen, J. *et al.* Graphene oxide exhibits broad-spectrum antimicrobial activity against bacterial phytopathogens and fungal conidia by intertwining and membrane perturbation. *Nanoscale* **6**, 1879-1889, doi:10.1039/c3nr04941h (2014).

118. Mejias Carpio, I. E., Santos, C. M., Wei, X. & Rodrigues, D. F. Toxicity of a polymer-graphene oxide composite against bacterial planktonic cells, biofilms, and mammalian cells. *Nanoscale* **4**, 4746-4756, doi:10.1039/c2nr30774j (2012).

119. Akhavan, O. & Ghaderi, E. Toxicity of graphene and graphene oxide nanowalls against bacteria. *ACS Nano* **4**, 5731-5736, doi:10.1021/nn101390x (2010).

120. Krishnamoorthy, K., Veerapandian, M., Zhang, L.-H., Yun, K. & Kim, S. J. Antibacterial efficiency of graphene nanosheets against pathogenic bacteria via lipid peroxidation. *J. Phys. Chem. C* **116**, 17280-17287, doi:10.1021/jp3047054 (2012).

121. Perreault, F., Fonseca de Faria, A. & Elimelech, M. Environmental applications of graphene-based nanomaterials. *Chem. Soc. Rev.* **44**, 5861-5896, doi:10.1039/c5cs00021a (2015).

122. Hu, W. *et al.* Graphene-based antibacterial paper. *ACS Nano* **4**, 4317-4323, doi:10.1021/nn101097v (2010).

123. Musico, Y. L. F., Santos, C. M., Dalida, M. L. P. & Rodrigues, D. F. Surface modification of membrane filters using graphene and graphene oxide-based

nanomaterials for bacterial inactivation and removal. *ACS Sustainable Chem. Engin.* **2**, 1559-1565, doi:10.1021/sc500044p (2014).

124. Santos, C. M. *et al.* Antimicrobial graphene polymer (PVK-GO) nanocomposite films. *Chem. Commun.* **47**, 8892-8894, doi:10.1039/c1cc11877c (2011).

125. Karimi, L., Yazdanshenas, M. E., Khajavi, R., Rashidi, A. & Mirjalili, M. Using graphene/TiO$_2$ nanocomposite as a new route for preparation of electroconductive, self-cleaning, antibacterial and antifungal cotton fabric without toxicity. *Cellulose* **21**, 3813-3827, doi:10.1007/s10570-014-0385-1 (2014).

126. Martinetto, P., Gariglio, M., Lombard, G. F., Fiscella, B. & Boggio, F. Bactericidal effects induced by laser irradiation and haematoporphyrin against gram-positive and gram-negative microorganisms. *Drugs Exp. Clin. Res.* **12**, 335-342 (1986).

127. Jori, G. *et al.* Photodynamic therapy in the treatment of microbial infections: basic principles and perspective applications. *Lasers Surg. Med.* **38**, 468-481, doi:10.1002/lsm.20361 (2006).

128. Gozhansky, M. Z. S. & Nitzan, Y. Effects of photoactivated haematoporphyrin derivative on bacteria and antibiotic resistance. *Microbios. Lett.* **21**, 103–112 (1982).

129. Nitzan, Y. M., Gutterman, S. & Malik, Z. Effect of photoactivated hematoporphyrin derivative on the viability of *Staphylococcus aureus*. *Curr. Microbiol.* **8**, 279–284 (1983).

130. Venezio, F. R. *et al.* Bactericidal effects of photoradiation therapy with hematoporphyrin derivative. *J. Infect. Dis.* **151**, 166-169 (1985).

131. Mital, G. S. & Manoj, T. A review of TiO$_2$ nanoparticles *Chin. Sci. Bull.* **56**, 1639-1657, doi:doi: 10.1007/s11434-011-4476-1 (2011).

132. Matsunaga, T., Tomoda, R., Nakajima, T. & Wake, H. Photoelectrochemical sterilization of microbial cells by semiconductor powders. *FEMS Microbiol. Lett.*

29, 211-214, doi:10.1111/j.1574-6968.1985.tb00864.x (1985).

133. Ibáñez, J. A., Litter, M. I. & Pizarro, R. A. Photocatalytic bactericidal effect of TiO_2 on *Enterobacter cloacae*. *J. Photochem. Photobiol. A* **157**, 81-85, doi:10.1016/s1010-6030(03)00074-1 (2003).

134. Amezaga-Madrid, P., Nevarez-Moorillon, G. V., Orrantia-Borunda, E. & Miki-Yoshida, M. Photoinduced bactericidal activity against *Pseudomonas aeruginosa* by TiO_2 based thin films. *FEMS Microbiol. Lett.* **211**, 183-188, doi:10.1111/j.1574-6968.2002.tb11222.x (2002).

135. Herrera Melián, J. A. *et al.* The photocatalytic disinfection of urban waste waters. *Chemosphere* **41**, 323-327, doi:10.1016/s0045-6535(99)00502-0 (2000).

136. Saito, T., Iwase, T., Horie, J. & Morioka, T. Mode of photocatalytic bactericidal action of powdered semiconductor TiO_2 on mutans *Streptococci*. *J. Photochem. Photobiol. B* **14**, 369-379, doi:10.1016/1011-1344(92)85115-b (1992).

137. Watts, R. J., Kong, S., Orr, M. P., Miller, G. C. & Henry, B. E. Photocatalytic inactivation of coliform bacteria and viruses in secondary wastewater effluent. *Water Res.* **29**, 95-100, doi:10.1016/0043-1354(94)e0122-m (1995).

138. Vohra, A., Goswami, D. Y., Deshpande, D. A. & Block, S. S. Enhanced photocatalytic inactivation of bacterial spores on surfaces in air. *J. Ind. Microbiol. Biotechnol.* **32**, 364-370, doi:10.1007/s10295-005-0006-y (2005).

139. Ireland, J. C., Klostermann, P., Rice, E. W. & Clark, R. M. Inactivation of *Escherichia coli* by titanium dioxide photocatalytic oxidation. *Appl. Environ. Microbiol.* **69**, 1668-1670 (1993).

140. Neamen, D. A. Semiconductor Physics and Devices: Basic Principles. (McGraw-Hill, 2003).

141. Anandan, S., Ikuma, Y. & Niwa, K. An overview of semi-conductor photocatalysis: modification of TiO_2 nanomaterials. *Sol. St. Phen.* **162**, 239-260, doi:10.4028/www.scientific.net/SSP.162.239 (2010).

142. Pauly, N., Yubero, F., Espinos, J. P. & Tougaard, S. Optical properties and electronic transitions of zinc oxide, ferric oxide, cerium oxide, and samarium oxide in the ultraviolet and extreme ultraviolet. *Appl. Opt.* **56**, 6611-6621, doi:10.1364/AO.56.006611 (2017).

143. Wang, Z. L. Zinc oxide nanostructures: growth, properties and applications. *J Phys-Condens Mat* **16**, R829-R858, doi:Pii S0953-8984(04)58969-510.1088/0953-8984/16/25/R01 (2004).

144. Xie, Y., He, Y., Irwin, P. L., Jin, T. & Shi, X. Antibacterial activity and mechanism of action of zinc oxide nanoparticles against *Campylobacter jejuni Appl. Environ. Microbiol.* **77** 2325-2331(2011).

145. Sirelkhatim, A. *et al.* Review on zinc oxide nanoparticles: Antibacterial activity and toxicity mechanism. *Nano-Micro Lett.* **7**, 219-242, doi:10.1007/s40820-015-0040-x (2015).

146. Jones, N., Ray, B., Ranjit, K. T. & Manna, A. C. Antibacterial activity of ZnO nanoparticle suspensions on a broad spectrum of microorganisms. *FEMS Microbiol. Lett.* **279**, 71-76, doi:10.1111/j.1574-6968.2007.01012.x (2008).

147. Liu, Y. *et al.* Antibacterial activities of zinc oxide nanoparticles against *Escherichia coli* O157:H7. *J. Appl. Microbiol.* **107**, 1193-1201, doi:10.1111/j.1365-2672.2009.04303.x (2009).

148. Janotti, A. & Van de Walle, C. G. Fundamentals of zinc oxide as a semiconductor. *Rep. prog. Phys.* **72**, 126501, doi:10.1088/0034-4885/72/12/126501 (2009).

149. Docampo, R., Moreno, S. N., Muniz, R. P., Cruz, F. S. & Mason, R. P. Light-enhanced free radical formation and trypanocidal action of gentian violet (crystal violet). *Science* **220**, 1292-1295 (1983).

150. Demidova, T. N. & Hamblin, M. R. Photodynamic inactivation of *Bacillus* spores, mediated by phenothiazinium dyes. *Appl. Environ. Microbiol.* **71**, 6918-6925, doi:10.1128/AEM.71.11.6918-6925.2005 (2005).

151. Wood, S., Metcalf, D., Devine, D. & Robinson, C. Erythrosine is a potential photosensitizer for the photodynamic therapy of oral plaque biofilms. *J. Antimicrob. Chemother.* **57**, 680-684, doi:10.1093/jac/dkl021 (2006).

152. Wainwright, M. Photodynamic antimicrobial chemotherapy (PACT). *J. Antimicrob. Chemother.* **42**, 13-28, doi:10.1093/jac/42.1.13 (1998).

153/ Vatansever, F. *et al.* Antimicrobial strategies centered around reactive oxygen species-bactericidal antibiotics, photodynamic therapy, and beyond. *FEMS Microbiol. Rev.* **37**, 955-989, doi:10.1111/1574-6976.12026 (2013).

154. Henderson, B. W. & Dougherty, T. J. How does photodynamic therapy work? *Photochem. Photobiol.* **55**, 145-157, doi:10.1111/j.1751-1097.1992.tb04222.x (1992).

155. Hamblin, M. R. & Hasan, T. Photodynamic therapy: a new antimicrobial approach to infectious disease? *Photochem. Photobiol. Sci.* **3**, 436-450, doi:10.1039/b311900a (2004).

156. Ozkan, E., Allan, E. & Parkin, I. P. The antibacterial properties of light-activated polydimethylsiloxane containing crystal violet. *RSC Adv.* **4**, 51711-51715, doi:10.1039/c4ra08503e (2014).

157. Piccirillo, C. *et al.* Antimicrobial activity of methylene blue and toluidine blue O covalently bound to a modified silicone polymer surface. *J. Mater. Chem.* **19**, 6167, doi:10.1039/b905495b (2009).

158. Noimark, S. *et al.* Incorporation of methylene blue and nanogold into polyvinyl chloride catheters; a new approach for light-activated disinfection of surfaces. *J. Mater. Chem.* **22**, 15388, doi:10.1039/c2jm31987j (2012).

159. Noimark, S., Allan, E. & Parkin, I. P. Light-activated antimicrobial surfaces with enhanced efficacy induced by a dark-activated mechanism. *Chem. Sci.* **5**, 2216-2223, doi:10.1039/c3sc53186d (2014).

160. Noimark, S. *et al.* Photobactericidal polymers; the incorporation of crystal

violet and nanogold into medical grade silicone. *RSC Advances* **3**, 18383, doi:10.1039/c3ra42629g (2013).

161. Sehmi, S. K. *et al.* Lethal photosensitisation of *Staphylococcus aureus* and *Escherichia coli* using crystal violet and zinc oxide-encapsulated polyurethane. *J. Mater. Chem. B* **3**, 6490-6500, doi:10.1039/c5tb00971e (2015).

162. Ayliffe, G. A. J., Collins, B. J., Lowbury, E. J. L., Babb, J. R. & Lilly, H. A. Ward floors and other surfaces as reservoirs of hospital infection. *J Hyg-Camb* **65**, 515-536, doi:10.1017/s0022172400046052 (2009).

163. Boyce, J. M. Environmental contamination makes an important contribution to hospital infection. *J. Hosp. Infect.* **65**, 50-54, doi:10.1016/s0195-6701(07)60015-2 (2007).

164. Morones-Ramirez, J. R., Winkler, J. A., Spina, C. S. & Collins, J. J. Silver enhances antibiotic activity against gram-negative bacteria. *Sci. Transl. Med.* **5**, 190ra181-190ra181 (2013).

165. Lakshmi Prasanna, V. & Vijayaraghavan, R. Insight into the mechanism of antibacterial activity of ZnO: surface defects mediated reactive oxygen species even in the dark. *Langmuir* **31**, 9155-9162, doi:10.1021/acs.langmuir.5b02266 (2015).

166. Visai, L. *et al.* Titanium oxide antibacterial surfaces in biomedical devices. *Int. J. Artif. Organs* **34**, 929-946, doi:10.5301/ijao.5000050 (2011).

167. Mahalakshmi, P. V., Vanithakumari, S. C., Gopal, J., Mudali, U. K. & Raj, B. Enhancing corrosion and biofouling resistance through superhydrophobic surface modification. *Curr. Sci.* **101**, 1328-1336 (2011).

168. Shateri Khalil-Abad, M. & Yazdanshenas, M. E. Superhydrophobic antibacterial cotton textiles. *J. Colloid Interface Sci.* **351**, 293-298, doi:10.1016/j.jcis.2010.07.049 (2010).

169. Chung, J. S. *et al.* Silver-perfluorodecanethiolate complexes having superhydrophobic, antifouling, antibacterial properties. *J. Colloid Interface Sci.* **366**,

64-69, doi:10.1016/j.jcis.2011.09.080 (2012).

170. Hong, S.-J., Li, Y.-F., Hsiao, M.-J., Sheng, Y.-J. & Tsao, H.-K. Anomalous wetting on a superhydrophobic graphite surface. *Appl. Phys. Lett.* **100**, 121601, doi:10.1063/1.3697831 (2012).

171. Larmour, I. A., Bell, S. E. J. & Saunders, G. C. Remarkably simple fabrication of superhydrophobic surfaces using electroless galvanic deposition. *Angew. Chem. Int. Ed.* **119**, 1740-1742, doi:10.1002/ange.200604596 (2007).

172. Fey, P. D. *et al.* A genetic resource for rapid and comprehensive phenotype screening of nonessential *Staphylococcus aureus* genes. *MBio.* **4**, e00537-00512, doi:10.1128/mBio.00537-12 (2013).

173. Bayles, K. Product Information sheet for NR-47222: *Staphylococcus aureus subsp. aureus*, Strain JE2, transposon mutant NE679 (SAUSA300_0629) (BEI resource, 2014).

174. O'Toole, G. A. & Kolter, R. Initiation of biofilm formation in *Pseudomonas fluorescens* WCS365 proceeds via multiple, convergent signalling pathways: a genetic analysis. *Mol. Microbiol.* **28**, 449-461, doi:10.1046/j.1365-2958.1998.00797.x (1998).

175. Lu, Y. *et al.* Repellent materials. Robust self-cleaning surfaces that function when exposed to either air or oil. *Science* **347**, 1132-1135, doi:10.1126/science.aaa0946 (2015).

176. Feng, G. *et al.* Bacterial attachment and biofilm formation on surfaces are reduced by small-diameter nanoscale pores: how small is small enough? *NPJ Biofilms Microbiomes* **1**, 15022, doi:10.1038/npjbiofilms.2015.22 (2015).

177. Ammar, Y., Swailes, D., Bridgens, B. & Chen, J. Influence of surface roughness on the initial formation of biofilm. *Surf. Coat. Technol.* **284**, 410-416, doi:10.1016/j.surfcoat.2015.07.062 (2015).

178. Cerca, N., Pier, G. B., Vilanova, M., Oliveira, R. & Azeredo, J. Quantitative

analysis of adhesion and biofilm formation on hydrophilic and hydrophobic surfaces of clinical isolates of *Staphylococcus epidermidis*. *Res. Microbiol.* **156**, 506-514, doi:10.1016/j.resmic.2005.01.007 (2005).

179. Pringle, J. H. & Fletcher, M. Influence of substratum wettability on attachment of freshwater bacteria to solid surfaces. *Appl. Environ. Microbiol.* **45**, 811-817 (1983).

180. Harapanahalli, A. K., Chen, Y., Li, J., Busscher, H. J. & van der Mei, H. C. Influence of adhesion force on icaA and cidA gene expression and production of matrix components in *Staphylococcus aureus* biofilms. *Appl. Environ. Microbiol.* **81**, 3369-3378, doi:10.1128/AEM.04178-14 (2015).

181. Harapanahalli, A. K., Younes, J. A., Allan, E., van der Mei, H. C. & Busscher, H. J. Chemical signals and mechanosensing in bacterial responses to their environment. *PLoS Pathog* **11**, e1005057, doi:10.1371/journal.ppat.1005057 (2015).

182. Shirtcliffe, N. J., McHale, G., Newton, M. I., Perry, C. C. & Pyatt, F. B. Plastron properties of a superhydrophobic surface. *Appl. Phys. Lett.* **89**, 104106, doi:10.1063/1.2347266 (2006).

183. Peñas-López, P., Parrales, M. A. & Rodríguez-Rodríguez, J. Dissolution of a spherical cap bubble adhered to a flat surface in air-saturated water. *J. Fluid Mech.* **775**, 53-76, doi:10.1017/jfm.2015.291 (2015).

184. Manley, D. M. J. P. Change of size of air bubbles in water containing a small dissolved air content. *Brit. J. Appl. Phys.* **11**, 38-42, doi:Doi 10.1088/0508-3443/11/1/307 (1960).

185. Fadeeva, E. *et al.* Bacterial retention on superhydrophobic titanium surfaces fabricated by femtosecond laser ablation. *Langmuir* **27**, 3012-3019, doi:10.1021/la104607g (2011).

186. Truong, V. K. *et al.* Air-directed attachment of coccoid bacteria to the surface of superhydrophobic lotus-like titanium. *Biofouling* **28**, 539-550, doi:10.1080/08927014.2012.694426 (2012).

187. Stallard, C. P., McDonnell, K. A., Onayemi, O. D., O'Gara, J. P. & Dowling, D. P. Evaluation of protein adsorption on atmospheric plasma deposited coatings exhibiting superhydrophilic to superhydrophobic properties. *Biointerphases* **7**, 31, doi:10.1007/s13758-012-0031-0 (2012).

188. Pernites, R. B. *et al.* Tunable protein and bacterial cell adsorption on colloidally templated superhydrophobic polythiophene films. *Chem. Mater.* **24**, 870-880, doi:10.1021/cm2007044 (2012).

189. Zhang, X., Wang, L. & Levänen, E. Superhydrophobic surfaces for the reduction of bacterial adhesion. *RSC Adv.* **3**, 12003, doi:10.1039/c3ra40497h (2013).

190. El-Sayed, G. O. Removal of methylene blue and crystal violet from aqueous solutions by palm kernel fiber. *Desalination* **272**, 225-232, doi:10.1016/j.desal.2011.01.025 (2011).

191. Green, F. The Sigma-Aldrich handbook of stains. 239-240 (Aldrich Chemical Co., Inc., 1990).

192. Ben-Hur, E. *et al.* The photodecontamination of cellular blood components: Mechanisms and use of photosensitization in transfusion medicine. *Transfus. Med. Rev.* **10**, 15-22, doi:10.1016/s0887-7963(96)80119-2 (1996).

193. Oleinick, N. L. & Evans, H. H. The photobiology of photodynamic therapy: cellular targets and mechanisms. *Radiat. Res.* **150**, S146, doi:10.2307/3579816 (1998).

194. Naik, A. J. T., Ismail, S., Kay, C., Wilson, M. & Parkin, I. P. Antimicrobial activity of polyurethane embedded with methylene blue, toluidene blue and gold nanoparticles against *Staphylococcus aureus*; Illuminated with white light. *Mater. Chem. Physi.* **129**, 446-450, doi:10.1016/j.matchemphys.2011.04.040 (2011).

195. Perni, S. *et al.* The antimicrobial properties of light-activated polymers containing methylene blue and gold nanoparticles. *Biomaterials* **30**, 89-93, doi:10.1016/j.biomaterials.2008.09.020 (2009).

196. Noimark, S. *et al.* Dual-mechanism antimicrobial polymer-ZnO nanoparticle and crystal violet encapsulated silicone. *Adv. Funct. Mater.* **25**, 1367-1373, doi:10.1002/adfm.201402980 (2015).

197. Link, S., Wang, Z. L. & El-Sayed, M. A. Alloy formation of gold−silver nanoparticles and the dependence of the plasmon absorption on their composition. *J. Phys. Chem. B* **103**, 3529-3533, doi:10.1021/jp990387w (1999).

198. Coury, A. J., Slaikeu, P. C., Cahalan, P. T., Stokes, K. T. & Hobot, C. M. Factors and interactions affecting the performance of polyurethane elastomers in medical devices. *J. Biomater. Appl.* **3**, 130-178 (1988).

199. Hernandez-Sierra, J. F. *et al.* The antimicrobial sensitivity of *Streptococcus mutans* to nanoparticles of silver, zinc oxide, and gold. *Nanomedicine* **4**, 237-240, doi:10.1016/j.nano.2008.04.005 (2008).

200. Cui, Y. *et al.* The molecular mechanism of action of bactericidal gold nanoparticles on *Escherichia coli*. *Biomaterials* **33**, 2327-2333, doi:10.1016/j.biomaterials.2011.11.057 (2012).

201. Shrivastava, S. *et al.* Characterization of enhanced antibacterial effects of novel silver nanoparticles. *Nanotechnology* **18**, 225103 (2007).

202. Dunnill, C. W. *et al.* Nanoparticulate silver coated-titania thin films—Photo-oxidative destruction of stearic acid under different light sources and antimicrobial effects under hospital lighting conditions. *J. Photochem. Photobiol. A* **220**, 113-123, doi:10.1016/j.jphotochem.2011.04.001 (2011).

203. Hyun, J. S. *et al.* Effects of repeated silver nanoparticles exposure on the histological structure and mucins of nasal respiratory mucosa in rats. *Toxicol. Lett.* **182**, 24-28, doi:10.1016/j.toxlet.2008.08.003 (2008).

204. Ji, J. H. *et al.* Twenty-eight-day inhalation toxicity study of silver nanoparticles in Sprague-Dawley rats. *Inhal. Toxicol.* **19**, 857-871 (2007).

205. Ahamed, M., Alsalhi, M. S. & Siddiqui, M. K. Silver nanoparticle applications

and human health. *Clin. Chim. Acta.* **411**, 1841-1848, doi:10.1016/j.cca.2010.08.016 (2010).

206. Moghimi, S. M., Hunter, A. C. & Murray, J. C. Long-circulating and target-specific nanoparticles: theory to practice. *Pharmacol Rev* **53**, 283-318 (2001).

207. Tolaymat, T. M. *et al.* An evidence-based environmental perspective of manufactured silver nanoparticle in syntheses and applications: a systematic review and critical appraisal of peer-reviewed scientific papers. *Sci Total Environ.* **408**, 999-1006, doi:10.1016/j.scitotenv.2009.11.003 (2010).

208. Kim, Y. S. *et al.* Twenty-eight-day oral toxicity, genotoxicity, and gender-related tissue distribution of silver nanoparticles in Sprague-Dawley rats. *Inhal. Toxicol.* **20**, 575-583, doi:10.1080/08958370701874663 (2008).

209. Lee, H.-Y. *et al.* Genomics-based screening of differentially expressed genes in the brains of mice exposed to silver nanoparticles via inhalation. *J. Nanopart. Res.* **12**, 1567-1578, doi:10.1007/s11051-009-9666-2 (2009).

210. *Carolina biological supply company, Safety Data Sheet: Toluidine Blue O.* <http://www.carolina.com/pdf/msds/TOLBLUEOGHS.pdf>

211. *American Mastertech, Material safety data sheet in accordance with ISO/DIS 11014: toluidine blue O.*
 <http://www.americanmastertech.com/PDF/SSSTTBO.PDF>

212. Lin, J., Bi, L. J., Zhang, Z. G., Fu, Y. M. & Dong, T. T. Toluidine blue-mediated photodynamic therapy of oral wound infections in rats. *Lasers Med. Sci.* **25**, 233-238, doi:10.1007/s10103-009-0700-5 (2010).

213. Nicolle, L. E. Catheter associated urinary tract infections. *Antimicrob. Resist. Infect. Control* **3**, 23, doi:10.1186/2047-2994-3-23 (2014).

214. Douglas Scott II, R. The Direct medical costs of healthcare-associated infections in US hospitals and the benefits of prevention 2009; The division of healthcare quality promotion, national center for preparedness, detection, and

control of infectious diseases, coordinating center for Infectious diseases, centers for disease control and prevention. (2009).

215 Magill, S. S. *et al.* Multistate point-prevalence survey of health care-associated infections. *N. Engl. J. Med.* **370**, 1198-1208, doi:10.1056/NEJMoa1306801 (2014).

216. Page, K. *et al.* Study of the adhesion of *Staphylococcus aureus* to coated glass substrates. *J. Mater. Sci.* **46**, 6355-6363, doi:10.1007/s10853-011-5582-9 (2011).

217. Ratkowsky, D. A., Olley, J., McMeekin, T. A. & Ball, A. Relationship between temperature and growth rate of bacterial cultures. *J. Bacteriol.* **149**, 1-5 (1982).

218. Theoret, C. & Schumacher, J. *Equine wound management*. (John Wiley & Sons, 2016).

219. Korppi-Tommola, J. & Yip, R. W. Solvent effects on the visible absorption spectrum of crystal violet. *Can. J. Chem.* **59**, 191-194, doi:10.1139/v81-030 (1981).

220. Si, W. H. & Zi, Y. Q. Studies on the interaction between RNA with methyl violet and determination of RNA by spectrophotometry. *Guang Pu Xue Yu Guang Pu Fen Xi* **25**, 1846-1849 (2005).

221. Lauth, C. On the new aniline dye, 'Violet de Paris'". *Laboratory* **1**, 138–139 (1867).

222. Docampo, R. & Moreno, S. N. The metabolism and mode of action of gentian violet. *Drug Metab. Rev.* **22**, 161-178, doi:10.3109/03602539009041083 (1990).

223. Littlefield, N. Chronic toxicity and carcinogenicity studies of gentian violet in mice. *Fundam. Appl. Toxicol.* **5**, 902-912, doi:10.1016/0272-0590(85)90172-1 (1985).

224. US department of health & human services. Carcinogenic potency database (CPDB): gentian violet (CAS 548-62-9), (2007). <https://toxnet.nlm.nih.gov/cpdb/chempages/GENTIAN%20VIOLET.html>

225. US Food and Drug Administration (FDA). Questions and answers on FDA's import alert on farm-raised seafood from china: what evidence is there that malachite green, gentian violet and nitrofuran cause cancer? (2009).

226. Zhang, X., Wang, L. & Levänen, E. Superhydrophobic surfaces for the reduction of bacterial adhesion. *RSC Advances* **3**, 12003, doi:10.1039/c3ra40497h (2013).

227. Berendjchi, A., Khajavi, R. & Yazdanshenas, M. E. Fabrication of superhydrophobic and antibacterial surface on cotton fabric by doped silica-based sols with nanoparticles of copper. *Nanoscale Res. Lett.* **6**, 594, doi:10.1186/1556-276X-6-594 (2011).

228. Yamauchi, K. *et al.* Antibacterial activity of hydrophobic composite materials containing a visible-light-sensitive photocatalyst. *J. Nanotech.* **2011**, 1-7, doi:10.1155/2011/380979 (2011).

229. Barlow, S. M. & Raval, R. Complex organic molecules at metal surfaces: bonding, organisation and chirality. *Surf. Sci. Rep.* **50**, 201-341, doi:10.1016/s0167-5729(03)00015-3 (2003).

230. Luo, X. *et al.* Electrospraying-assisted rapid dye molecule uptake on the surfaces of TiO_2 nanoparticles for speeding up dye-sensitized solar cell fabrication. *Sol. Energ. Mater. and Sol. Cells* **144**, 411-417, doi:10.1016/j.solmat.2015.09.042 (2016).

231. Cech, J. & Taboryski, R. Stability of FDTS monolayer coating on aluminum injection molding tools. *Appl. Surf. Sci.* **259**, 538–541 (2012).

232. Zhang, D., Li, G., Wang, F. & Yu, J. C. Green synthesis of a self-assembled rutile mesocrystalline photocatalyst. *Cryst. Eng. Comm.* **12**, 1759, doi:10.1039/b922477g (2010).

233. Tang, H. Z., Wang, H. & He, J. H. Superhydrophobic titania membranes of different adhesive forces fabricated by electrospinning. *J Phys Chem C* **113**, 14220-14224, doi:10.1021/jp904221f (2009).

234. Vilcnik, A. *et al.* Structural properties and antibacterial effects of hydrophobic and oleophobic sol-gel coatings for cotton fabrics. *Langmuir* **25**, 5869-5880, doi:10.1021/la803742c (2009).

235. Pai, K. R. N. *et al.* High surface area TiO_2 nanoparticles by a freeze-drying approach for dye-sensitized solar cells. *RSC Adv.* **4**, 36821-36827, doi:10.1039/c4ra04226c (2014).

236. Shang, B., Wang, Y., Peng, B. & Deng, Z. Bioinspired polydopamine particles-assisted construction of superhydrophobic surfaces for oil/water separation. *J. Colloid Interface Sci.* **482**, 240-251, doi:10.1016/j.jcis.2016.07.081 (2016).

237. McCullagh, C., Robertson, J. M. C., Bahnemann, D. W. & Robertson, P. K. J. The application of TiO_2 photocatalysis for disinfection of water contaminated with pathogenic micro-organisms: A review. *Res Chem Intermediat* **33**, 359-375, doi:Doi 10.1163/156856707779238775 (2007).

238. Tortora, G., Funke, R. B. & Case, L. C. Microbiology; An Introduction. (Addison-Wesley Longman, Inc., 2001).

239. Daoud, W. A., Xin, J. H. & Zhang, Y.-H. Surface functionalization of cellulose fibers with titanium dioxide nanoparticles and their combined bactericidal activities. *Surf. Sci.* **599**, 69-75, doi:10.1016/j.susc.2005.09.038 (2005).

240. Zhao, L., Chu, P. K., Zhang, Y. & Wu, Z. Antibacterial coatings on titanium implants. *J. Biomed. Mater. Res. B Appl. Biomater.* **91**, 470-480, doi:10.1002/jbm.b.31463 (2009).

241. Kazuhito, H., Hiroshi, I. & Akira, F. TiO_2 photocatalysis: a historical overview and future prospects. *Jpn. J. Appl. Phys.* **44**, 8269–8285 (2005).

242. Wu, T., Liu, G., Zhao, J., Hidaka, H. & Serpone, N. Evidence for H_2O_2 generation during the TiO_2-assisted photodegradation of dyes in aqueous dispersions under visible light illumination. *J.of Phys. Chem. B* **103**, 4862-4867, doi:10.1021/jp9846678 (1999).

243. Saquib, M. TiO$_2$-mediated photocatalytic degradation of a triphenylmethane dye (gentian violet), in aqueous suspensions. *Dyes Pigm.* **56**, 37-49, doi:10.1016/s0143-7208(02)00101-8 (2003).

244. Maisch, T. Resistance in antimicrobial photodynamic inactivation of bacteria. *Photochem. Photobiol. Sci.* **14**, 1518-1526, doi:10.1039/c5pp00037h (2015).

245. Zhang, W. *et al.* Superhydrophobic and superoleophilic PVDF membranes for effective separation of water-in-oil emulsions with high flux. *Adv Mater* **25**, 2071-2076, doi:10.1002/adma.201204520 (2013).

246. National Institute of Environmental Health Sciences, Perfluorinated chemicals (PFCs)(2016).
<https://www.niehs.nih.gov/health/materials/perflourinated_chemicals_508.pdf>

247. United States Environmental Protection Agency, Emerging contaminants fact sheet–perfluorooctane sulfonate (PFOS) and perfluorooctanoic acid (PFOA) (2014).

248. Barry, V., Winquist, A. & Steenland, K. Perfluorooctanoic acid (PFOA) exposures and incident cancers among adults living near a chemical plant. *Environ. Health Perspect* **121**, 1313-1318, doi:10.1289/ehp.1306615 (2013).

249. Ducatman, A. M., Zhang, J. & Fan, H. Response to prostate cancer and PFOA. *J. Occup. Environ. Med.* **57**, e61, doi:10.1097/JOM.0000000000000470 (2015).

250. The US Centers for Disease Control and Prevention (CDC). Perfluorochemicals (PFCs) (2009).

251. International Agency for Research on Cancer (IARC), Monographs on the Evaluation of Carcinogenic Risks to Humans (2010).

252. US Food and Drug Adminstration (FDA). Code of federal regulations title 21 (2016).
<https://www.accessdata.fda.gov/scripts/cdrh/cfdocs/cfcfr/cfrsearch.cfm>